Cross-Modal Interactions in the Optic Tectum of *Xenopus laevis* Tadpoles

Daniel L. Felch
M.S., Brandeis University, 2005

THESIS

Submitted in partial fulfillment of the requirements for the degree of Doctor of Philosophy in the Department of Neuroscience at Brown University

Providence, Rhode Island

May 2015

This dissertation by Daniel L. Felch is accepted in its present form by the Neuroscience Graduate Program as satisfying the dissertation requirement for the degree of Doctor of Philosophy.

Date_____ _____
Carlos Aizenman, Advisor

Recommended to the Graduate Council

Date_____ _____
David Berson, Reader

Date_____ _____
Julie Kauer, Reader

Date_____ _____
Barry Connors, Reader

Date_____ _____
Chinfei Chen, Reader

Approved by the Graduate Council

Date_____ _____
Peter M. Weber, Dean of the Graduate School

Daniel L. Felch

Daniel_Felch@brown.edu

EDUCATION

Doctor of Philosophy (candidate), Neuroscience, Brown University, Providence, RI (2009–present)
Thesis Title: *Cross-Modal Interactions in the Optic Tectum of* Xenopus laevis *Tadpoles*

Master of Science, Neuroscience, Brandeis University, Waltham, MA (2003–2005)
Thesis Title: *Molecular Compartmentalization of Thalamocortical Visual Pathways in the Gray Squirrel, a Highly Visual Diurnal Rodent*

Bachelor of Arts, Psychology, Brandeis University, Waltham, MA (1998–2002)

RESEARCH EXPERIENCE

Neuroscience Graduate Program, Brown University, Providence, RI (2009–preseent)
Doctoral Thesis research in the laboratory of Dr. Carlos Aizenman

Department of Pathology, Brigham and Women's Hospital, Boston, MA (2006–2009)
Technical Research Assistant in the laboratory of Dr. Mel Feany

Dept. of Anesthesia & Critical Care, Massachusetts General Hospital, Charlestown, MA (2005–2006)
Research Technologist for Dr. Gary Brenner, in laboratory of Dr. Clifford Woolf

Neuroscience Program, Brandeis University, Waltham, MA (2003–2005)
Master's Thesis research conducted with Dr. Sacha Nelson

Department of Biology, Brandeis University, Waltham, MA (2002–2003)
Laboratory Assistant for Dr. Sacha Nelson

PUBLICATIONS

Daniel L. Felch and Stephen D. Van Hooser. (2012) Molecular compartmentalization of lateral geniculate nucleus in the gray squirrel (*Sciurus carolinensis*). *Frontiers in Neuroanatomy*: Epub 2012 Apr 10.

Michelle L. Steinhilb, Dora Dias-Santagata, Tudor A. Fulga, **Daniel L. Felch**, and Mel B. Feany. (2007) Tau phosphorylation sites work in concert to promote neurotoxicity in vivo. *Molecular Biology of the Cell* 18: 5060–5068.

CONFERENCE PRESENTATIONS

Brown Institute for Brain Science, Center for Vision Research: 'art + science PERCEPTION' (5th Anniversary Celebration), November 9 2012, Granoff Center for the Creative Arts, Brown University

Video Poster Title: "Contribution of Excitatory and Inhibitory Synaptic Conductances to Multi-Modal Integration in the Optic Tectum of *Xenopus laevis* Tadpoles"

NIH-Brown Neuroscience Graduate Program Partnership: Second Scientific Retreat, April 15–17 2012, Marine Biological Laboratory, Woods Hole, MA

Poster Title: "Multisensory interactions in single neurons of the *Xenopus* tadpole optic tectum"

Society for Neuroscience Annual Meeting, November 12–16 2011, Washington DC

Poster Title: "Multisensory interactions in single neurons of the *Xenopus* tadpole optic tectum"

AWARDS AND FELLOWSHIPS

Interdisciplinary Vision Training Grant (2010–2013)
Center for Vision Research, Brown University

TEACHING EXPERIENCE

Graduate Teaching Assistant (2011)
Principles of Neurobiology, Department of Neuroscience, Brown University
– Wrote and graded exams, conducted section meetings and lectures

PROFESSIONAL AFFILIATIONS

Society for Neuroscience (2009–present)

Acknowledgment

This is work undertaken as an exploration, and in many respects. A push into the unknown on many levels, only a few of which are addressed in study that follows. And the arrival of that journey here, at the writing of this dissertation, is not the product of my efforts alone; individuals in many roles, places, and capacities gave a part of themselves — their energy and time, their expertise and knowledge, their smile and love, or simply their pause and consideration — to create the result which is presented, in part (the *scientific* part), in the text below. This is a large group indeed, but one in which every person has made an irreplaceable contribution. So whether your work here was days on end, hours at a time, or simply a small aside at a crucial time, then please know that, at least to me, it has made all the difference in the world.

Table of Contents

List of Tables

List of Illustrations

INTRODUCTION

With rare exceptions, our experience of the world is effortless, and seamless. When standing roadside as a bicycle approaches, when it rings its bell we notice and locate it quickly, and can then either wave hello or jump out of the way. And, as we step out of bed and onto a fragile child's toy, the combination of crunching sound and odd texture creates an immediacy which disperses grogginess quite effectively. The particular efficiency with which our brain merges these pairs of sensations — vision and sound, sound and touch — into a single perception is quite notable, and attests to the fundamental importance of this phenomenon to sensory perception, generally.

Indeed, in humans and all other animals, the nervous system must rapidly transform external stimuli into information about external events, in the form of internal representations, and then use that information to initiate an appropriate reaction. But, as Fetsch and colleagues note in a recently-published review of theoretical and experimental work on sensory integration (2013), these internal representations contain inaccuracies. Energy generated by external events is randomly lost or distorted as it passes through space on it's way to an animal's sensory organs and, due to stochastic variability inherent in these sensory organs and their downstream cellular targets, any internal representation conveys, at best, only an estimate of the original event. By logic, this uncertainty within

sensory representations limits the accuracy of an animal's perception of the external world. Given the probabilistic nature of internal representations, however, one way that the nervous system of any animal can improve perceptual accuracy is to combine information from multiple, statistically-independent representations of external events.

In sensory physiology, any event-triggered energy that impinges upon, and changes the activity of, a sensory organ can be classified as a stimulus to that sensory system. Very often, the energy produced by a single external event is transmitted over a range of frequencies, and animals have evolved distinct peripheral sensory systems to detect different frequencies of energy — from 400–790 THz (visible frequencies), to 20–20,000 Hz (audible frequencies), to the range below 250 Hz (tactile and proprioceptive frequencies).

In vertebrates, after information is extracted from energy in the environment and transferred by peripheral sensory systems to the central nervous system, the central representations of external space often take the form of coordinate maps in spatial dimensions. Such coordinate maps are ideally suited to integrate and transform sensory information about events in space (Knudsen et al., 1987), and are also used by motor systems to guide and efficiently execute responses of the skeletal musculature (Graziano and Gross, 1998). Behaviorally-relevant interactions between sensory information and motor output plans are therefore likely to involve some combination of information from these different coordinate spatial representations – i.e., those containing information from sensory systems as well as those containing information about motor targets. One

biological substrate in which to study these interactions is the vertebrate optic tectum (OT). This midbrain structure, also known as the superior colliculus (SC) in mammals, receives both sensory information and motor feedback, and transforms that information into signals that direct motor outputs. It contains laminae that are segregated both anatomically and functionally – its superficial layers receive a direct retinal projection that maintains its topographic, coordinate map of visual space in the tangential dimension (Gaze et al., 1972; Graybiel, 1975; Straznicky and Gaze, 1972) and its deep and intermediate layers receive inputs carrying both auditory information (Knudsen, 1982; Knudsen and Knudsen, 1983; Lowe, 1986) as well as somato- and mechano-sensory information and motor feedback signals (Deeg et al., 2009; Drager and Hubel, 1975a, b, 1976; Harting and Van Lieshout, 1991; Lowe, 1986; Wallace and Stein, 1997); for a review, see May (2006). Non-visual sensory modalities also maintain coordinate maps of external space in the tangential dimension of the intermediate and deeper layers, and in all instances described to date the spatial coordinates of visual and non-visual maps are in register along the superficial-deep axis of the tectum (for example: Drager and Hubel, 1976; Hiramoto and Cline, 2009; Knudsen, 1982; Knudsen and Knudsen, 1983). Motor output signals are generated by neurons in the intermediate and deep layers, and these output signals are similarly organized into a coordinate representation of positions in space that likewise maps onto the tangential dimension of the tectum (Lee et al., 1988; Robinson, 1972). Importantly, observations that the coordinate system of the topographic motor map is in spatial register with the coordinate systems of the topographic sensory maps, as seen in studies of functional output (Jay and Sparks, 1987; Sparks, 1986 (review)) and synaptic connectivity (Doubell et al., 2003; Lee et al., 1997; Meredith and

King, 2004; Skaliora et al., 2004), strongly suggest that local interactions among cross-modal sensory signals may participate in the transformation of information about events occurring in space into motor signals that shape a behavioral response.

MULTISENSORY INTEGRATION

Integration of multimodal inputs is evident when the response to a given stimulus, measured in either cellular output or gross behavioral performance, is altered by the presence of a second stimulus in a defined temporal and/or spatial window (Stein and Stanford, 2008; Stein et al., 2009). In the output of neurons in the intermediate and deeper layers of the mammalian superior colliculus, this manner of integration is highly robust for stimuli delivered to different sensory pathways. For neurons that receive input from multiple sensory modalities, *in vivo* experiments have shown that after stimulation of two different sensory pathways the neuronal response can be either significantly enhanced or depressed relative to that elicited by stimulation of either pathway in isolation (Meredith and Stein, 1983). Notably, these changes in cellular output do not occur when two stimuli are delivered via the same sensory pathway — for such within-modality pairs, the output is either unchanged or depressed relative to the responses evoked by a single stimulus presentation (Alvarado et al., 2007b). And as researchers have developed different metrics to quantify and observe these effects, different aspects of this phenomenon have been discovered.

Phenomenology: Response Magnitude

The earliest observations of multisensory integration in cellular output were based on examination of the total number of action potentials, or "spikes," generated in a given post-stimulus time window (Meredith et al., 1987; Meredith and Stein, 1983, 1985, 1986a, b; Stein et al., 1988). By comparing, for each cell, the total spike count observed after a paired stimulus presentation with that observed after a single stimulus — that is, presentation of just one of the two component stimuli in the paired condition — it is therefore possible to assess the spike "gain" due to paired stimulation. In their original report, Meredith and Stein (1983) quantify this effect as:

Equation 1: $$MSI = (CM - SM_{max})/SM_{max}$$

where SM_{max} is the average number of action potentials evoked by the most effective of the two single-stimulus presentations (Single Modality), *CM* is the average number of action potentials evoked by the paired-stimulus presentation (Combined Modality), and *MSI* is the Multisensory Index. This measure thus indicates the difference (or "gain") in a cell's response (positive or negative) resulting from the addition of a second stimulus, corrected for the cell's maximal single-stimulus response. Because MSI corrects for each neuron's maximal output in the single-stimulus condition, it is a normalized measure that can be compared across neurons that may vary in overall spike output. And, as discussed by Stein et al. (2009) in their paper "Challenges in quantifying multisensory integration:

alternative criteria, models, and inverse effectiveness," this metric has remained central to the multisensory field.

Phenomenology: Inverse Effectiveness

MSI is itself a proportional measure of the change in response elicited by the addition of a second stimulus (i.e., in the creation of a stimulus pair), versus output evoked by a single stimulus; there is no *a priori* expectation of the relationship between the maximal output attributable to the single stimulus and this index of paired efficacy. Empirical observations of this relationship, however, have revealed that for cellular data in which MSI values are positive (that is, indicating a response enhancement) there is a negative relationship between single stimulus efficacy and the MSI metric — for a given paired stimulus, as the magnitude of a cell's responsiveness to either one of the component stimuli increases, the associated MSI value tends to decrease (Alvarado et al., 2007a; Alvarado et al., 2007b; Jiang et al., 2001; Meredith and Stein, 1986b; Stanford et al., 2005; Wallace and Stein, 1997) (**see Figures 1 and 2**). A similar, but inverse, relationship appears to hold for cellular output in which MSI values are negative (indicating a response depression). In these circumstances, as the magnitude of a cell's responsiveness to a component stimulus increases, the *absolute value* of the MSI metric tends to decrease (Jiang and Stein, 2003).

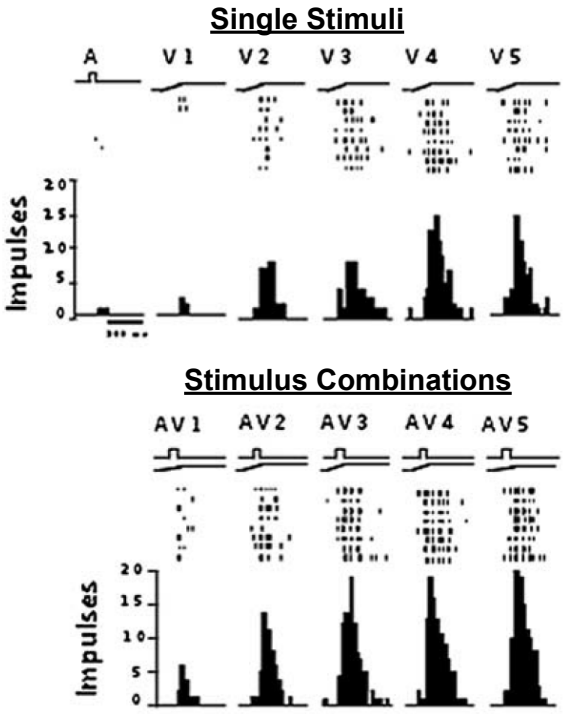

Figure 1: Inverse effectiveness in cross-modal response enhancement: Examples.
Top: Raster plots and cumulative histograms showing the responses of a SC neuron to an isolated auditory stimulus ("*A*") and an isolated visual stimulus, at five different intensities ("*V1*" through "*V5*").
Bottom: Raster plots and cumulative histograms showing responses of the same SC neuron to combinations of the auditory stimulus and each of the five intensities of the visual stimulus ("*AV1*" through "*AV5*"). Note that there are differences in output between combinations that include the strongest of the visual stimuli.
(Figure from Stein et al. (2009))

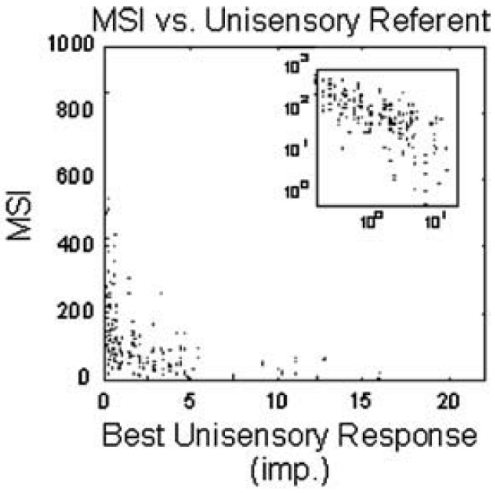

Figure 2: Inverse effectiveness in cross-modal response enhancement: Population data.
Scatter plot of data from a population of SC neurons, displaying the Multisensory Index for each cell (MSI) versus the number of impulses generated by the most effective of the two cross-modal stimuli ("imp" = impulses). Note the sharply negative relationship between these two measures, especially cells in which the most effective single stimulus is relatively weak. *Inset*: A log-log plot for the same data.
(Figure from Stein et al. (2009))

Data from studies of perceptual performance are also consistent with the principle of inverse effectiveness. For example, auditory stimuli are more accurately located when presented in conjunction with visual stimuli just at the perceptual threshold, versus visual stimuli above it (Bolognini et al., 2007), and accurate detection of a variable-contrast visual target is improved by a paired sound, but only if that sound is presented alone and without other, additional stimulus cues (Lippert et al., 2007). These observations

establish an important link between cellular output and behavioral context, and in doing so provide support for the notion that the principle of inverse effectiveness is widespread in multi-modal phenomena.

Phenomenology: Response Timing

The preceding metrics are based on the total number of action potentials that occur in an interval of time, post-stimulus. These measures, therefore, cannot detect or describe changes in the temporal distribution of action potentials within that interval. Recent multisensory studies have begun to show, however, that stimulus pairings can indeed produce a temporal redistribution in spike output. Specifically, two reports by Rowland and colleagues not only demonstrated that a pair of cross-modal stimuli decreases what latency to action potential generation, relative to action potential onset after either of the component stimuli presented in isolation (Rowland et al., 2007a), but also that cross-modal stimuli shift the entire temporal distribution of cellular output earlier in time and more closely aligned with the stimulus, even after controlling for the difference in onset latency (Rowland and Stein, 2007) (**see Figure 3**). Under multisensory conditions, it is important to note that no expectation exists of a link between the temporal distribution of action potentials a cell produces and the total number of action potentials it produces (i.e., the "magnitude" of the response); there is not a principled or mechanistic reason to connect the two measures. However, Ghose, Barnett, and Wallace (2012) demonstrated this very association between the duration of OT/SC neurons' responses upon

multisensory stimulation and the MSI values calculated from the total number of action potentials generated — cell by cell, higher MSI values for response magnitude are associated with shorter duration responses after cross-modal stimulation. This finding is notable because it suggests that the timing of neuronal responses, in addition to their magnitude, represents a key metric of multisensory processes.

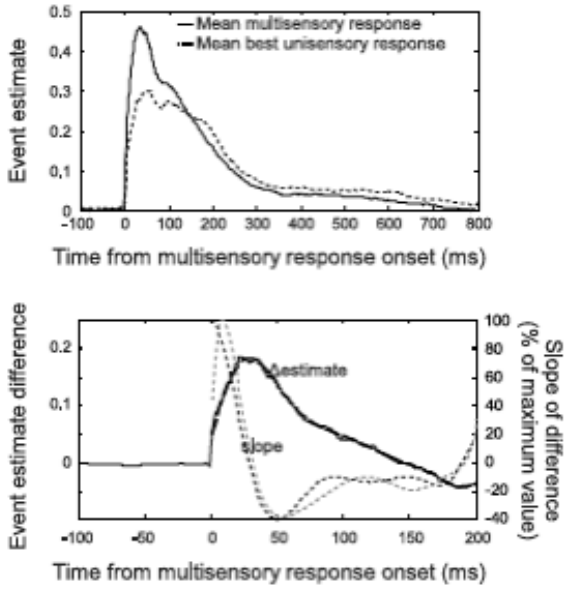

Figure 3: Temporal characteristics of cross-modal phenomena.
Top: Shown are event estimates of spike data recorded in mammalian SC after cross-modal stimulus pairs and after presentations of the most effective single stimulus, aligned to the onset of cross-modal response. Note that the curves are most differentiated early in the response.
Bottom: Plotted is the raw difference between these curves, as well as the difference in their slope. The solid line demonsrates how this difference peaks soon after response onset.
(Figure from Rowland and Stein (2007))

Behavioral studies of multisensory perception have also provided data that parallel this temporal redistribution of cellular responses. Whether in tasks of stimulus localization (Hecht et al., 2008b), simple stimulus detection (Diederich and Colonius, 2004), or detection during participant self-motion (Hecht et al., 2008a), increasingly heterologous stimulus sets were associated with progressively faster reaction times. Moreover, in each of these reports, instances of relatively greater multisensory effect were generated by combinations of relatively weaker individual stimuli; their results thus extend the concept of inverse effectiveness to measures of response timing, in addition to measures of response magnitude. Overall, studies such as these provide clear evidence that changes in the temporal domain are fundamental to multisensory processes at all levels, from cellular to behavioral.

These dimensions of cell output indicate the manner in which neurons demonstrate their integration of multisensory information. An exploration of the specific stimulus characteristics that generate such responses — that is, the aspects of multisensory patterns to which neurons are most sensitive — continues below.

Stimulus Dependencies: Spatial Factors

One well-characterized property of multisensory integration is its dependence on overlap between spatial receptive fields (RF's) for the respective modalities of sensory input that impinge on a multisensory collicular neuron. In the vast majority of cases, RF alignment is associated with response enhancement to a multimodal stimulus pair (with each stimulus in its respective RF), whereas RF disparity is associated with either response depression or no response change to a multimodal stimulus pair (again, with each stimulus in its RF) (Meredith and Stein, 1996). A detailed account of the consequences of RF alignment was recently provided by Ghose and Wallace (2014) — their data not only address the spatial heterogeneity in efficacy that exists within the multi-modal receptive fields of SC neurons, but also show that the strongest multisensory effects are evoked from the locations in space that correspond to the least effective regions of one or both uni-modal receptive fields, when stimulated individually. These results thus extend the principle of inverse effectiveness in multisensory interactions to spatially-arrayed stimuli, as well. A behavioral manifestation of the spatial sensitivity of SC neurons can be seen in

the accuracy of orienting responses to stimuli presented in space. Specifically, in an awake-behaving animal, the accuracy of trained movements to the presentation of one stimulus modality (e.g., visual or auditory) is either enhanced or depressed by the simultaneous presentation of a stimulus of the alternate modality. The degree of enhancement or depression is again dependent on spatial factors — response accuracy is enhanced as the second, cross-modal stimulus approaches the position of the first stimulus, while response accuracy is depressed as the second stimulus moves farther from the position of the first (Stein et al., 1989). Together these functional observations provide further support for a behaviorally-relevant integrative mechanism that operates locally within the topographic sensory maps of the OT/SC, in local neural circuits or within individual neurons.

Stimulus Dependencies: Temporal Factors

Temporal factors also influence multisensory integration in OT/SC neurons. For example, cross-modal stimulus pairs produce a maximal enhancement of action potential generation when the two inputs are staggered such that overlap occurs between the peaks of the timecourses of each unimodal response. When the temporal offset between stimuli varies from the offset which elicits maximal enhancement, in either the positive or negative direction, action potential generation decreases to the point where the cross-modal stimulus pair produces a response depression (relative to the response elicited by either stimulus in isolation) or a response in which there is no apparent interaction

between the two input modalities (Meredith et al., 1987). Repeated exposure to temporal patterns of cross-modal stimuli can also alter the timecourse of action potential generation in OT/SC neurons, even in an anesthetized adult animal. If stimuli delivered to two different sensory systems are offset by the smallest time interval that permits the resolution of separate evoked responses, and then delivered in the same sequence for 50-80 trials, the response to each stimulus in the sequence increases in magnitude and the distribution of the total responses to the stimulus sequence compresses towards the midpoint of the interval between the pair. This form of response plasticity occurs only after exposure to cross-modal sequences — no changes are observed after repetitions of same-modality pairs (Yu et al., 2009). It is consistent, then, with a mechanism that operates specifically in multisensory integration.

What remains unknown is how exposure to patterns of cross-modal stimuli during development might impact the maturation of multisensory integration and the overall function of the tectum/superior colliculus. Yet in order to address this and other questions about the development of multisensory integration in a systematic way, the core characteristics of its maturation must serve as a reference. The findings described below outline the basic developmental trajectory of this phenomenon.

Development of Multisensory Integration

The developmental onset of multisensory integration in tectal/collicular neurons is delayed relative to the onset of non-integrating multisensory responsiveness. In cat superior colliculus, for example, somatosensory responses are present at birth, auditory responses are detectable by the end of the first postnatal week, and visual responses can be recorded between the first and second postnatal week (Stein, 1984; Stein et al., 1973). Only between the fourth and fifth postnatal week does an initial subset of multisensory neurons demonstrate integrative responses. On a cell-by-cell basis, the appearance of this integrative ability is all-or-none — one multisensory neuron may fail to support any interaction between cross-modal stimuli while a neighboring multisensory neuron integrates stimuli delivered to different sensory pathways just as robustly as would a neuron in the adult SC. Furthermore, at least for the temporal resolution of the data currently available, for a given neuron RF refinement occurs synchronously for all sensory inputs and takes place abruptly, as with the transition to integrative capability. Indeed, in an individual cell the presence or absence of integrative capability is directly associated with the spatial refinement of its modality-specific RFs; if the RF size for a particular input pathway remains greater than 150% of its average size in the adult, the probability of observing multisensory integration in that neuron drops to 0.5 and quickly approaches zero as the RF size continues to increase. Despite this abrupt onset of multisensory integration between the fourth and fifth postnatal week, the complete development of integrative capabilities in cat SC is prolonged and continues cell-by-cell

through the third postnatal month, until the adult population of integrating neurons is established (Wallace and Stein, 1997).

The mechanisms that mediate this transition to multisensory integration are currently unknown. One hypothesis describes topographic projections from higher-order sensory areas in cortex as the source of instructive signals for the development of multisensory integration in the OT/SC. In the cat, for example, the anterior ectosylvian sulcus (AES; a higher-order multisensory area) and the rostral aspect of the lateral suprasylvian sulcus (rLS; a higher-order visual area) send projections to the intermediate and deeper SC layers. Although each area contains cells with multisensory response properties, in both cases the axons that enter the SC are exclusively unisensory and align their modality-specific topographic projections with the coordinate maps in SC laminae (Wallace et al., 1993). Temporary de-activation of AES and/or rLS has been shown to specifically eliminate the integrative capabilities of multisensory SC neurons, leaving their responses to each component stimulus intact. Cortical inactivation most often produces redundant or synergistic affects in individual SC neurons – in cases of redundancy, the elimination of multisensory integration will occur after inactivation of either AES or rLS, and in cases of synergy, the elimination of integrative responses requires simultaneous inactivation of both AES and rLS (Jiang et al., 2001). These affects of AES and/or rLS inactivation can also be demonstrated in newly-integrating multisensory SC neurons in very young animals, at the end of the fourth postnatal week (Wallace and Stein, 2000). The early appearance of functional interactions between higher-order sensory areas in cortex and multisensory neurons in the SC suggests that, at least in the cat, topographic

sensory input from cortex has some role in the establishment or refinement of the mechanisms underlying multisensory integration.

Current Hypotheses Regarding the Biological Mechanisms for Multisensory Integration

To date, the literature on multisensory integration's biological underpinnings contains exceedingly few direct investigations of cellular or synaptic mechanisms. One significant report by Binns and Salt (1996) assessed the sensory-evoked responses of multimodal neurons in cat SC (i.e., those responsive to more than one sensory modality) after single stimuli and multisensory stimulus pairs, both before and during the intracollicular iontophoretic injection of AP5, a NMDA receptor antagonist. This pharmacological blockade of NMDA receptors decreased stimulus-evoked responses, generally. Cells' responses to multisensory stimuli, however, were decreased by a greater fraction than were their responses to single stimuli (via each modality in isolation). These data have provided a rare insight into the biological mechanisms for multisensory integration, and continue to inform biologically-inspired models of the phenomenon.

Indeed, a range of computational models currently exist that postulate, and seek to account for, the biological mechanisms underlying various aspects of multisensory phenomenology. There are two principal types of such biologically-inspired models. The first focuses on the integration of sensory inputs within a single neuron, and the second

introduces network-level interactions between neurons, both within afferent areas and within the OT/SC itself.

The first biologically-realistic model created is a single-neuron model, proposed by Rowland and colleagues (2007b) to account for how, in the cat, multisensory integration depends on NMDA-receptor-mediated currents (Binns and Salt, 1996) and projections from higher-order sensory cortex (Jiang et al., 2001), and also demonstrates characteristic phenomenology such as supralinear enhancement, inverse effectiveness, and temporal sensitivity. This multi-compartment model suggests that supra-linear responses to specific combinations of inputs are possible when those inputs converge on the same electrotonic compartment of the neuron, where their summed strength can then undergo local, non-linear amplification — by NMDA receptors. To reproduce the empirical finding that multisensory integration in cat SC depends on higher-order sensory cortices (Jiang et al., 2001), these authors group heterologous single-modality inputs from cortex on a single dendritic compartment and segregate the equivalent set of inputs from first-order sensory relays to separate dendritic compartments, so that these compartments only integrate input from a single source. Rowland et al. (2007b) further propose that inhibitory inputs modulate excitation in a divisive manner. Specifically, inhibitory inputs driven by all single-modality sources (higher-order and first-order) are summed directly, without any non-linear operations, and this single value then serves as the denominator in the final ratio of excitation-to-inhibition. The biological instantiation of this divisive inhibition is envisioned in terms of subcellular synaptic location, as well: all inhibitory input converges on the neuron's soma which, being electrotonically closer to the point of

final input integration (the axon initial segment), is thought to enable shunting (divisive) inhibition of inputs that are electrotonically more distant (for a detailed consideration see: Koch, 1999). These specific elements of synaptic architecture are currently without support from empirical work in the colliculus, however.

More recently, this same group proposed a simplified algebraic model that reproduces the temporal profile of cat SC neuronal responses after stimulation with pairs of single-modality inputs (Rowland and Stein, 2014). Here, each excitatory single-modality input is constructed as an independent, biologically-realistic post-stimulus waveform, and at each post-stimulus time point all such inputs undergo a simple summation. The model posits that inhibition: 1) is subtractive, rather than divisive; 2) is present only after net excitation has reached it's peak; and 3) reflects non-linear dynamics within the SC itself — at each time point it's value is calculated from, in part, the product of all excitatory input values at that same time. The role of inhibition is further constrained, here, by it's inclusion exclusively for pairs of stimuli, and not for isolated inputs, which follows from the idea that particular combinations of stimuli are uniquely able to drive non-linear dynamics within the colliculus. As for their first model, the inhibitory dynamics that Rowland et al. (2014) propose here have yet to be validated by experimental data.

The second type of biologically-inspired model of multisensory phenomena incorporates hypotheses not only about synaptic integration in single SC neurons, but also about interactions among the structures and cell types which send inputs to those SC neurons. Similar to the first cell-intrinsic model described by Rowland and colleagues (2007b),

these network models reference two heterologous single-modality excitatory projections from first-order sensory pathways, and two excitatory single-modality inputs from higher-order sensory cortex (the same two modalities are represented in each pair of projections). As introduced by Cuppini and colleagues (2010), this class of model accounts for spatial interactions in multisensory phenomena by specifying — within two heterologous single-modality areas each SC afferent structure and within the SC itself — populations of units with spatiotopically-organized receptive fields. Furthermore, this spatiotopic organization is conserved in the projections from each of these areas onto individual SC units. One critical assumption of this model is that lateral connections within each such population vary in sign according to the spatiotopic distance between units: connections between units responsive to adjacent or nearby positions in space are excitatory, while there is a gradual, continuous transition to inhibitory connectivity for units responsive to progressively more disparate regions of space. Graphically, this relationship follows a 'Mexican hat' distribution of connection sign & strength versus spatiotopic distance. As instantiated within each of the single-modality afferent structures, this lateral connectivity enables the model to reproduce response suppression for spatially disparate uni-modal inputs and, as implemented between SC neurons, allows the model to also reproduce response suppression for spatially disparate cross-modal inputs.

Other hypotheses incorporated into this network structure relate to how SC afferent structures interact with each other and how they differentially influence SC neurons. While this model follows the cell-intrinsic models (Rowland et al., 2007b; Rowland and Stein, 2014) in incorporating the postsynaptic action of NMDA receptors for afferent

inputs onto SC neurons, it makes several additional hypotheses regarding inhibitory connections within the multisensory network. First, each single-modality afferent area sends a collateral projection to a dedicated population of inhibitory units within the SC, with spatiotopically-conserved unit-to-unit connectivity. In turn, each unit within each of these four SC inhibitory populations sends a projection to the spatiotopically-matched multisensory neuron. The second hypothesis accounts for the empirical finding that in cats, the phenomenon of cross-modal enhancement is dependent on both single-modality projections from higher-order sensory cortex (Jiang et al., 2007; Jiang et al., 2002). Cuppini et al. (2010) speculate that projections from each of the two cortically-activated SC inhibitory populations shunt the excitatory inputs from the first-order sensory streams, and that such shunting would be manifested as divisive inhibition, applied only to the first-order excitatory inputs. Direct input from the two cortical afferents would therefore represent the primary influence on SC neurons. The third hypothesis accounts for the empirical finding that, in the cat, when cortical inputs are acutely deactivated, SC neurons' responses to cross-modal stimuli largely resemble responses to the most effective of the two first-order sensory projections (Alvarado et al., 2009; Alvarado et al., 2007a; Jiang et al., 2001). Cuppini et al. (2010) reproduce this finding by introducing two interactions between the first-order sensory streams: 1) shunting, divisive inhibition of each excitatory first-order input by the SC inhibitory population driven by the opposite pathway, and 2) spatiotopically-matched reciprocal connections between units of these two SC inhibitory populations. This mutual inhibition of inhibition is responsible for a "winner-take-all" outcome among the first-order sensory pathways — when these projections are unmasked by acutely silencing higher-order sensory cortex, SC

multisensory neuron responses are driven by the strongest of the two first-order inputs. The creators of this network model (Cuppini et al., 2010) emphasize its sensitivity to changes in the inhibitory connections proposed within the colliculus. As one significant example, they note that when the strength of first-order sensory inputs to the respective SC inhibitory populations is sufficiently decreased, cross-modal enhancement is possible even in the absence of projections from higher-order sensory cortex.

In a subsequent work, Cuppini and colleagues (2012) extend this network model to propose candidate mechanisms for the development of multisensory phenomena in cat superior colliculus. Based on Hebbian rules of synaptic plasticity, which strengthen connections between neurons active in orthodromic sequence, this form of the network model predicts, in part, that in order for cross-modal suppression to appear in the adult, maturation of lateral connectivity between multisensory collicular neurons must be delayed relative to the maturation of descending projections from higher-order sensory cortex. As such, to allow for cross-modal suppression, these lateral synapses must mature only after the network has developed it's capacity for integrative cross-modal enhancement. This work further predicts that in an adult animal: 1) overall synaptic drive from lateral connections between multisensory SC neurons is strongly inhibitory, with excitatory inputs arriving only from multisensory neurons with spatiotopically-matched receptive fields, and 2) a multisensory collicular neuron's capacity for cross-modal suppression, in addition to cross-modal enhancement, varies with the strength of the inhibitory lateral inputs to that cell. Thus, this dependence on intra-collicular feedback inhibition augments the emphasis placed earlier on feed-forward inhibition, from each of

the four inhibitory populations receiving input from single-modality afferents(Cuppini et al., 2010), and underscores the potential for inhibitory connectivity to shape the multisensory response. As for the hypotheses generated by single-cell models, however, it should be noted that these predictions have yet to be confirmed or refuted by direct experimental data.

The hypotheses regarding intra-collicular connectivity are particularly amenable to experimental interrogation in the *Xenopus* tadpole, which engages in active navigation through a multisensory environment and yet, as representing a larval stage of vertebrate development, does so without fully-developed inputs from higher-order sensory areas. The results of the work that follows, therefore, will later be discussed in the context of these hypothetical mechanisms for multisensory phenomena.

Multiple Sensory Projections to the Optic Tectum of *Xenopus laevis*, and Their Development

In the adult *Xenopus laevis* (African clawed frog), the internal structure, afferent and efferent connections, and functional properties of the optic tectum are well characterized and demonstrate a clear homology to the adult mammalian superior colliculus. **Figure 4** presents a detailed schematic of the homology between amphibian, bird, and mammalian SC/OT. As in the superior colliculus,, for instance, the *Xenopus* optic tectum receives a primarily contralateral projection from retinal ganglion cells (RGC's); this projection

targets the superficial neuropil layers and there forms synapses with tectal cell dendrites (Székely and Lázár, 1976). In developing *Xenopus* tadpoles, RGC axons can first be visualized entering the tectum during the Nieuwkoop and Faber (1956) developmental

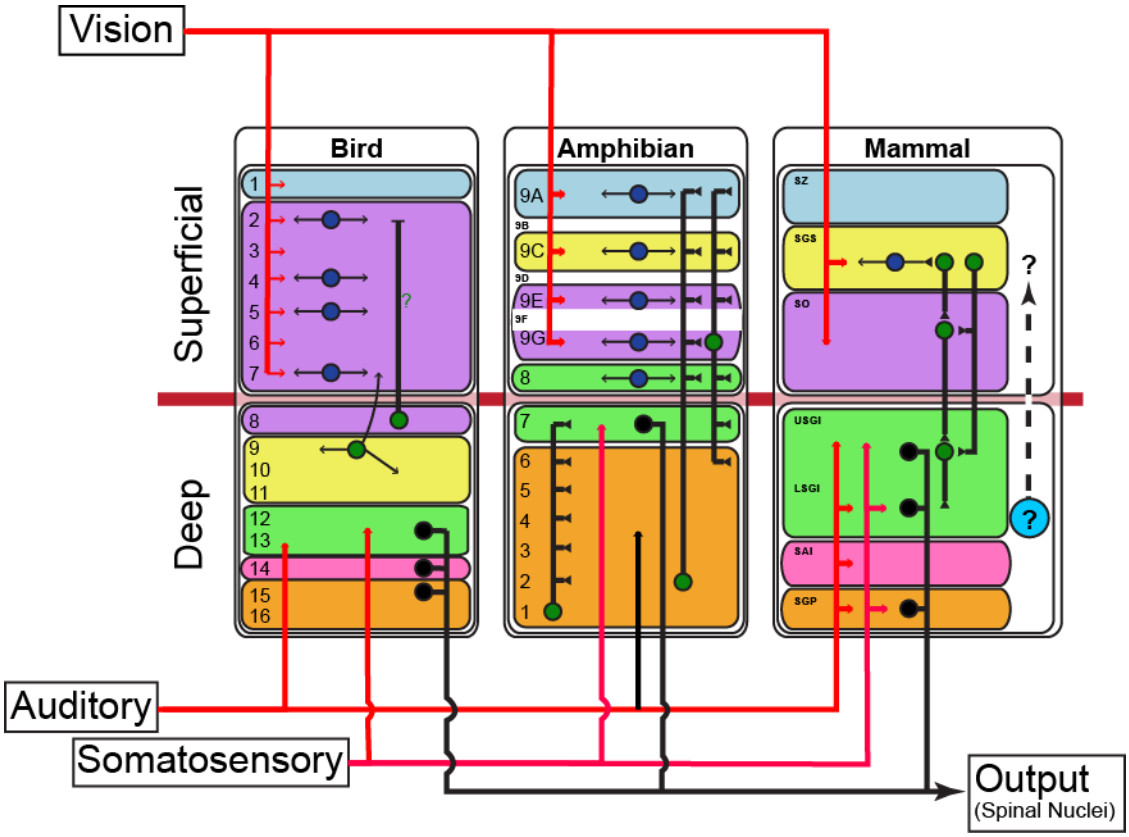

Figure 4: Comparative neuroanatomy of the vertebrate OT/SC.
Simplified wiring diagram of the bird, amphibian, and mammalian OT/SC. Sensory inputs are labeled in red. The primary output cells and pathways to motor planning circuits are labeled in black. Blue cells represent intrinsic connectivity within layers. Green cells represent intrinsic connectivity between layers. The background colors represent likely functional conservation of layers between the bird, amphibian, and mammal, and the layers are labeled after the prevailing nomenclature. In the mammalian SC, the blue cell outside the specific layering represents a putative projecting cell type that would provide auditory input to the superficial cells as postulated by Ghose and colleagues. Abbreviations: SZ, stratum zonale; SGS, stratum griseum superficiale; SO, stratum opticum; USGI, upper stratum griseum intermediale; LSGI, lower stratum griseum intermediale; SAI, stratum album intermediale; SGP, stratum griseum profundum. Connectivity drawn from Székely and Lázár (Székely and Lázár, 1976); Wilczynski and Northcutt (1977); Hardy et al. (1985); Luksch (2003); and May (2006). (Figure provided by T. Truszkowski; personal communication)

stages 39-41 (Gaze et al., 1974; Holt, 1989). Functional synaptic connections between RGC's and tectal neurons can also be detected during this period, at stage 40-41 (Zhang et al., 1998). Once RGC projection has fully innervated the tectum, a period of rapid

tectal circuit growth then occurs between stages 45 and 49, wherein concomitant increases in excitatory synaptic drive and retinotectal synapse number are constrained by a decrease in intrinsic excitability (Pratt and Aizenman, 2007). The result is a refinement of retinotectal connectivity manifested in a sharpening of visual RF's (Dong et al., 2009), a reduction in the latency and variability of recurrent intratectal excitation (Pratt et al., 2008), and an increase in visual acuity (Dong et al., 2009).

The adult *Xenopus* optic tectum also receives direct projections from mechanosensory nuclei in the hindbrain that carry somatosensory input, lateral line (water-wave sensitive) input, and auditory input. The dorsal column nucleus (DCN), for example, collects somatosensory information from ascending spinal afferents and afferents from cranial nerves including V (trigeminal) and VII (facial). It then transmits those signals via medial lemniscal axon projections to the contralateral tectum, where its processes arborize in the intermediate and deep layers (Munoz et al., 1995) and mediate peripherally-evoked synaptic events in tectal neurons (Tsurudome et al., 2005). The lateral line system in amphibians enables the detection and discrimination of water movements, and movement frequencies, with specific hair cell receptors arrayed on the external body wall (Behrend et al., 2006). In the dorsal medulla, lateral line inputs enter via the anterior and posterior lateral line nerves (NLLa and NLLp, respectively) and converge on the medially-situated lateral line nucleus (LLN) (Will et al., 1985a). The LLN, too, sends a direct projection to the contralateral optic tectum (Zittlau et al., 1988), where its component axons arborize in the intermediate and deep layers (Will et al., 1985b) and generate field potentials and multi-unit spiking activity upon stimulation of peripheral lateral line nerves (Lowe, 1986).

Processes from auditory organs in the inner ear travel through nerve VIII (acousticovestibular) and terminate in the dorsal medullary nucleus (DMN) (Will et al., 1985a). Although tracer injections in the dorsal-lateral aspect of the medulla – including the DMN – seem to label axon projections in the optic tectum (Will et al., 1985b), the presentation of a simple acoustic stimulus (e.g., a 1200Hz tone burst) in the animal's environment is not sufficient to elicit a distinct peak in the field potential from within the tectal laminae (Lowe, 1986). However, the DMN sends a strong projection to the torus semicircularis, a midbrain structure homologous to mammalian inferior colliculus and located just ventral to the optic tectum (Edwards and Kelley, 2001; Will et al., 1985b), and acoustic stimuli evoke a large field potential at center of its principal nucleus (Lowe, 1986); given the extensive topographic projection from the torus semicircularis to the overlying tectum (Zittlau et al., 1988), acoustic information could potentially enter the *Xenopus* OT from this nearby sensory relay.

Our laboratory and others have recently characterized the development of hindbrain mechanosensory projections to the tectum in *Xenopus* tadpoles. Experiments with dual tracer injections into retina and hindbrain demonstrate that RGC projections first enter the contralateral anterior tectum at stage 37 and arborize in the dorsal tectum at stage 40, and that projections from dorsolateral hindbrain also begin to arborize in the contralateral dorsal tectum at stage 40. By stage 43, axon arbors from RGC's and the hindbrain have together expanded through the anterior-posterior extent of the tectum and occupy most of the length of the tectal neuropil (Hiramoto and Cline, 2009). Furthermore, at each developmental stage examined, there is tight spatial concordance between the center of

the RGC axon arborization and the center of the hindbrain axon arborization, as measured in the plane tangential to the tectal surface (Deeg et al., 2009). Along the superficial-deep axis of the tectum, the adult pattern of superficial RGC terminations and deeper hindbrain terminations is evident as soon as both sets of axons begin to arborize in the neuropil layer of the tadpole tectum. This spatial segregation becomes more distinct through progressive stages of development, such that by stage 48 hindbrain axonal arbors are confined to a band immediately adjacent to the cell body layer and RGC axonal arbors are restricted to a well-prescribed band at the core of the tectal neuropil, with a distinct gap between these two laminar arborizations and between the RGC arborization and the superficial boundary of the tectum (Hiramoto and Cline, 2009). But even from the earliest stages and throughout the course of development, the dendritic arbors of many neurons in the tadpole tectum extend through the entire depth of the tectal neuropil (Lázár, 1973; Wu and Cline, 2003); these morphological observations together suggest that a sensitivity to multiple sensory inputs in single tectal neurons might underlie the key role of cross-modal integration in the development of normal tectal function (Knudsen, 1983, 2002; Knudsen and Brainard, 1991; Wallace and Stein, 2007). Indeed, as soon as RGC and hindbrain projections converge in the tectum, stimulation of either sensory pathway can evoke excitatory synaptic events (Deeg et al., 2009) and increases in somatic intracellular calcium (Hiramoto and Cline, 2009) in single tectal neurons. Furthermore, behavioral data demonstrate that *Xenopus* tadpoles at this same early stage of development produce motor responses to visual and mechanosensory stimuli (Dong et al., 2009; Roberts et al., 2009). Knowledge of how such convergent inputs are integrated by local tectal circuitry and individual postsynaptic neurons, both on a moment-to-moment

basis and over the course of development, will therefore define mechanisms and principles that allow the tectum to maintain its sensitivity to complex events even as an animal's sensory environment and neural architecture are constantly changing.

The Mechanistic Investigation of Cross-Modal Interactions in the Developing *X. laevis* Optic Tectum

However, despite great interest within the field in understanding these fundamental mechanisms and principles (for example: Anastasio and Patton, 2003; Anastasio et al., 2000; Cuppini et al., 2012; Patton and Anastasio, 2003; Rowland et al., 2007b), very few experimental reports are known to exist (Binns and Salt, 1996; Ghose et al., 2014). The prevalent experimental models of multisensory integration have been and are currently the optic tectum (OT) of the barn owl and its mammalian homolog, the superior colliculus (SC), in the cat; their location within the animal makes these structures difficult to access with whole-cell recording techniques *in vivo* and impossible to isolate *in vitro* without significantly disrupting the neural networks in which they operate. The studies that follow exploit the advantages of *X. laevis* tadpoles, where the optic tectum is superficially located and thus accessible for whole-cell recordings *in vivo* (Zhang et al., 1998) and can be isolated in an intact whole-brain preparation for recordings *in vitro* (Wu et al., 1996). Furthermore, because tectally-mediated behaviors appear almost immediately after axonal projections from sensory systems first contact OT neurons during *X. laevis* larval development (Dong et al., 2009; Zhang et al., 1998), this

preparation also enables one to study the maturation of both tectal circuitry and tectal function, in parallel.

The investigation that follows is the first to elucidate the relationship between synaptic conductances to, and spike output from, neurons of the optic tectum / superior colliculus when this midbrain structure receives stimulation from different sensory pathways. Moreover, this study characterizes how this relationship changes with tectal development; the specific period of development under consideration begins at Nieuwkoop and Faber (1956) stage 44 and ends at stage 49. Two key developmental epochs are defined from within this range — tadpoles from stages 44, 45, and 46 possess tectal circuitry that has yet to undergo experience-dependent refinement of connectivity and stimulus selectivity, and tadpoles from stages 48 and 49 begin to demonstrate a more refined connectivity. As noted above, this refinement is evident as an increased number of synapses per RGC axon (Pratt and Aizenman, 2007), a more compact temporal distribution of recurrent activity with shorter latency (Pratt et al., 2008), smaller visual receptive field (RF) sizes, and a concomitant increase in visual acuity (Dong et al., 2009). *X. laevis* larval development progresses rapidly through stage 47 and with few reliable morphometric markers; to ensure reproducibility in the assignment of tadpoles to the two developmental groups, larvae without clear morphometric features of either stage 46 or stage 48 will be excluded.

The first set of experiments examines neuronal output recorded extracellularly, at the cell membrane. These data will reveal whether, and to what degree, *Xenopus* OT responds

uniquely to cross-modal pairs of stimuli, using the same metrics and criteria that multisensory researchers have used previously to analyze extracellularly-recorded action potentials in the OT/SC of birds, cats, and rodents. The phenomenology I detail here not only enables a comparative assessment of how the *Xenopus* tadpole model system agrees with — or differs from — the established vertebrate models, but also provides an essential reference against which to evaluate data on the inputs to these cells; that is, synaptic conductances recorded under the same stimulus protocols.

My expectations are: 1) even without fully-developed higher-order sensory inputs, neurons in the *Xenopus* tectum demonstrate multisensory phenomenology in their output (e.g., it is dependent on stimulus strength and inter-stimulus interval), and 2) the strength of these multisensory effects increases over the two stages of tadpole development under investigation here, as the tectal network undergoes experience-dependent refinement.

The second set of experiments directly addresses, for the first time, whether corollaries to the integrative properties of *X. laevis* OT neurons are evident in the excitatory and inhibitory conductances they receive. Because much is already known about the development of excitatory and inhibitory circuits in the *Xenopus* tectum, the results generated in this study represent the first step towards connecting the cross-modal sensitivity of individual tectal neurons to the circuit- and cellular-level mechanisms known to underlie such selective responses in other paradigms.

I expect, first, that synaptic inhibition will be critical to the expression of multisensory phenomenology in *Xenopus* OT, in accordance with hypotheses about its contributions in mammalian colliculus (Cuppini et al., 2012; Cuppini et al., 2010; Rowland et al., 2007b) and existing data on its influence on visual receptive field structure and output properties of neurons in *Xenopus* tectum (Shen et al., 2011). Second, I anticipate that influence of synaptic inhibition on multisensory output will increase with tadpole development, based on experimentally-observed changes to its visually-driven topography(Tao and Poo, 2005) and fundamental biophysical properties(Akerman and Cline, 2006) over the same developmental stages under investigation here.

Lastly, to assess the degree of overlap between excitatory feedback circuits activated by each of two cross-modal stimuli, I will block $GABA_A$-receptor mediated inhibition with picrotoxin and test whether excitatory circuits activated by one stimulus modality can be fatigued by repeated presentations of stimuli delivered to the other sensory stream. Based on the observation that the magnitude and spread of such "recurrent" excitatory circuits decreases over development (Pratt et al., 2008), as the tectal network undergoes experience-dependent refinement, I expect that degree of overlap between excitatory circuits activated by the two stimulus modalities will decrease, as well.

Altogether, by utilizing the methodological advantages inherent to the *Xenopus* tadpole preparation, the work described herein is able to shed first light on the cellular and circuit-level bases of a phenomenon that is studied widely and yet largely evades explanation — cross-modal integration.

METHODS

Experimental Animals

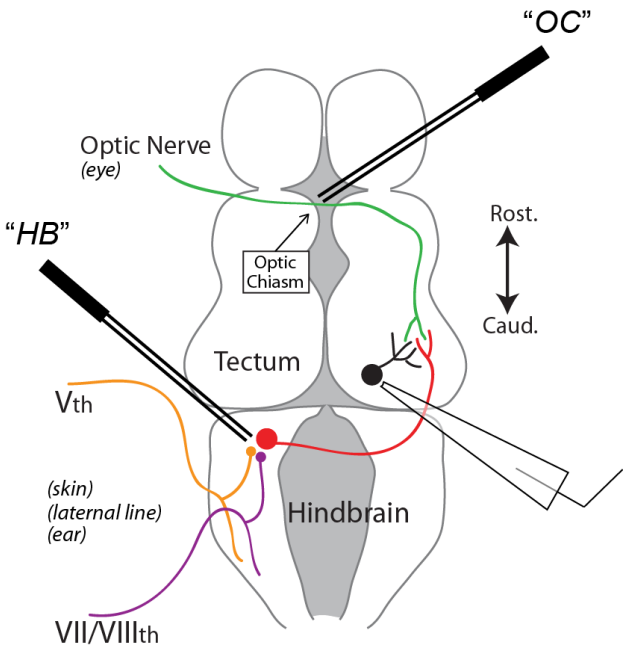

Figure 5: Isolated whole-brain preparation.
Diagram showing placement of the "OC" and "HB" bipolar electrodes relative to tectal afferents and recording location.

Wild-type *Xenopus laevis* tadpoles were raised on a 12 hour light/dark cycle at 18°C in 10% Steinberg's solution. In our laboratory, tadpoles reach the Nieuwkoop and Faber (1956) developmental stages 42–43 at 5–6 days postfertilization (dpf), stages 44–46 at 7–10 dpf, and stage 49 at 14 dpf.

Xenopus laevis tadpoles between developmental stages 44 and 49 are utilized for this study. In the experiments that follow, two key developmental epochs are defined from within this range — tadpoles from stages 44, 45, and 46 possess tectal circuitry that has yet to undergo experience-dependent refinement of connectivity and stimulus selectivity, and tadpoles from stages 48, and 49 begin to demonstrate a more refined connectivity. This

refinement is evident in an increased number of synapses (Pratt and Aizenman, 2007), a more compact temporal distribution of recurrent activity with shorter latency (Pratt et al., 2008), smaller receptive field (RF) sizes, and a concomitant increase in visual acuity (Dong et al., 2009).

Whole-Brain Preparation

The whole-brain preparation is as follows, after Wu et al. (1996): animals were first anesthetized in 0.01% tricaine methane sulphonate (MS-222) in 10% Steinberg's, the dorsal surface of skin was then be opened to expose brain, the dorsal midline was cut at all levels from base of spinal cord through the olfactory bulbs, and the brain dissected out. The preparation was transferred to a recording chamber with room temperature HEPES-buffered extracellular saline (containing: 115mM NaCl, 4mM KCl, 3mM $CaCl_2$, 3mM $MgCl_2$, 5mM HEPES, and 10mM glucose; pH 7.2, 255mOsm) and positioned on top of a block of Sylgard, with the exposed walls of the ventricle facing upwards. Shortened insect pins were then be inserted through the caudal extent of hindbrain and through one or both olfactory bulbs. For stimulation of retinal ganglion cell axons, a bipolar stimulating electrode consisting of two adjacent 25-µm platinum leads (CE2C75; FHC, Bowdoin, ME) was placed at the optic chiasm (OC), and for stimulation of mechanosensory projections, a second bipolar stimulating electrode was placed in the rostral hindbrain (HB) contralateral to the recording site (see **Figure 5**). Individual neurons in the optic tectum were visualized through a light microscope with a 60× water-

immersion objective, in combination with a infrared CCD camera. To achieve access to the tectal cells at the recording site I used the jagged tip of a broken glass micropipette to lift away the periventricular membrane, with the aid of a micromanipulator. These recording sites were selected consistently from within in the middle third of the optic tectum's rostral-caudal dimension, to avoid introducing variability in the maturational state of neurons studied at a given stage of tadpole development, given that the tectal circuit matures along a rostral-to-caudal gradient in individual animals (Pratt et al., 2008; Wu et al., 1996).

Electrophysiology

Glass micropipettes were pulled for tip resistances of 8–15 MΩ. For whole-cell recording mircopipettes were filled with filtered Cs^+-methane sulfonate/TEA intracellular saline (containing: 80mM Cs^+-methane sulfonate, 20mM TEA, 5mM $MgCl_2$, 20mM HEPES, 10mM EGTA, 2mM ATP, and 0.3mM GTP; pH 7.2, 255mOsm), and for loose cell-attached (LCA) recording of action potentials, the same micropipettes were filled with filtered extracellular saline. In experiments where blocking $GABA_A$-receptor mediated inhibition was required, 0.1mM picrotoxin was added to the extracellular solution. Electrophysiological signals were detected with an Axopatch 200B amplifier, digitized at 10kHz by a Digidata 1322A analog-to-digital converter, and formatted for recording by pClamp 9 acquisition software. Leak subtraction was performed on-line, in real-time by the acquisition software. In our recording conditions the junction potential is predicted to

be 12mV, but was uncorrected in the recorded traces. To detect changes in access resistance over the course of a recording, a 5mV depolarizing square wave was applied at the start of each trace. In all experiments, only cells demonstrating responses to both optic chiasm and hindbrain stimulation were chosen for recording.

Stimulus Properties

Electrical stimulation was initiated automatically by the acquisition software. At pre-specified time points, ISO-Flex stimulus isolators (A.M.P.I., Jerusalem, Israel) were activated for 0.2msec by an ON-OFF command signal from the digitizer. The output of each stimulus isolator (one for each stimulus electrode) was manually set, based on the responsiveness and dynamic range of each cell, to deliver between 10μA and 800μA across the poles of it's bipolar electrode, for the duration of the command signal. The criteria for setting the stimulation strength are specified below.

Experimental Design: Varying Inter-Stimulus Interval

In mammalian superior colliculus the inter-stimulus interval (ISI) between two cross-modality inputs is one factor that determines the direction and magnitude of the integrative response (Meredith et al., 1987). To determine the best ISI or range of ISI's for driving the inputs (synaptic conductances) and outputs (action potentials) of *Xenopus*

tectal neurons, I systematically varied both the interval between electrical stimuli. For cross-modal pairs, stimuli were delivered to the optic chiasm and hindbrain in the order of OC-then-HB as well as HB-then-OC. In each case, the time interval between stimulus presentations ranged between 0ms to 1000ms, in 100ms increments; the ISI began at 1000ms and decreased to 0ms. Uni-modal pairs of OC stimuli and HB stimuli were presented in the same way, but without the 0ms interval — because only one bipolar stimulating electrode was used for each sensory pathway, a simultaneous presentation of two inputs to a single pathway was not possible.

For experiments assessing multisensory integration, the strength of each stimulus was calibrated as follows: in loose cell-attached recordings of action potentials, the stimulus strength was set such that a single pulse would evoke between 0 and 2 action potentials, on average, and in whole-cell recordings, the stimulation to each pathway was set to evoke the half-maximal monosynaptic conductance, on average.

Experimental Design: Cross-Modal Rundown of Recurrent Activity

Previous experiments in the laboratory have shown that recurrent excitation evoked by stimulation of RGC axons runs down over the course of successive stimulus presentations at 1 Hz, with excitatory currents isolated by 0.1mM picrotoxin in the external solution and membrane voltage clamped at –60mV in whole-cell mode (Pratt et al., 2008). The present set of experiments will assess the degree to which successive presentations to one

stimulus pathway effect recurrent activity evoked by it's cross-modal counterpart. Specifically, this protocol will first run down the recurrent excitation driven by one sensory pathway, by applying a stimulus five times at 1 Hz, and then at the next 1 Hz period (i.e., 1 second later) will apply a test stimulus to the second, cross-modal sensory pathway. Currents were integrated over two windows: 0–20ms to isolate monosynaptic responses, and 20–600ms to isolate polysynaptic recurrent responses. These values will compared to those obtained before cross-modal rundown, in the same cell and for the same pathway. For these experiments, stimulation strength was set at the level which evoked the maximal response.

Recording Excitatory and Inhibitory Synaptic Conductances Evoked by Paired Stimuli

Experiments to examine the temporal characteristics of excitatory and inhibitory synaptic conductances will utilize the intracellular, whole-cell patch-clamp technique. The general methodology for electrophysiological recording appears in detail above. In these experiments, voltage-clamp mode was used to isolate synaptic conductances mediated by excitatory neurotransmitter receptors and those mediated by inhibitory neurotransmitter receptors. By using the voltage-clamp to hold the cell's membrane potential at the reversal potential of a given synaptic current, it is possible to eliminate the driving force on the ions mediating that current and thus "zero" the amplitude of that particular type of synaptic event. Previous work in the laboratory's tectal preparation has shown that when

$GABA_A$-receptor-mediated currents are blocked with picrotoxin, the reversal potential of excitatory AMPA and NMDA receptor-mediated currents is +5mV, and when AMPA and NMDA receptor-mediated currents are blocked by NBQX and APV, respectively, the reversal potential of synaptic currents mediated by inhibitory $GABA_A$ receptors is –45mV (Bell et al., 2011). Thus, by holding the membrane potential at –45mV, I was able to "zero" the inhibitory synaptic events and record only excitatory synaptic events, and by holding the membrane potential at +5mV I was able to accomplish the inverse, "zero-ing" the excitatory synaptic events and recording only the inhibitory synaptic events.

It is essential to note that the absolute magnitudes of the excitatory and inhibitory events recorded with this method do not reflect the physiological currents mediated by their respective ionotropic receptors. The amplitudes of receptor-mediated currents are dependent on the relative concentration of ions on either side of the cell membrane — as this relationship determines the driving force that acts on each type of ion as it passes from one side of the membrane to the other — and thus the disruption of ionic concentrations during the course of an experimental preparation means that the absolute magnitudes of the currents recorded no longer reflect the native, physiological condition. Nevertheless, because the excitatory and inhibitory currents recorded in these experiments were both be measured at holding potentials 50mV away from their respective potentials, the driving force for each will be the same. This shared physical constant leaves synaptic conductance as the variable that determines the relative magnitudes of excitatory and inhibitory events.

Recording Action Potential Responses to Multisensory Stimuli: Loose Cell-Attached Recordings

The loose-cell attached mode enabled the recording of action potentials without breaking through the cell membrane and without electrical access, and is defined as seal resistances in the 40–200MΩ range. The pipette tip was dirtied prior to cell contact to prevent formation of a tight seal. Action potentials were detected off-line by importing the digitized traces into the AxoGraphX analysis environment and by using an amplitude threshold to identify events and determine post-stimulus onset times.

Data Analysis

All analyses were performed offline, using AxoGraphX software and the MATLAB programming environment. Prism software (GraphPad) was used for curve fitting and statistical tests.

Determination of the predicted neuronal response to paired stimuli, both uni-modal and cross-modal, was performed in the manner of Stanford and colleagues (2005). For each cell, responses after each trial of the individual (baseline) stimulus presentations were collected and, as appropriate for the type of paired responses being predicted, all possible uni-modal trial-by-trial combinations or all possible cross-modal trial-by-trial

combinations were determined. For each such combination of trials, the sum of spike counts recorded in each was calculated. Thus, with 33 single-stimulus trials delivered through each modality, in each cell, $33 \times 33 = 1089$ possible sums exist. In the actual experiments, however, at each ISI 4 trials of paired stimuli were presented, and the mean response over these trials was determined. To mirror these procedures in the predictive analysis, for each cell and for each type of stimulus pair, 4 of the possible sums were randomly selected (with replacement) and their mean taken. This randomly sampling and averaging was repeated 10,000 times for each pair type, to create an approximately normal distribution of predicted mean sums. In each cell, *Z*-score comparisons of the actual mean response, at each ISI of each pair type, were then performed against this distribution.

RESULTS

NEURONAL OUTPUT — ACTION POTENTIAL COUNT, AND TIMING

Previous descriptions of cross-modal integration, evidenced in either the number or temporal distribution of action potentials, reveal that the inter-stimulus interval (ISI) between two cross-modal inputs is a key factor that determines the direction and magnitude of the integrative response (Meredith et al., 1987). To assess how ISI influences the ability of *Xenopus* tectal neurons to integrate both cross-modal and uni-modal stimulus pairs, I systematically varied the time interval between the two electrical stimuli, whether delivered to different sensory pathways (cross-modal pairs) or to the same sensory pathway (uni-modal pairs). **Figure 6** shows examples of raw data at different ISI's (**a**) and extracted spike times across the range of ISI's, in both developmental groups (**b**).

a. Action Potentials Recorded in Loose Cell-Attached Configuration

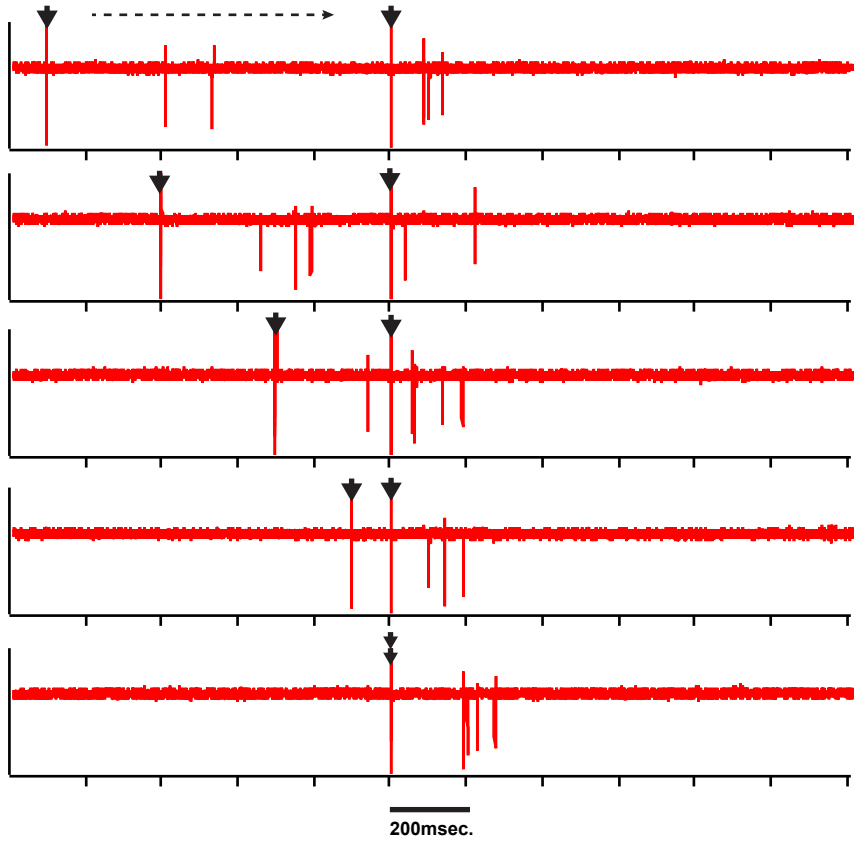

b. Cell Output Varies Over Development, and is Sensitive to ISI

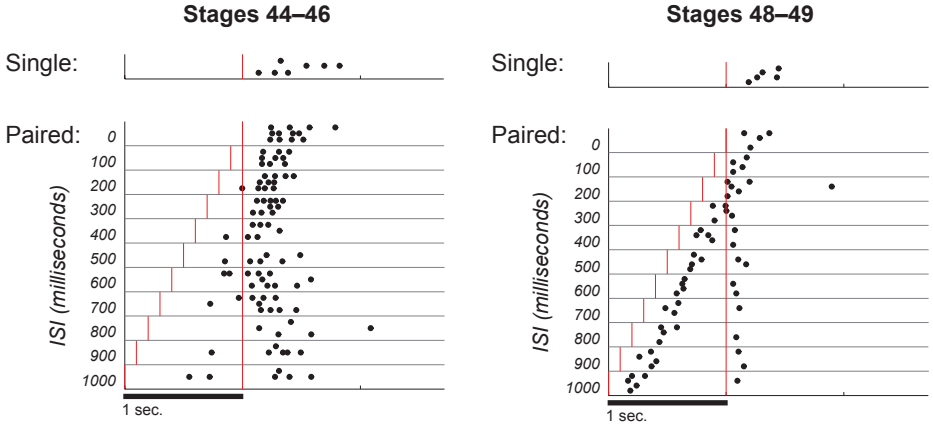

Figure 6: Action potentials recorded in loose cell-attached configuration.
a. Raw traces of capacitive currents generated during paired stimulation (four sweeps are represented in each trace). Arrows indicate times of stimulus presentation. **b.** Example raster plots from two cells, one from a stages 44–46 animal (*left*) and one from a stages 48–49 animal (*right*).

Temporal Tuning of Cross-Modal and Uni-Modal Integration

In **Figure 7** this dependence on inter-stimulus interval (ISI) is revealed in the population means of Multi-Sensory Index (MSI; see **Equation 1**) values from both developmental

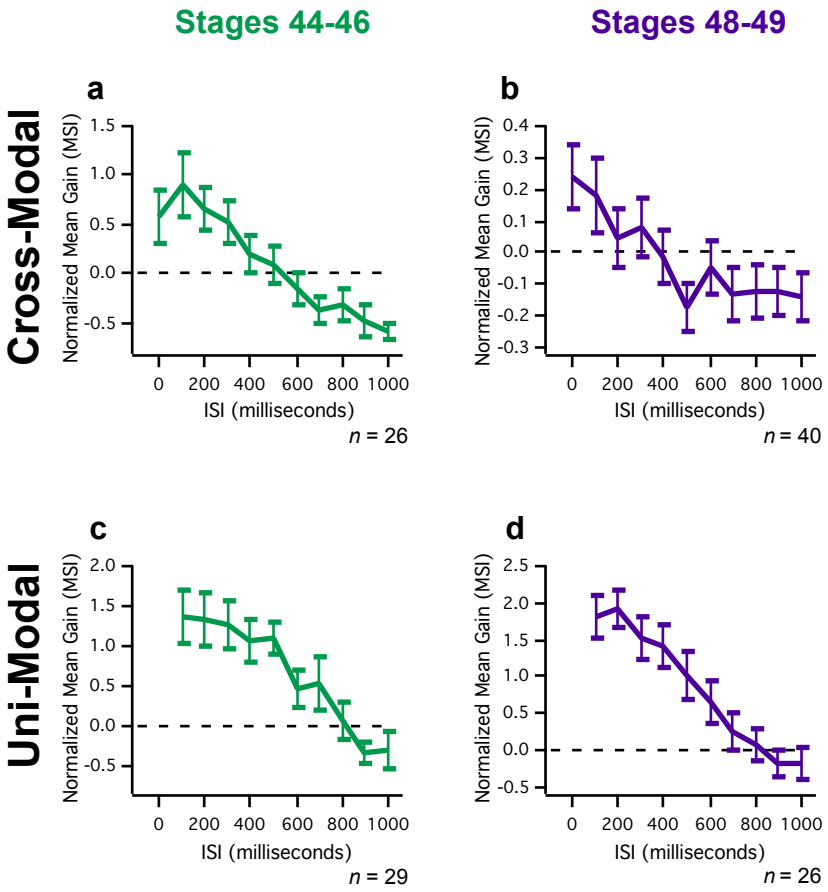

Figure 7: Cross-modal and uni-modal integration occur in both developmental groups.
In a given cell, data are averaged over trials at each ISI, to determine the MSI ratio. Plotted here are the population means of these trial-averaged MSI ratios, at the ISI's tested in each condition. Error bars show +/– S.E.M.

groups (stages 44–46 and stages 48–49), and after cross-modal as well as uni-modal stimuli. Some phenomena are evident in all experimental data: Greater, more-positive MSI values are produced by shorter inter-stimulus intervals, whereas negative MSI values —indicating a suppression of responses due to paired stimuli — are produced exclusively by longer inter-stimulus intervals, of up to 1000ms. The fact that a leading

stimulus will influence responses to a subsequent, reference stimulus even at a separation of 1 second shows that the refractory period for these single-cell responses is longer than that interval. That is, more than 1 second is required for the underlying mechanisms to return to their baseline state, be they related to cellular excitability, short-term synaptic plasticity, circuit dynamics, or some combination thereof. While no specific experiments were designed to assess the refractory/recovery period after a single stimulus, data collected on feed-forward circuit dynamics can provide clues as to how the lingering effects of a leading stimulus can effect responses to a second stimulus, presented some time later.

One notable difference between data shown in **Figure 7** is that after cross-modal pairs in the older, stages 48–49 developmental group, specifically, the population mean MSI's appear lower relative to those from the other data sets (see **Fig. 7b**, *y*-axis). But precisely because the values at each ISI represent a population mean, calculated across cells, there remains the possibility that at stages 48–49 individual cells are strongly selective for one or only a few ISI's, but that these neurons vary widely with respect to the ISI at which the peak of this selectivity (i.e., the 'tuning curve') is centered.

To investigate this possibility, that tectal neurons become sensitive to different cross-modal ISI's over development, I noted the ISI's at which their maximal MSI values were generated. Against the right axis of the graphs in **Figure 8**, these maximum MSI values are plotted at the ISI's which evoked them. Against the right axis of each graph, a histogram shows the number of peak values found to occur at each of the ISI's tested.

Among the four charts, it is evident that after cross-modal pairs in the stages 48–49 developmental group, specifically (see **Fig. 8b**), maximum MSI responses occur at a relatively broad range of ISI's, across cells, in contrast to the younger tadpoles, where maximal MSI mostly occurs at short ISIs. Thus these data are consistent with the possibility that 'tuning' to cross-modal ISI's does indeed occur at stages 48–49, but that in different cells the peak selectivity of these responses is found at different ISI's.

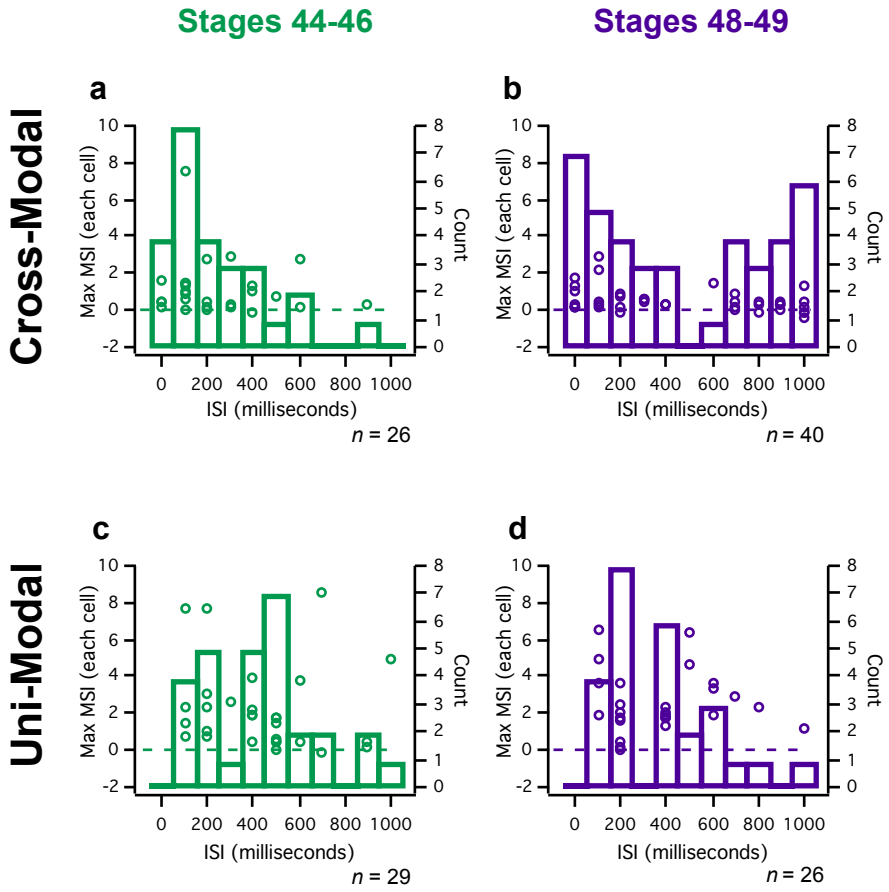

Figure 8: The distribution of inter-stimulus intervals (ISI's) that evoke the maximal response differs between developmental groups and stimulus types.
For each cell, the maximum trial-averaged MSI ratio, over all ISI's tested (*left axis*), is plotted at the ISI which elicits it. Histogram bars show the total number of max MSI ratios at each ISI (*right axis*).

Interestingly, the qualitative appearance of a bimodal distribution of peak responses to cross-modal stimuli at stages 48–49 (**Fig. 8b**), does suggest two distinct physiological classes of tectal neurons, one integrating cross-modal stimuli at short latencies, and

another that prefers longer latencies. With the tools employed here, however, it is not possible to identify particular cell types: although both excitatory and inhibitory neurons are present in *Xenopus* tectum at these developmental stages (Miraucourt et al., 2012) they cannot be readily distinguished by morphology or electrophysiological characteristics. A unique physiological cell type has recently been discovered more superficially in the tadpole tectum (Pratt and Aizenman, 2009), however it is not likely to have been encountered in these recordings from the deep cell body layer.

One additional confound in the preceding analysis is that data for cross-modal stimuli, as well as for uni-modal stimuli, are derived from two distinct patterns of stimulation. For

		Stages 44–46			**Stages 48–49**		
		Mean MSI *± S.E.M.*	*P-value*	*Summary*	***Mean MSI*** *± S.E.M.*	*P-value*	*Summary*
Cross-Modal	***VH***	0.98 ± 0.57 (*n* = 13)	*P* = 0.605	n.s.	0.50 ± 0.17 (*n* = 20)	*P* = 0.628	n.s.
	HV	1.31 ± 0.26 (*n* = 13)			0.60 ± 0.12 (*n* = 20)		
Uni-Modal	***HH***	2.54 ± 0.74 (*n* = 13)	*P* = 0.554	n.s.	2.58 ± 0.47 (*n* = 13)	*P* = 0.973	n.s.
	VV	2.01 ± 0.53 (*n* = 16)			2.56 ± 0.46 (*n* = 13)		
		Median ISI *(msec.)*	*IQR*	*P-value*	*Summary*	***Median ISI*** *(msec.)*	*IQR*	*P-value*	*Summary*
Cross-Modal	***VH***	200 (*n* = 13)	250	*P* = 0.964	n.s.	350 (*n* = 20)	675	*P* = 0731	n.s.
	HV	100 (*n* = 13)	350			500 (*n* = 20)	875		
Uni-Modal	***HH***	400 (*n* = 13)	300	*P* = 0.785	n.s.	200 (*n* = 13)	250	*P* = 0.040	*
	VV	450 (*n* = 16)	400			400 (*n* = 13)	300		

Table 1: Comparisons between presentation order for cross-modal stimuli and modality type for uni-modal pairs do not reveal consistent differences in MSI ratios, in either developmental group. *Top*: Within both developmental groups, maximum MSI ratios are compared between the two cross-modal sequences and between the two types of uni-modal pair. n.s.: not significant (unpaired *t*-test). *Bottom*: The identity of the ISI's responsible for the maximal response is compared between the two cross-modal sequences and between the two uni-modal pairs, within each developmental group. * : $P < 0.05$ (Mann-Whitney rank-sum test); n.s.: not significant (Mann-Whitney rank-sum test).

uni-modal stimulus pairs, specifically, all data have been considered equivalent, regardless of whether the stimuli were delivered to the visual pathway (OC→OC) or to the mechanosensory, hindbrain pathway (HB→HB). Similarly, all data for cross-modal stimulus pairs have been considered equivalent and were grouped together, regardless of whether two stimuli were presented in the OC→HB sequence or the HB→OC sequence.

If either of these assumptions of equivalence prove incorrect, however, this analysis would miss the differential effectiveness of these stimuli and overgeneralize the relevance of the findings. **Table 1** shows the results of statistical tests for differences between the two cross-modal stimuli, and between the two uni-modal stimuli, at each developmental stage. As indicated, there are no consistent differences between the uni-modal target pathways or the cross-modal stimulus sequences with respect to either peak MSI values or the particular inter-stimulus interval at which this peak enhancement is found.

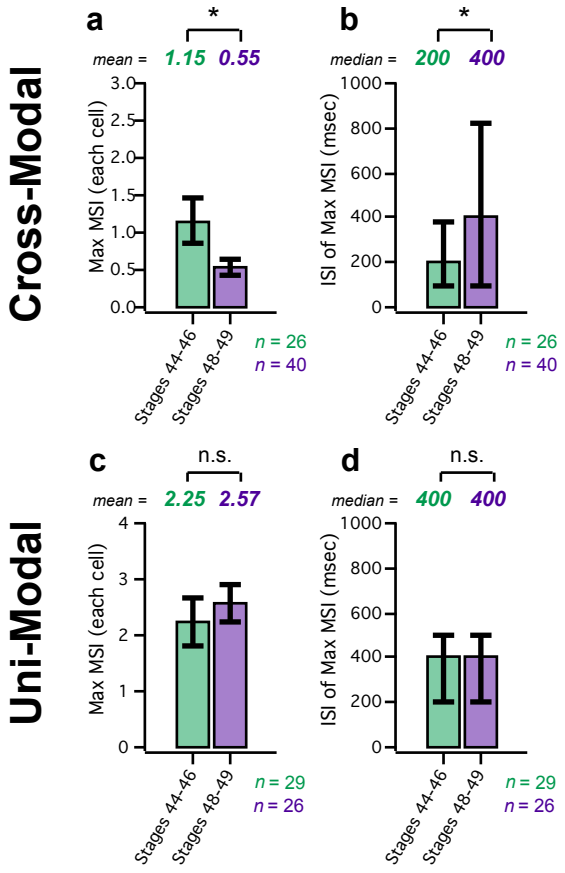

Figure 9: Differences between developmental groups and stimulus types are evident in individual cells' maximum MSI ratios.
a, **c**: Maximum MSI ratios are compared across developmental stages. Error bars indicate +/– S.E.M. ∗ : $P < 0.05$ (unpaired *t*-test); n.s.: not significant (unpaired *t*-test). **b**, **d**: The identity of the ISI's responsible for the maximal response (and thus the maximum MSI ratio) in each developmental group are compared. Error bars show interquartile range. * : $P < 0.05$ (Mann-Whitney rank-sum test); n.s.: not significant (Mann-Whitney rank-sum test).

Having established the operational equivalence of the stimulus sub-types used to generate uni-modal and cross-modal data, I conducted statistical tests on the uni-modal and cross-modal data blocs to assess developmental changes in peak MSI values, as well as in the

particular ISI's that generate them. As seen in **Figure 9**, on the left (**Fig. 9a**, **c**) are shown comparisons between the population means of peak (maximum) MSI values from each cell, for the two developmental groups, and on the right (**Fig. 9b**, **d**) are comparisons between the population medians for the particular ISI (in milliseconds) responsible for each cell's peak MSI value, again for the two developmental groups. **Figure 9** shows that only for cross-modal stimuli are there significant developmental changes in the maximum enhancement index (**Fig. 9a**) and temporal selectivity (**Fig. 9b**) of integrative responses. Specifically, at later developmental stages the maximum MSI indices are lower, confirming the suggestion of a lower range for all MSI indices in **Figure 7b**, and are produced by relatively longer inter-stimulus intervals.

Both of these results were unexpected, given current knowledge of the development of uni-modal and cross-modal sensitivity in vertebrate OT/SC. The first finding, that maximal MSI values after cross-modal stimuli specifically tend to decrease over development, contradicts developmental findings in mammalian SC of an increase in enhancement after cross-modal stimuli (Wallace and Stein, 1997). The origin of this discrepancy will be explored in greater detail below, in the context of data on the contribution of synaptic inhibition to integrative responses of *Xenopus* tectal neurons. The second observation, that cells' maximal responses tend to occur at relatively longer inter-stimulus intervals in the later developmental group, was unexpected in light of previous findings in vertebrate OT/SC that single neurons become sensitive to finer temporal frequencies (i.e., shorter inter-stimulus intervals) as the animal matures (Wallace and Stein, 1997). Furthermore, as seen in the relatively broad inter-quartile

range for cross-modal data in **Figure 9b**, cells become selective for a more diverse set of ISI's in later stage tadpoles. What these results do not address, however, is the breadth of temporal selectivity in each cell, independent of the inter-stimulus interval at which peak responsiveness is found. That is, the degree to which the neuron's responses at that most-effective ISI are differentiated from it's responses to the other ISI's tested.

Independent of a cell's responses to its maximally-effective (i.e., "preferred") stimulus, described above, another measure of developmental refinement is the degree of its selectivity for that particular stimulus combination. Because responses to paired stimuli peak at different ISI's in different cells, to study the tuning of ISI selectivity across cells it is necessary to align their MSI-versus-ISI distributions at the peak MSI value in each. This alignment of all 'ISI tuning curves' at their peak (maximal) MSI values should provide a common reference point for comparing the shapes of the entire curve, across cells. For cross-modal stimuli (**Fig. 10a**), responses after HB→OC pairs were arrayed in order of decreasing ISI, and positioned to the left of the central reference point on the bottom axis, and responses after OC→HB pairs were arrayed in order of increasing ISI, and positioned to the right of the central reference point. For each cell, then, MSI values for all intervals were shifted by the same amount, such that the peak value sits at the central reference point on the bottom axis. For uni-modal stimuli (**Fig. 10b**), responses after both OC→OC and HB→HB pairs were arrayed in order of increasing ISI and, as was done for cross-modal pairs, peak MSI values were aligned to the common reference point. For cross-modal stimuli in **Figure 10a**, therefore, the difference in peak size between developmental groups represents the same effect as shown in the direct

comparison between maximum cross-modal MSI values in **Figure 9a**. And, by controlling for differences in the specific ISI's at which peak MSI selectivity occurs, this

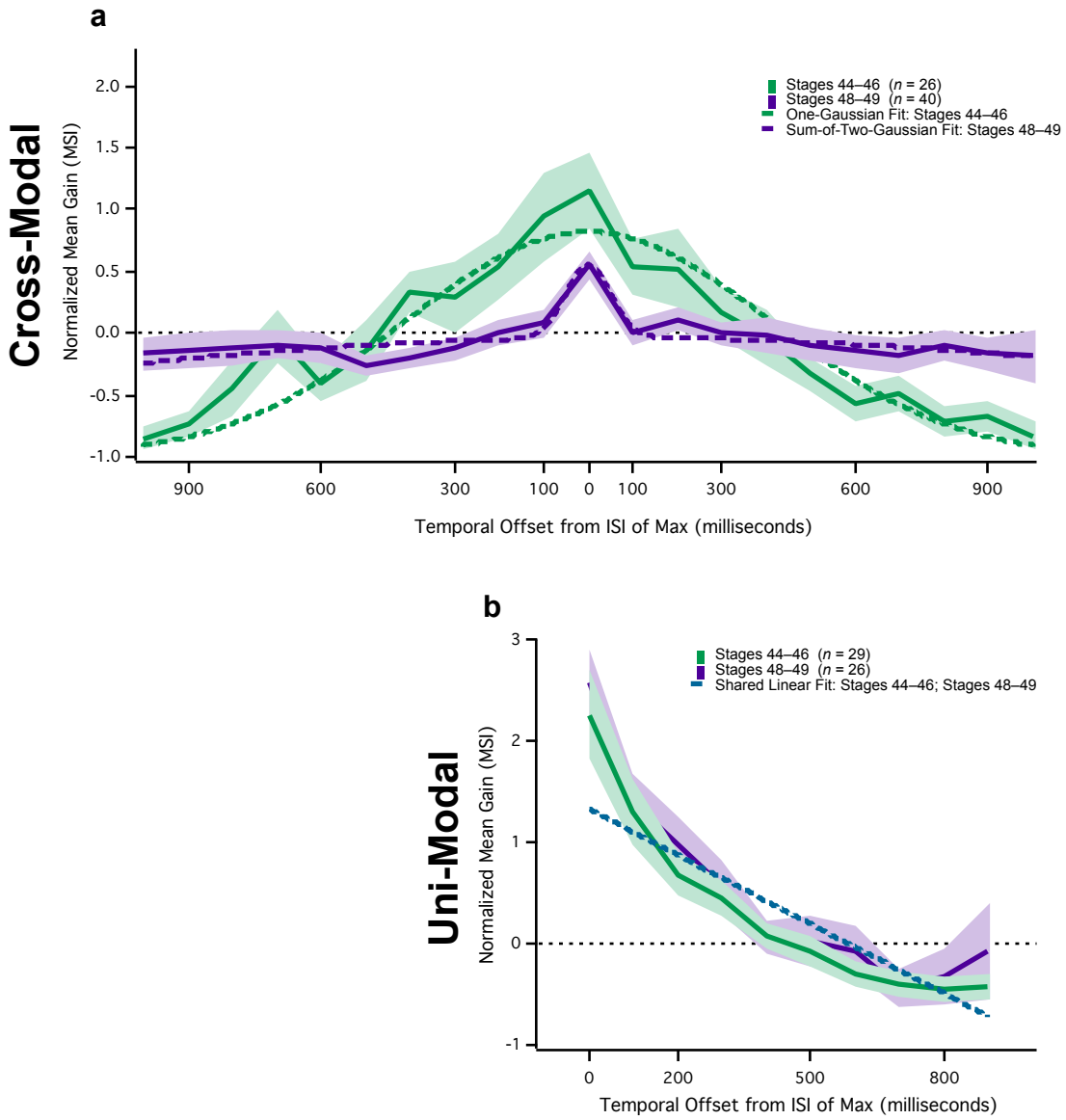

Figure 10: Population tuning to cross-modal ISI's changes significantly over development, but to uni-modal ISI's remains the same.
a: MSI-versus-ISI curves from HB-then-OC pairs were aligned at their peak values, and then averaged across cells as indicated in the text. Solid lines connect the population means. Solid lines connect the population means. Shaded areas demarcate +/– S.E.M. Dashed lines show the separate curves that are best fit to the population data. See **Table 2** for curve fitting method and statistics. **b**: Each cell's MSI values, again averaged over trials for the range of ISI's, were shifted to center on the ISI of that cell's maximal MSI ratio, and these peak-aligned MSI's were averaged across cells. Solid lines connect the population average MSI ratio at peak and the ratios at ISI's longer than that of the peak. Shaded areas mark +/– S.E.M. A single blue dashed line represents the single linear fit which sufficiently describes data from both developmental groups. For statistical results of curve fitting, see **Table 2**.

plot of cross-modal responses reveals that peak values appear more highly differentiated from off-peak values in data from stages 48–49 than in data from stages 44–46; that is, each neuron's selectivity for a particular cross-modal ISI seems to become more refined over development. For peak-aligned MSI values after uni-modal stimuli in **Figure 10b**, on the other hand, there appears to be no developmental change in the differentiation of MSI values around the most-effective inter-stimulus interval for each cell. Thus, these data suggest a developmentally-regulated refinement of temporal selectivity, specifically for cross-modal stimulus pairs.

To confirm these results quantitatively, each data set was fit to a curve, and the resulting curves were compared statistically. The candidates for curves of best fit were selected empirically — that is, each represents a visual approximation of the distribution of data — and not because of theoretical assumptions tied to the shapes of, and equations for, the types of curves under consideration. For instance, at the top left of **Table 2** are two F-tests of distributions, to determine whether the cross-modal data from each developmental group are best fit by a Gaussian curve, or by a curve that represents the sum of two Gaussians. The results of these tests indicate that the peak-aligned MSI values from each group are best fit by a different type of curve. At top right of **Table 2**, a subsequent F-test — to determine whether pooled cross-modal data from both developmental groups are best fit by a single, common curve or two separate curves — supports the conclusion that aligned cross-modal data from stages 44–46 and stages 48–49 tadpoles come from separate populations. For uni-modal data from the two developmental groups, the bottom of **Table 2** shows the results of an F-test to determine

whether pooled, peak-aligned MSI values are best described by a common linear fit or two distinct linear fits. This test shows that a shared linear model best describes the uni-modal data from both groups, consistent with the minimal differences observable between their peak-aligned averages. These results confirm, statistically, the refinement of temporal selectivity for cross-modal, but not uni-modal, stimulus pairs during early *Xenopus* development.

CM	H_0:	Gaussian*		Single fit for all data	
	H_1:	Sum of Two Gaussians**		Separate fits, one per data set	
		Results	*Summary*	*Results*	*Summary*
	St. 44–46	F(3,281) = 1.976; $P < 0.0001$ ($n = 26$)	Gaussian	F(2,716) = 9.966; $P < 0.0001$	Separate fits
	St. 48–49	F(3,435) = 11.95; $P < 0.0001$ ($n = 40$)	Sum of Two		
UM	H_0:	Single linear fit for all data			
	H_1:	Separate linear fits, one per data set			
		Results	*Summary*		
	St. 44–46	F(2,544) = 1.394; $P = 0.249$ ($n = 45$)	Single fit		
	St. 48–49				

Table 2: Statistical comparisons between MSI-versus-ISI tuning curves, across developmental groups.
Top: Cross-modal data from both developmental groups. *Top Left*: Determination of best-fit curves for cross-modal data from each developmental group. Model constraints: *: Mean = 0, S.D. > 0; **: Mean of first Gaussian = 0, S.D. of first Gaussian > 0, S.D. of second Gaussian > 0. *Top Right*: Comparison between developmental groups confirms that total cross-modal data are best modeled by separate curve fits, one for each developmental group. *Bottom*: Uni-modal data from both developmental groups. Statistical comparison between developmental groups shows that a single linear fit best describes the data from both groups. *For all statistical tests*: H_0: null hypothesis; H_1: alternative hypothesis.

Inverse Effectiveness

Existing literature on multisensory integration in mammals has found that the principle of inverse effectiveness — segregating data by response magnitude, even without isolating the maximum — can further differentiate responses to cross-modal and uni-modal pairs. For instance, Alvarado and colleagues (2007b) in their report on *in vivo* data from cat SC, found that this phenomenon of inverse effectiveness describes the range of response magnitudes after cross-modal pairs better than the range of magnitudes generated by uni-

modal pairs. This difference was especially robust when responses to paired stimuli were greatest. For the present data, therefore, I examined how the relationship between the peak MSI value and the response to a single stimulus (delivered to whichever modality appears second in the respective pair) differs for cross-modal and uni-modal pairs. **Figure 11** contrasts how responses to uni-modal and cross-modal stimuli express this relationship, in each developmental group. Clearly, the phenomenon of inverse

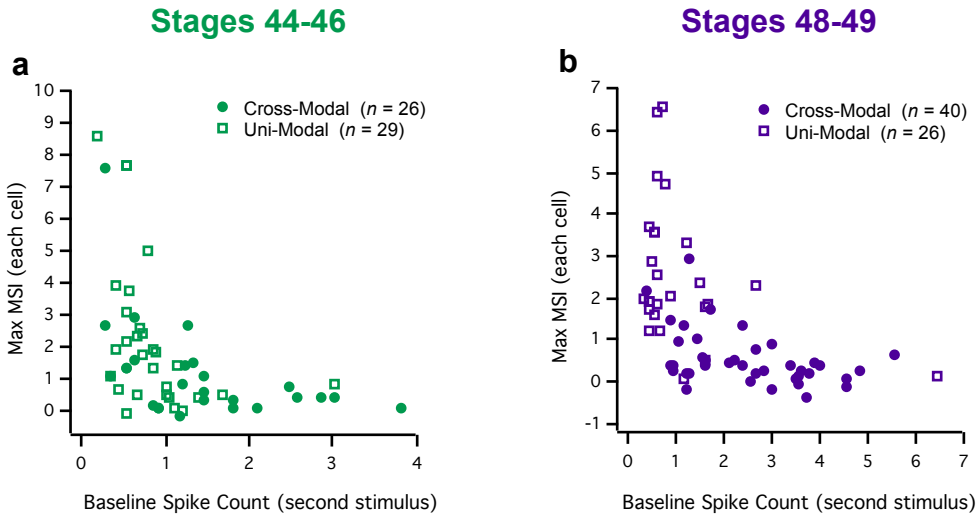

Figure 11: In each developmental group, maximum MSI ratios for both cross-modal and uni-modal stimuli demonstrate inverse effectiveness.
For both uni-modal and cross-modal data sets, and for each cell, the maximum, trial-averaged MSI value is plotted against the average number of action potentials recorded after the control stimulus, defined as a single pulse delivered to whichever modality is presented second in the corresponding stimulus pair.

effectiveness is evident in data from both developmental groups. These plots show that in neither developmental group, however, is there a clear difference between cross-modal and uni-modal data in its expression. This set of results was unexpected given the assumption of this principle's universality in mammalian literature. It may also serve to indicate that the MSI metric is not sufficient to describe all aspects of integrative phenomena.

Deviations from Linearity

Indeed, while the MSI metric reveals how the response to a given stimulus is changed by a preceding input, when the two are presented as a stimulus pair, it does not quantitatively address the manner in which the two inputs interact. The method of Stanford et al. (2005), however, compares the actual output of these processes to what is expected from a purely additive combination of responses to the each of the inputs, when presented individually (for details of how their predicted sum is determined, see *Methods*). In the present data, **Figure 12** shows that the actual raw responses to cross-modal and uni-modal pairs, at the maximal value per cell, differ in how the two component inputs are integrated relative to the response predicted by a linear sum. First, the raw relationship between the two values — actual and predicted — is compared between cross-modal and uni-modal stimulus pairs, in both developmental groups (**Fig. 12a**, **b**). At stages 48–49 especially, data points for cross-modal stimuli seem to cluster below the line of unity (predicted > actual) and data points for uni-modal stimuli seem lie mostly above the line of unity (predicted < actual). After statistical treatment of the predicted vs. actual relationship with cumulative frequency distributions (CFD's) for each pair type (**Fig. 12c**, **d**), it is shown that in both developmental groups — not just at stages 48–49 — uni-modal pairs and cross-modal pairs have different *Z*-score distributions, such that uni-modal pairs may be more likely to generate actual maximal responses that exceed the predicted linear sum (*stages 44–46*: Kolmogorov-Smirnov test, D = 0.5119, $P = 0.001$; *stages 48–49*: Kolmogorov-Smirnov test, D = 0.7096, $P < 0.001$). If all data within each developmental group are considered together, without regard to stimulus type,

then a simple visual comparison between these groups suggests that a greater proportion of cells at stages 48–49 show responses that match or exceed what is predicted by linear summation. This result would support the general hypothesis that the OT/SC becomes

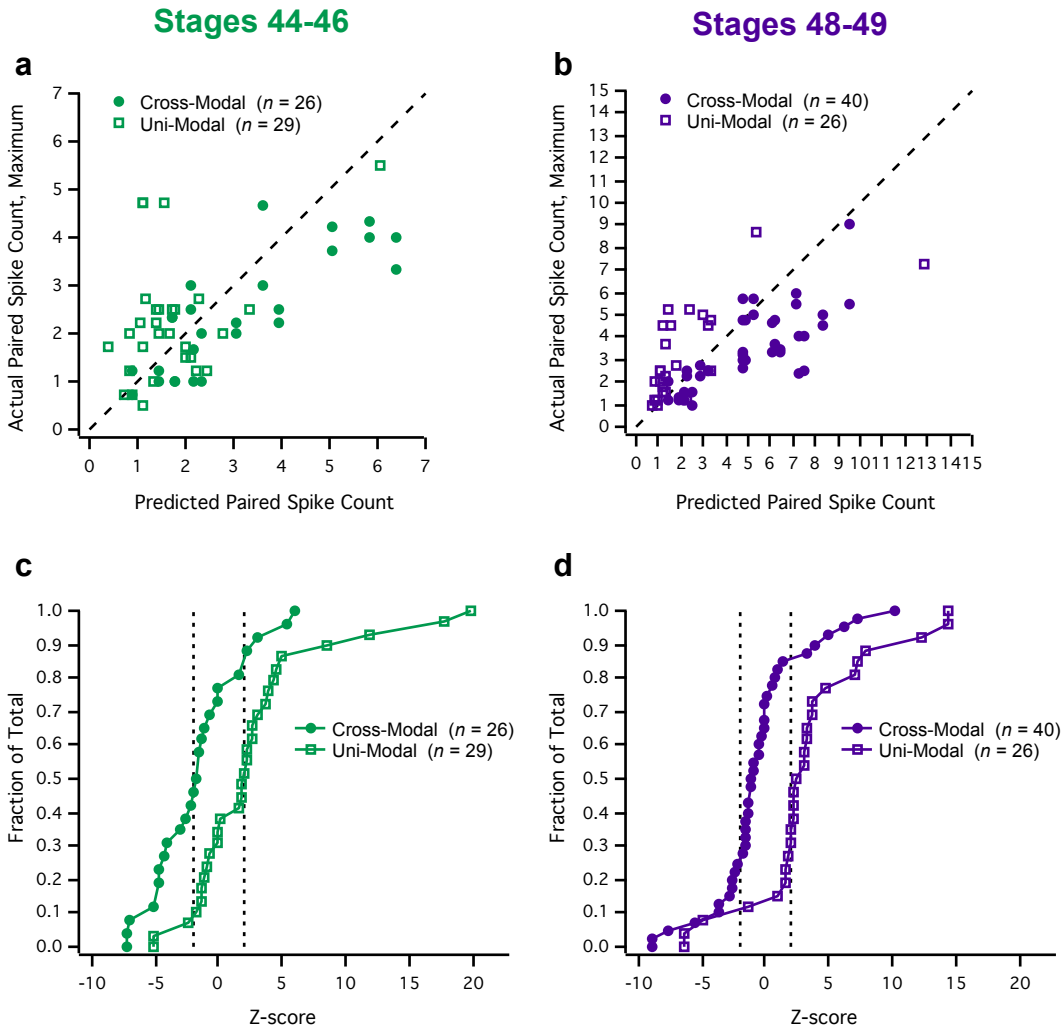

Figure 12: In both developmental groups, the underlying operations for cross-modal and uni-modal integration differ significantly.
a, **b**: For both uni-modal and cross-modal data sets, and for each cell, the maximum raw spike count after paired stimulation (averaged across trials) is plotted against the spike count predicted by random additive pairings between the responses recorded after the two respective control stimuli, that is, single pulses delivered to the each component of the stimulus pair. Dashed lines each represent the line of unity. **c**, **d**: For both uni-modal and cross-modal data sets, Cumulative Frequency Distributions of *Z*-score values are plotted for the comparison between predicted and actual number of action potentials recorded after paired stimulation, in each cell. Vertical dashed lines indicate $Z = +/-1.97$, the point at which actual responses are +/–2 S.D.'s away from the respective predicted response. For greater detail on generation of the predicted responses and calculation of *Z*-scores, see *Methods*. Kolmogorov-Smirnov tests of distributions confirm the apparent differences in both the stages 44–46 developmental group ($D = 0.5119$, $P = 0.001$) and the stages 48–49 developmental group ($D = 0.7096$, $P < 0.001$).

more sensitive to combinations of stimuli, as the animal matures. However, if uni-modal and cross-modal stimuli are considered separately, it is clear that in both developmental

groups uni-modal responses actually show more enhancement than cross-modal responses, relative to what is predicted by linear summation. Therefore, this unexpected outcome seems to reflect a relatively more inhibitory computation for cross-modal stimuli — relative to the processes which drive responses to uni-modal pairs — which is present to some degree at all developmental stages studied.

Role of Inhibition

The above data show that neuronal responses to cross-modal stimuli change over development by exhibiting decreased maximal MSI (**Fig. 9**) and narrower selectivity to inter-stimulus interval (**Fig. 10**). In contrast, uni-modal stimulus pairs do not show such changes. These observations led me to investigate whether mechanisms known to change over a similar time course, and influence other aspects of *X. laevis* neural circuit development, might be partially responsible. $GABA_A$-receptor expression, for example, is known to increase in the OT over tadpole development (Miraucourt et al., 2012), and $GABA_A$-receptor mediated inhibition has been shown to affect the refinement of tectal neuron dendrites (Shen et al., 2009), visual receptive field structure and correlated neuronal output (Richards et al., 2010), as well as stimulus-guided behavior (Shen et al., 2011). Thus, I tested the hypothesis that functional changes observed in pair-driven enhancement over development are linked to the maturation of inhibitory circuits within the tectum. To do so, I used 0.1mM picrotoxin to block $GABA_A$-receptors and examined whether the differential sensitivity of action potential number to uni-modal and cross-

modal stimuli, particular to the stages 48–49 developmental group, would change in the absence of synaptic inhibition.

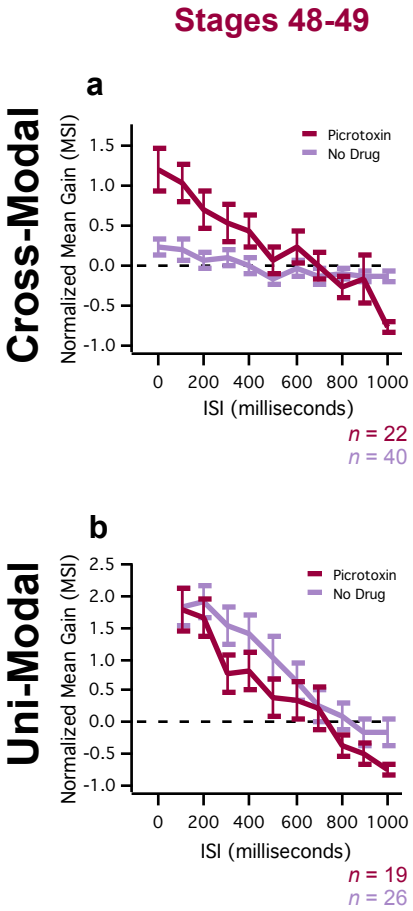

Figure 13: Across cells, blocking inhibition has different qualitative effects on cross-modal and uni-modal integration.
In a cell, data are averaged over trials at each ISI, to determine the MSI ratio as ISI varies. Plotted here are the population means of these trial-averaged MSI ratios, at the ISI's tested in each condition. To aid in comparison, data from the no drug condition are plotted on the same set of axes. Error bars show +/– S.E.M.

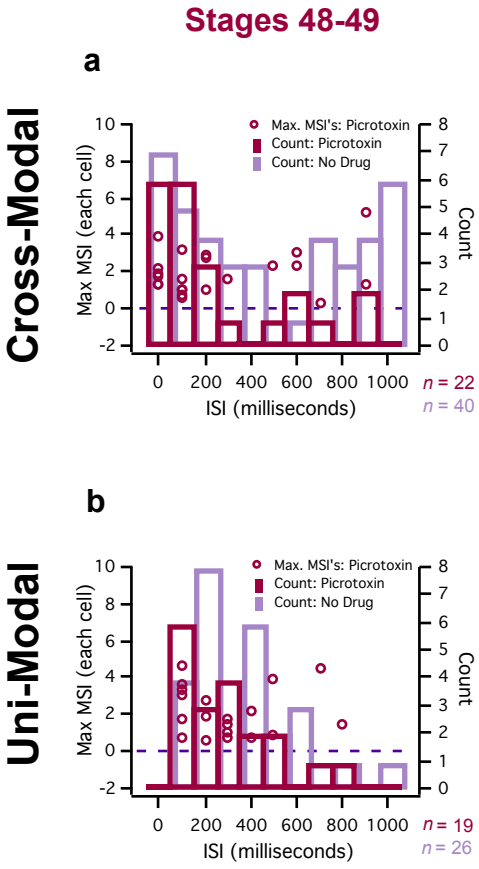

Figure 14: Blocking inhibition alters the distribution of inter-stimulus intervals which produce maximal cell output.
For each cell, the maximum trial-averaged MSI ratio, over all ISI's tested (*left axis*), is plotted at the ISI which elicits it. Histogram bars show the total number of max MSI ratios at each ISI (*right axis*). Shown also are histogram bars for the No Drug condition, for comparison.

As seen in **Figure 13**, when population means of MSI values are taken at each ISI, blocking inhibition in the stages 48–49 developmental group seems to specifically affect responses after cross-modal stimuli — it increases the range of MSI values and shifts them higher, especially at shorter ISI's (**Fig. 13a**). No such changes are evident after uni-

modal stimuli (**Fig. 13b**). The possibility of a similar stimulus-specific effect of inhibitory blockade on ISI preference was explored by isolating the peak (maximum) MSI value from each cell and plotting it at the specific ISI which evoked it, as in **Figure 8**, above. In **Figure 14**, data collected with inhibition blocked in the stages 48–49 developmental group reveal a shift in the distribution of peak MSI values towards shorter ISI's, versus experiments performed in this group with inhibition intact, but only for responses after cross-modal stimuli (**Fig. 14a**). This result again demonstrates the

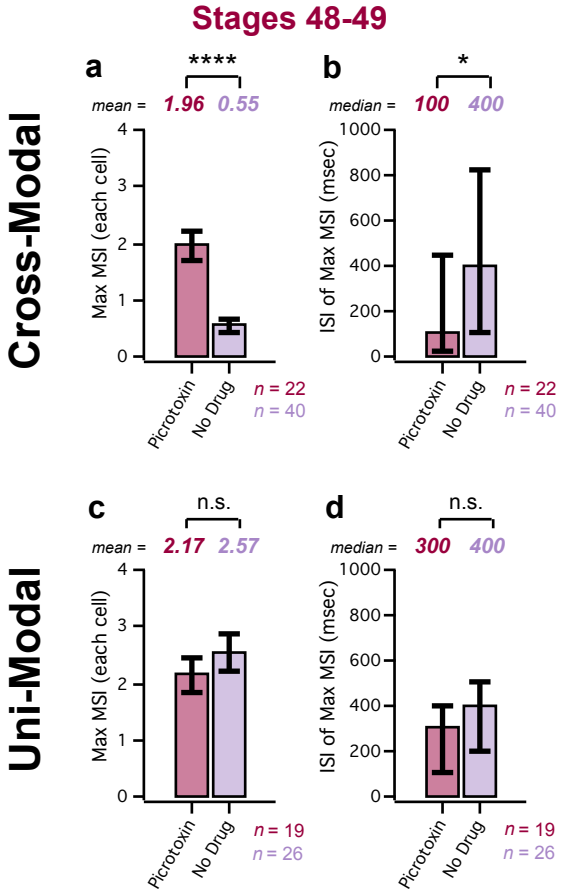

Figure 15: Blocking inhibition alters maximum MSI values and their dependence on inter-stimulus interval for cross-modal, but not uni-modal, stimulation.
a, **c**: Maximum MSI ratios are compared across between Picrotoxin and No Drug conditions. **** : $P < 0.0001$ (unpaired *t*-test), n.s.: not significant (unpaired *t*-test). **b**, **d**: The identity of the ISI's which evoke each cell's maximal response are compared between No Drug and Picrotoxin conditions. * : $P < 0.05$ (Mann-Whitney rank-sum test); n.s.: not significant (Mann-Whitney rank-sum test).

selective effect of picrotoxin application on cross-modal responsiveness. To confirm these patterns statistically I compared the No Drug and Picrotoxin conditions with respect to the population means of these peak MSI values, and also with respect to the population

medians for the ISI which evokes them, on a cell-by-cell basis for both uni-modal and cross-modal stimulus pairs. **Figure 15** confirms that the block of synaptic inhibition leads to both a significant increase in peak MSI after cross-modal stimulation (**Fig. 15a**) and a significant decrease in most-effective ISI (in milliseconds) between the cross-modal stimuli (**Fig. 15b**). This pharmacological manipulation produced no such changes for responses to uni-modal stimuli, however (**Fig. 15c**, **d**). Additionally, to test for the possibility that this treatment could expose previously undetected differences between processes activated by the two types of uni-modal stimuli, or between those activated by the two sequences of cross-modal stimuli, I compared data from these stimulus subtypes in the same manner as in **Table 1**, above. As shown here in **Table 3**, these

		Stages 48–49; picrotoxin				**Stages 48–49; no drug**			
		Mean MSI *± S.E.M.*		*P-value*	*Summary*	***Mean MSI*** *± S.E.M.*		*P-value*	*Summary*
Cross-Modal	***VH***	1.52 ± 0.26 (*n* = 11)		*P* = 0.075	n.s.	0.50 ± 0.17 (*n* = 20)		*P* = 0.628	n.s.
	HV	2.41 ± 0.40 (*n* = 11)				0.60 ± 0.12 (*n* = 20)			
Uni-Modal	***HH***	1.77 ± 0.40 (*n* = 10)		*P* = 0.171	n.s.	2.58 ± 0.47 (*n* = 13)		*P* = 0.973	n.s.
	VV	2.62 ± 0.44 (*n* = 9)				2.56 ± 0.46 (*n* = 13)			
		Median ISI *(msec.)*	*IQR*	*P-value*	*Summary*	***Median ISI*** *(msec.)*	*IQR*	*P-value*	*Summary*
Cross-Modal	***VH***	100 (*n* = 11)	600	*P* = 0.622	n.s.	350 (*n* = 20)	675	*P* = 0731	n.s.
	HV	100 (*n* = 11)	200			500 (*n* = 20)	875		
Uni-Modal	***HH***	250 (*n* = 10)	300	*P* = 0.706	n.s.	200 (*n* = 13)	250	*P* = 0.040	*
	VV	300 (*n* = 9)	500			400 (*n* = 13)	300		

Table 3: When synaptic inhibition is blocked, no significant differences are found between the MSI ratios calculated from different presentation sequences, for cross-modal stimuli, or from different modalities, for uni-modal stimulus pairs.
Top Left: With inhibition blocked, maximum MSI ratios are compared between the two cross-modal sequences and between the two types of uni-modal pair. *Top Right*: Data from the same developmental stage, but with intact synaptic inhibition, are shown for comparison. *Bottom Left*: The identity of the ISI's responsible for the maximal response is compared between the two cross-modal sequences and between the two uni-modal pairs, with inhibition blocked. *Bottom Right*: Data from the same developmental stage, but with synaptic inhibition intact, are shown for comparison. * : $P < 0.05$ (Mann-Whitney rank-sum test); n.s.: not significant (Mann-Whitney rank-sum test).

pharmacological conditions do not reveal differences between the OC→OC and HB→HB subtypes of uni-modal pairs or between the HB→OC and OC→HB sequences for cross-modal pairs. To aid in comparison, results from the 'no drug' condition are presented, again, at right. The table's results confirm that all cross-modal and uni-modal can be considered of equal validity. Taken as a whole, therefore, these data are consistent

with the conclusion that, in the stages 48–49 developmental group, pharmacological blockade of synaptic inhibition counteracts at least some processes — related to $GABA_A$-receptor-mediated inhibition — that are selectively engaged by pairs of cross-modal stimuli.

But while maximal responses can demonstrate an effect of picrotoxin application, they cannot provide any insight into the mechanism (or mechanisms) implicated in this change. If, for instance, inhibitory blockade purely alters the "gain" of output after cross-modal stimulation, then responses to a cell's most-effective ISI and responses to other, "off-peak" ISI's would change by the same magnitude. But if blocking inhibition alters the selectivity (or "contrast") of responses to cross-modal stimulation, then a cell's responses to "off-peak" ISI's and its responses to the most-effective ISI would change by different magnitudes, such that the distinction between these two classes of response would increase or decrease. Because an examination of maximum values alone cannot address either of these potential scenarios, further analysis of the full range of multisensory responses in each cell is necessary to establish evidence for the influence of one or both mechanisms.

Therefore, as was performed for the investigation of developmental effects in peak-aligned ISI selectivity under No Drug conditions (**Fig. 10**), for data collected during pharmacological blockade of inhibition in the later developmental group, MSI values at all ISI's were shifted and averaged in the same manner. The resulting curves are presented in **Figure 16**, with data from the No Drug condition shown again, for reference.

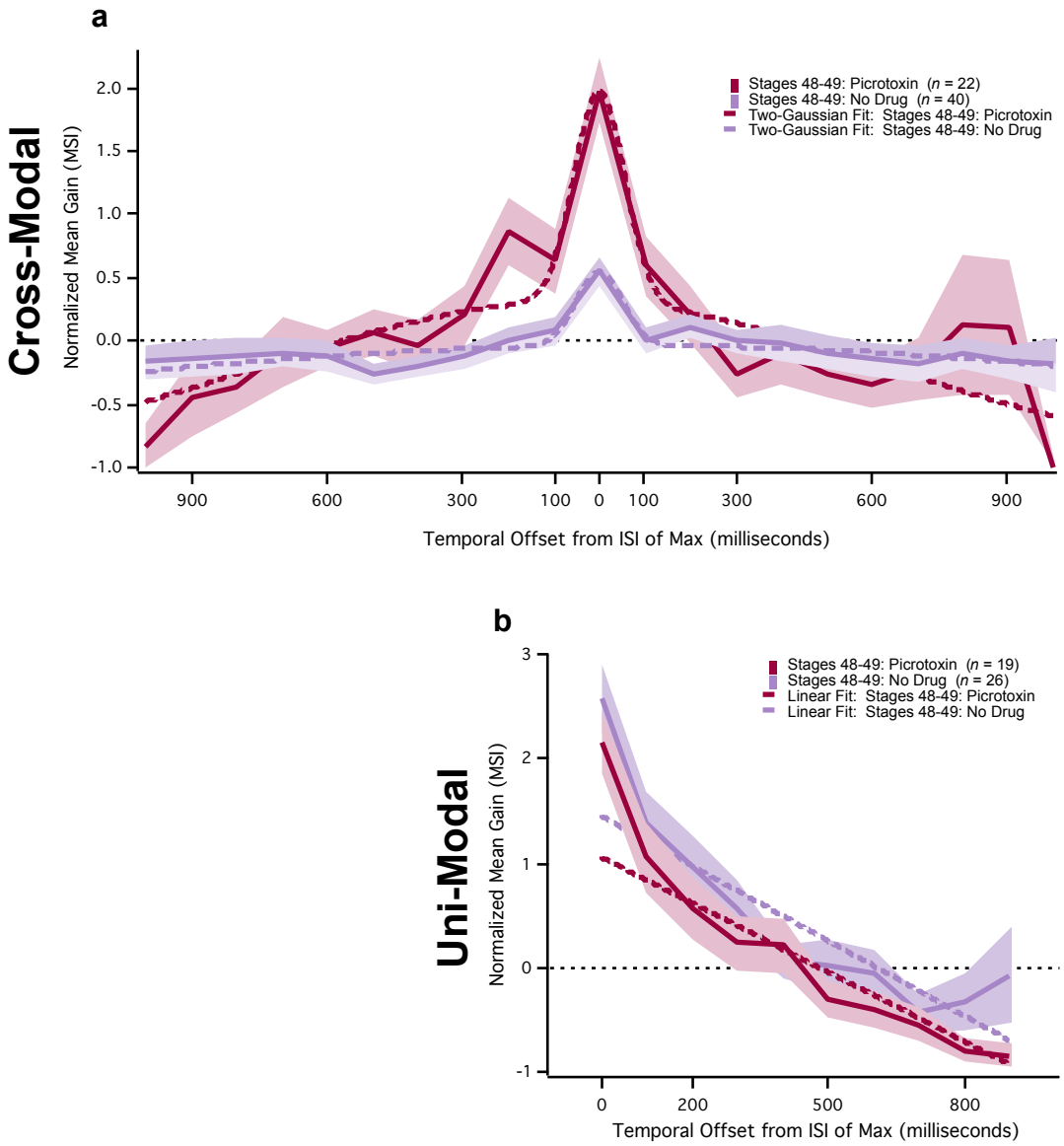

Figure 16: Population tuning to both cross-modal ISI's and uni-modal ISI's changes significantly when inhibition is blocked.
a: MSI-versus-ISI curves from HB-then-OC pairs were aligned at their peak values, and then averaged across cells. Solid lines connect the population means. Shaded areas demarcate +/– S.E.M. Results from the no drug experiments are displayed in light purple, and dashed lines reflect that separate Gaussian curves best describe the data from picrotoxin and no drug experiments ($F(2, 672) = 4.305$, $P = 0.0139$). **b**: Each cell's uni-modal MSI values, again averaged over trials for the range of ISI's, were shifted to center on the ISI of that cell's maximal MSI ratio, and these peak-aligned MSI's were averaged across cells. Solid lines connect the population average MSI ratio at peak and the ratios at ISI's longer than that of the peak. Shaded areas mark +/– S.E.M. Results from the no drug experiments are displayed in light purple, and dashed lines show the separate linear fits that best describe the data from picrotoxin and No Drug experiments ($F(2, 446) = 4.310$, $P = 0.014$).

When calculated after cross-modal pairs (**Fig. 16a**), the 'tuning' of MSI values around the peak becomes somewhat broader, while the raw differences between peak and off-peak MSI values appear much greater. After uni-modal stimulus pairs (**Fig. 16b**), though,

no sizeable differences are apparent between No Drug and Picrotoxin conditions in the breadth of tuning around the peak MSI value. Therefore, for responses to cross-modal stimuli, specifically, this analysis does not find any evidence for indiscriminate changes in response gain, but does suggest two changes in stimulus selectivity, in opposite directions. That is, the blockade of synaptic inhibition broadens (i.e., decreases) selectivity of response enhancement for cross-modal inter-stimulus intervals that are similar to the most-effective ISI, but also increases selectivity for that central range of intervals, around the ISI at peak, versus those that differ from it by more than several hundred milliseconds.

Statistical assessment of, and comparisons between, curves of best fit were again used to quantify differences between treatment groups. Specifically, the F-tests at the top left of **Table 4** indicate that the each of the cross-modal data sets is best described by a sum of

CM	H_0:	Gaussian*		Single fit for all data	
	H_1:	Sum of Two Gaussians**		Separate fits, one per data set	
		Results	*Summary*	*Results*	*Summary*
Picrotoxin		F(3,237) = 16.79; $P < 0.0001$ ($n = 22$)	Two Gauss.	F(2,672) = 4.305; $P = 0.0139$	Separate fits
No Drug		F(3,435) = 11.95; $P < 0.0001$ ($n = 40$)	Two Gauss.		
UM	H_0:	Single linear fit for all data			
	H_1:	Separate linear fits, one per data set			
		Results	*Summary*		
Picrotoxin		F(2,446) = 4.310; $P = 0.014$ ($n = 45$)	Separate fits		
No Drug					

Table 4: Statistical comparisons between MSI-versus-ISI tuning curves from experiments with and without blockade of synaptic inhibition.
Top: Cross-modal data from Stage 48–49 animals, for both the "No Drug" and "Picrotoxin" treatment conditions. *Top Left*: Determination of best-fit curves for cross-modal data from each treatment condition. Model constraints: *: Mean = 0, S.D. > 0; **: Mean of first Gaussian = 0, S.D. of first Gaussian > 0, S.D. of second Gaussian > 0. *Top Right*: Comparison between the two treatment conditions shows that while each group is best fit by a sum of two Gaussians, the data as a whole is best fit by separate curves, one for each treatment group. *Bottom*: Uni-modal data from the Stage 48–49 developmental group, for both the "No Drug" and "Picrotoxin" treatment conditions. Statistical comparison between treatment groups shows that the whole of the data can be best described by a single linear fit. *For all statistical tests*: H_0: null hypothesis; H_1: alternative hypothesis.

two Gaussians, and a further statistical test, at top right of **Table 4**, shows that these two aligned data sets can best be described by different mathematical fits. These results

support the notion that the ISI selectivity of the two data sets are distinguishable. The F-test at the bottom of **Table 4** demonstrates that uni-modal data in the two treatment groups are, in fact, best described by different linear fits to the respective data sets. Thus, while there is no significant difference between peak uni-modal MSI values from these two groups (**Fig. 15c**) and only a small visually-identifiable discrepancy between their ISI sensitivity curves (**Fig. 16b**), the breadth of temporal selectivity for uni-modal stimuli is indeed significantly different with picrotoxin application. These results nevertheless confirm that the major trends apparent graphically, in **Figure 16**, can be supported by statistics.

As detailed above, this analysis has found changes both in the gain of response enhancement at and around the most-effective inter-stimulus interval, for a given cell, and in a greater selectivity for intervals inside this broader peak region, versus those that differ by more than several hundred milliseconds. Multiple cellular and/or circuit-level mechanisms could underlie these changes. For instance, selectivity for temporal intervals might broaden (i.e., decrease) under these pharmacological conditions because the network operates free of an inhibitory influence that is preferentially recruited, in normal conditions, by the less-effective inter-stimulus intervals. Lacking this damping of enhancement for ISI's just around the most-effective interval, temporal selectivity would broaden. The cellular manifestation of these circuit-level processes will be addressed later in the work. The same processes, however, cannot be invoked for data at intervals that differ by more than several hundred milliseconds from the most-effective ISI, as these enhancement indexes show no evidence for an increase of similar proportions under the

same pharmacological conditions. Because the pharmacological block of $GABA_A$-receptor-mediated inhibition and the release from its effects does not increase MSI values for these, less-effective cross-modal intervals, the data suggest that synaptic inhibition either has no influence or is actually facilitative for responses to longer ISI's. Potential circuit-level and cellular mechanisms will be discussed in the context of additional experimental data, below.

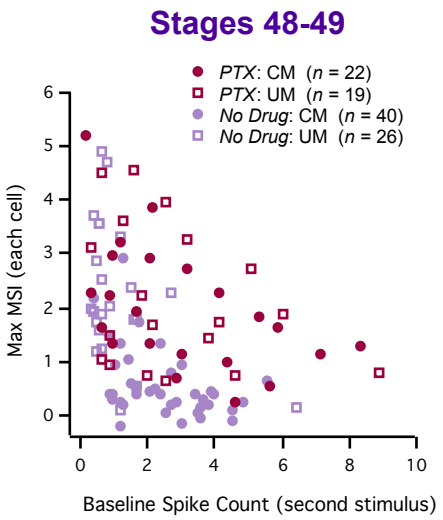

Figure 17: Blocking inhibition with picrotoxin qualitatively weakens the phenomenology of inverse effectiveness.
For both uni-modal and cross-modal data sets, and for each cell, the maximum, trial-averaged MSI value is plotted against the average number of action potentials recorded after the control stimulus, defined as a single pulse delivered to whichever modality is presented second in the corresponding stimulus pair. For reference, data from no drug experiments are also displayed, in light purple.

While the preceding analyses address the magnitude and temporal selectivity of response enhancement, other metrics for characterizing the interaction between two stimuli, such as inverse effectiveness and the assessment of actual-versus-predicted output, can reveal how blocking synaptic inhibition affects the very nature of multisensory processes. For example, when inhibition is blocked and maximal MSI values are isolated and compared to neuronal output after single control stimuli, as in **Figure 17**, responses to cross-modal as well as uni-modal pairs show markedly less robust inverse effectiveness than in the same developmental group — stages 48–49 — with inhibition intact. That is, without synaptic inhibition, these data show a weaker dependence on the baseline responsiveness to the second input in the pair, when presented in isolation, relative to the response enhancement observed after the two inputs are presented together

(for both cross-modal *and* uni-modal combinations). This gives some indication that the block of synaptic inhibition has removed constraints on the enhancement of responses; even strong responses, to highly effective individual stimuli, can be increased further in the context of a stimulus pair.

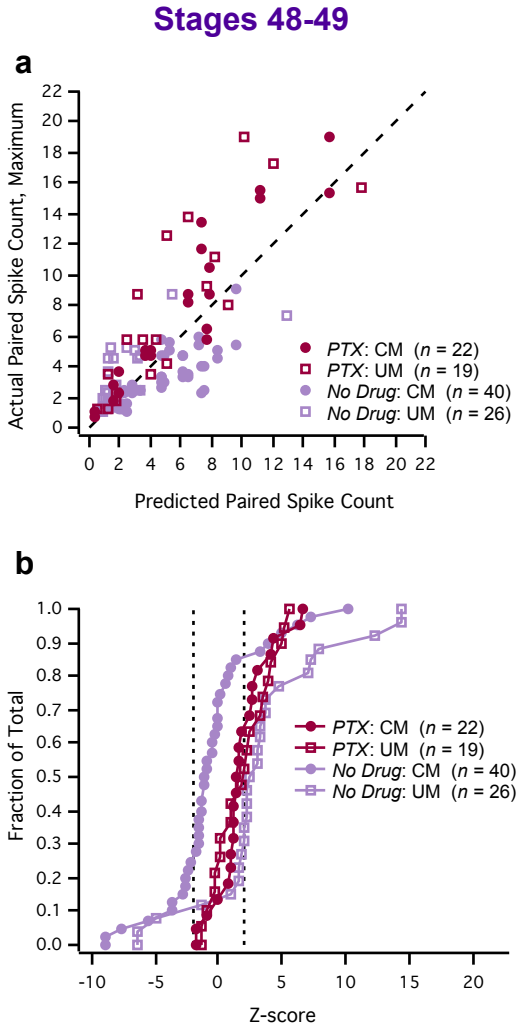

Figure 18: When inhibition is blocked, no difference is evident between the underlying operations for uni-modal and cross-modal integration.
a: For both uni-modal and cross-modal data sets, and for each cell, the maximum raw spike count after paired stimulation (averaged across trials) is plotted against the spike count predicted by random additive pairings between the responses recorded after the two respective control stimuli, that is, single pulses delivered to the each component of the stimulus pair. Dashed line represents the line of unity. For reference, data from no drug experiments are also displayed, in light purple. **b**: For both uni-modal and cross-modal data sets, Cumulative Frequency Distributions of *Z*-score values are plotted for the comparison between predicted and actual number of action potentials recorded after paired stimulation, in each cell. Vertical dashed lines indicate $Z = +/-1.97$, the point at which actual responses are +/–2 S.D.'s away from the respective predicted response. For greater detail on generation of the predicted responses and calculation of *Z*-scores, see *Methods*. As above, data from the no drug experiments are also displayed, in light purple, for reference. A Kolmogorov-Smirnov test of the distributions for uni-modal and cross-modal data shows no statistical difference (D = 0.2153, $P = 0.676$).

Additional insight on effects of blocking synaptic inhibition are made possible by accounting for the baseline responsiveness to each of the inputs comprising a pair, not just to the second of the two inputs, and then assessing the computational principles which guide their interaction. Following the same analytical methods as for **Figure 12**, **Figure 18a** shows that the actual responses to these stimulus pairs, at the maximum value

per cell, seem greater than what would be predicted by simple addition of the responses evoked by each of the two stimuli when presented separately. Moreover, when compared to the relationships observed under normal pharmacological conditions in this developmental group, the actual-versus-predicted data points for both uni-modal and cross-modal pairs seem to lie further above the line of unity. A quantitative account of the changes in the underlying integrative processes is shown in **Figure 18b**. CDF plots of the *Z*-scores for individual actual-versus-predicted comparisons not only highlight the near-absence of statistically significant negative values, but also reveal that the uni-modal / cross-modal difference that had existed between *Z* distributions with inhibition intact, in the same developmental group, has here collapsed (Kolmogorov-Smirnov test, D = 0.2153, $P = 0.676$). These results, therefore, are consistent with the observation that blocking synaptic inhibition increases the raw magnitude of maximal enhancement for cross-modal stimuli, for each cell (see **Figure 15a**), and they also confirm that this selective increase occurs independent of any changes in the efficacy of each input, since these baseline responses have been accounted for and controlled by the *Z*-score transformation. However, while the results of **Figure 18** show that blocking inhibition has eliminated subadditive interactions for cross-modal pairs, specifically, it has also reduced the diversity of computational modes evident for combinations of both cross-modal *and* uni-modal inputs. Thus there are both general and stimulus-specific roles of inhibition in the computational processes underlying multisensory interactions.

Timing of Action Potentials

The effect of cross-modal stimulus pairs on action potential timing, in addition to action potential count, has been acknowledged relatively recently in the multi-sensory literature. Specifically, in a pair of 2007 reports from the anesthetized cat SC, Rowland and colleagues were first to describe how cross-modal stimulus pairs evoke faster and more temporally-compact responses than single stimuli, presented individually (Rowland et al., 2007a; Rowland and Stein, 2007). Similar effects have since been shown in the OT of awake barn owls (Zahar et al., 2009). To assess whether cross-modal stimuli might induce similar temporal shifts in the output of neurons in the OT of *Xenopus* tadpoles — and whether this effect could be developmentally-regulated — I compared the time of response onset across experimental conditions.

Figure 19 shows the .25, .50 (median), and .75 quartiles of the post-stimulus time at which the first action potential responses occur after each of the ISI's, and the appropriate control stimulus, for each experimental group. The grouping of data, here, is according to the same conventions as in **Figure 7**. More specifically, the cross-modal group combines data derived from both OC→HB and HB→OC stimulus sequences (therefore with Control stimuli being a combination of single HB and single OC stimuli, respectively). The uni-modal group combines data collected after both HB→HB and OC→OC pairs (with Control stimuli representing a combination of single HB and single OC stimuli). Note that in all cases, the distribution of onset latencies after paired stimuli appears more narrow and to cover shorter post-stimulus times relative to the distributions after single

control stimuli. These plots also suggest that cross-modal stimulus pairs evoke spikes faster, and over a narrower interquartile range, than do uni-modal pairs in both developmental groups, and that some decrease in latency might occur over development.

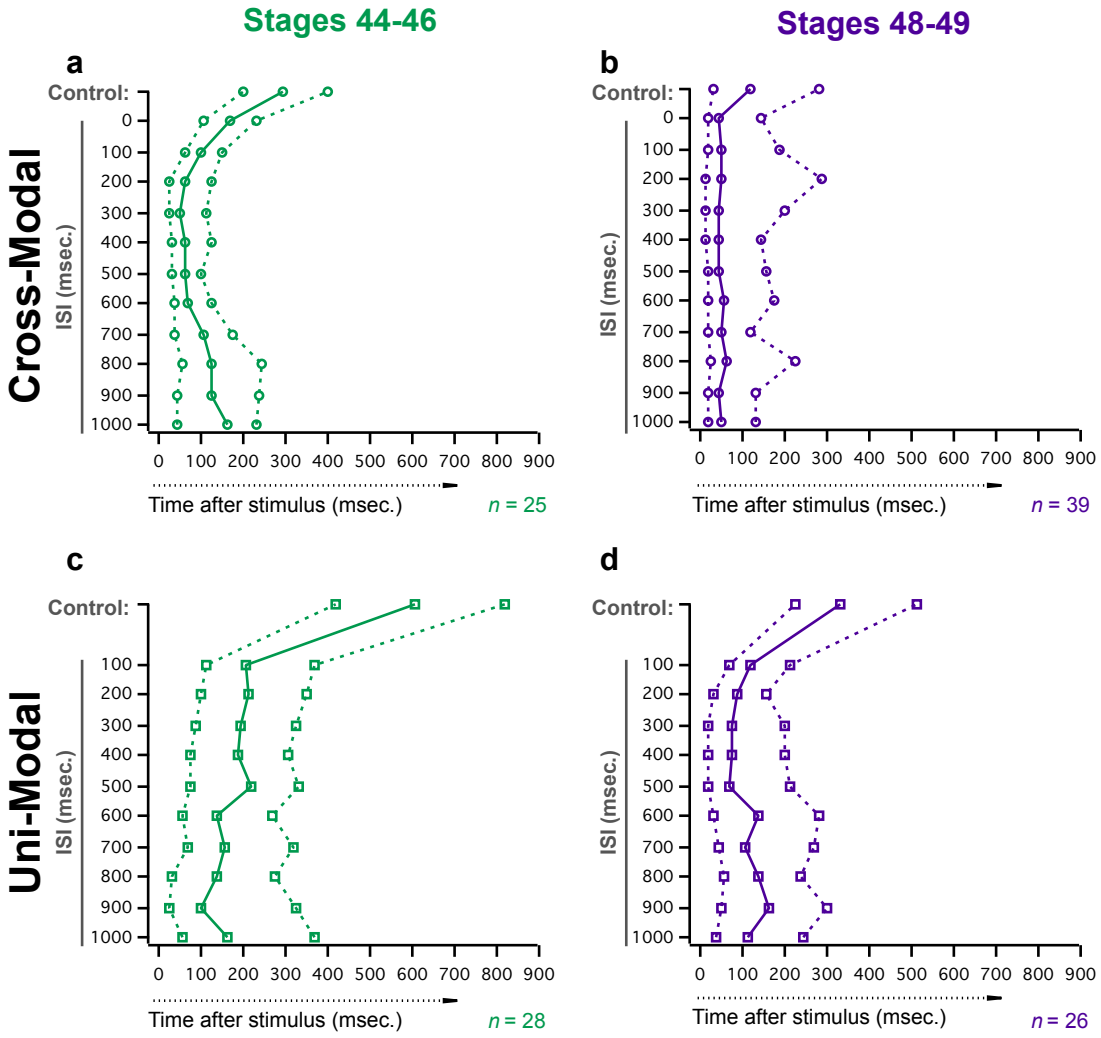

Figure 19: Population data suggest that the latency to first spike may differ after cross-modal and uni-modal stimuli, and between developmental groups.
For each paired ISI, as well as the appropriate control stimulus (*left axis*), the .25, .50 (median), and .75 quartiles of post-stimulus times for all first spikes generated under the indicated stage / stimulus conditions are plotted on the bottom axis. Dashed lines connect 0.25 and 0.75 quartile values, and solid lines connect .50 quartile (median) values.

To quantify these differences across experimental groups, one set of values for interquartile range and median of first spike times was compared per cell. These values were taken at the same ISI as was used to compare effects on spike count; that is, the ISI

which evoked the greatest number of action potentials (and likewise the maximal MSI) after paired stimulation. **Figure 20** addresses the first of these questions, and in each developmental group compares the median and interquartile range of onset latencies, in single neurons, after uni-modal and cross-modal stimuli. As shown, these two measures

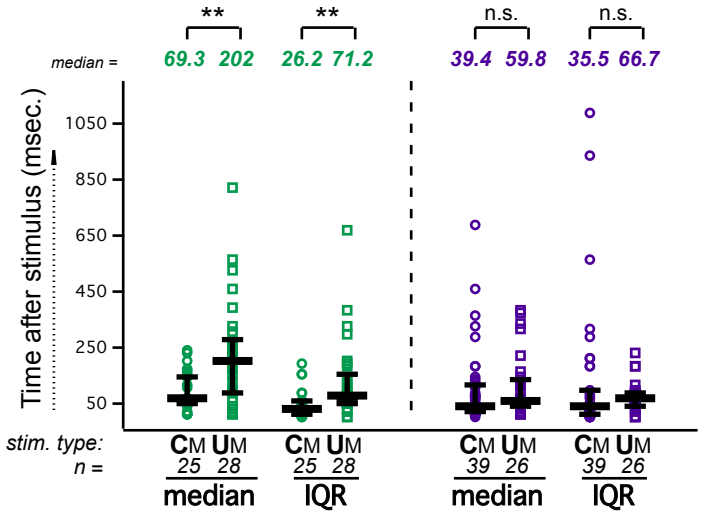

Figure 20: Versus uni-modal pairs, cross-modal stimuli initiate first spikes faster and with less variability at stages 44–46, but not at stages 48–49, when determined at the maximum MSI for each cell.
Values for the median time and interquartile time range of first spikes following uni- and cross-modal stimulus pairs are plotted by post-stimulus time (*left axis*) and directly compared in the stage 44–46 developmental group (*bottom axis, left side*) and the stage 48–49 developmental group (*bottom axis, right side*). UM: uni-modal; CM: cross-modal. ** : $P < 0.01$; n.s.: not significant (Mann-Whitney rank-sum test).

reflect an acceleration and refinement of response onset times after cross-modal stimuli, versus after uni-modal stimuli, for cells from the stages 44–46 developmental group only (Mann-Whitney rank-sum test, $P < 0.01$). **Figure 21** addresses the question of a developmental change in the distribution of response onsets after cross-modal pairs, specifically, and shows that no significant difference is found between the developmental groups studied here (Mann-Whitney rank-sum test). These findings are unexpected in

light of the results shown in **Figure 9**, where only for cross-modal stimuli are there developmentally-regulated changes in both maximal enhancement of responses (**Fig. 9a**) and the inter-stimulus interval at which it occurs (**Fig. 9b**). The results shown in **Figures 20** and **21** also contradict the subjective appearance of response onset data taken from all inter-stimulus intervals, and not just from the interval of maximum spike count (see **Figure 19**, and accompanying description in previous paragraph). Nevertheless, for the data overall, although the precise differences between experimental groups may be unexpected, these results do reveal an instance where cross-modal stimulation, specifically, affects response onset time — as has been found in *in-vivo* mammalian preparations — and also show how this stimulus dependence changes over development.

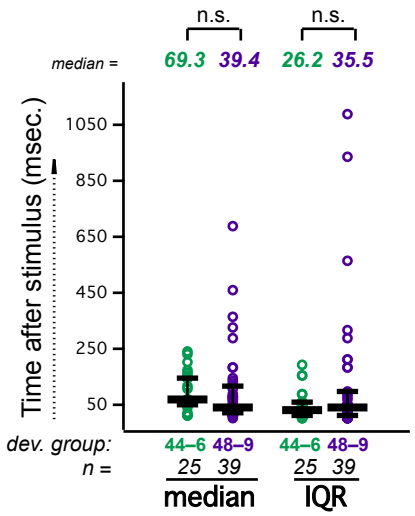

Figure 21: At maximum MSI after cross-modal stimuli, no developmental change in temporal position or spread of first spikes. Values for the median time and interquartile time range of first spikes following cross-modal stimulation are plotted by post-stimulus time (*left axis*), and data from the two developmental groups are compared. n.s.: not significant (Mann-Whitney rank-sum test).

To determine whether additional stimulus dependencies can be found in these combined data for both cross-modal and uni-modal pairs, **Table 5** presents statistical tests for differences between data taken after each of the stimulus subtypes which comprise these groups. As shown, there are no differences in either median time or inter-quartile range between single-cell data taken after the two subtypes of cross-modal stimuli, in either developmental group. A significant difference is found between the median onset latency of data from these the two subtypes of uni-modal stimuli, and

only in the earlier developmental group, and in both developmental groups there is only a weakly significant difference between the interquartile range of onset times from individual neurons.

		Stages 44–46			Stages 48–49		
		***Median* 1st spike latency (s)**	*P-value*	*Summary*	***Median* 1st spike latency (s)**	*P-value*	*Summary*
Cross-Modal	***VH***	0.069 (*n* = 13)	*P* = 0.462	n.s.	0.052 (*n* = 19)	*P* = 0.474	n.s.
	HV	0.069 (*n* = 12)			0.034 (*n* = 20)		
Uni-Modal	***HH***	0.271 (*n* = 13)	*P* = 0.006	**	0.118 (*n* = 13)	*P* = 0.138	n.s.
	VV	0.094 (*n* = 15)			0.054 (*n* = 13)		
		***IQR* 1st spike latency (s)**	*P-value*	*Summary*	***IQR* 1st spike latency (s)**	*P-value*	*Summary*
Cross-Modal	***VH***	0.046 (*n* = 13)	*P* = 0.494	n.s.	0.044 (*n* = 19)	*P* = 0.206	n.s.
	HV	0.022 (*n* = 12)			0.023 (*n* = 20)		
Uni-Modal	***HH***	0.106 (*n* = 13)	*P* = 0.015	*	0.078 (*n* = 13)	*P* = 0.039	*
	VV	0.054 (*n* = 15)			0.048 (*n* = 13)		

Table 5: At maximum MSI, some significant differences are found between uni-modal stimuli to different pathways, but not between different sequences of cross-modal stimuli, in the temporal position and spread of first spikes within both developmental groups.
Top: Within both developmental groups, the median temporal position of first spikes is compared between the two cross-modal sequences and the two types of uni-modal pair. *Bottom*: The temporal spread of first spikes — represented by their interquartile range (IQR) — is compared between the two cross-modal sequences and the two types of uni-modal pair, within each developmental group. *: $P < 0.05$ (Mann-Whitney rank-sum test); **: $P < 0.01$ (Mann-Whitney rank-sum test); n.s.: not significant (Mann-Whitney rank-sum test).

The discrepancy between these measures of response onset time (**Figures 20** and **21**) and the measures of maximal response enhancement (of spike count; **Figure 9**) is notable because in each cell, the raw data for both are taken after the same inter-stimulus interval. One possible explanation is that, across cells, the inter-stimulus interval producing the strongest effect on response onset latency differs from the inter-stimulus interval which evokes the maximal enhancement of spike count. A second potential explanation, not mutually exclusive to the first, is that the mechanisms involved in the developmental regulation of response magnitude after cross-modal stimuli, specifically, do not play a similar role in the maturation of response timing. Because acute pharmacological blockade of $GABA_A$-receptor-mediated synaptic inhibition has already been shown to disrupt developmentally-regulated changes in enhancement of response magnitude (i.e.,

count), the latter possibility — of different mechanisms for the maturation of response magnitude and response timing — can be evaluated in data from this treatment condition.

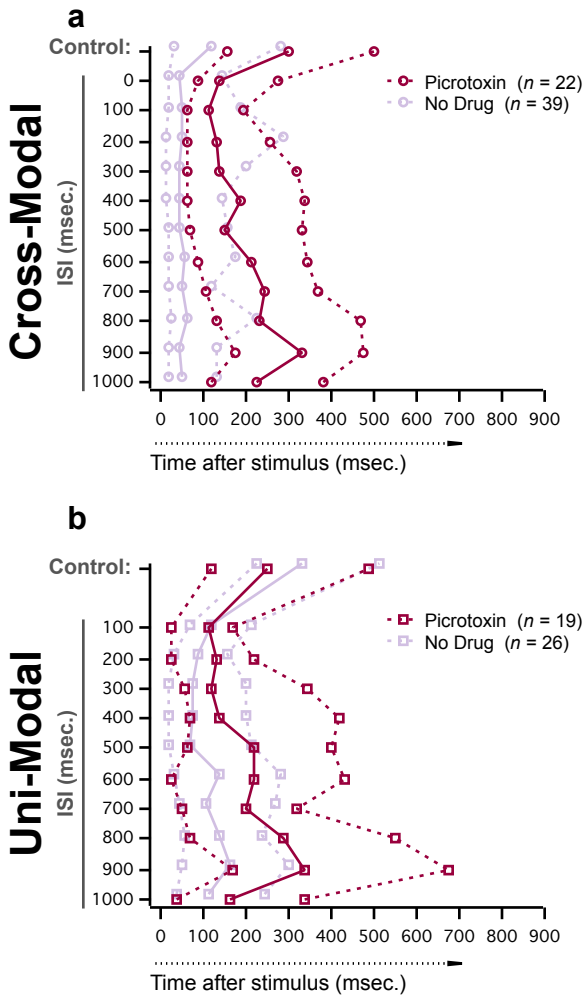

Figure 22: Inhibitory blockade produces apparent shifts in first spike latency after both cross-modal and uni-modal stimulus pairs.
For each paired ISI, as well as the appropriate control stimulus (*left axis*), the .25, .50 (median), and .75 quartiles of post-stimulus times for all first spikes generated under the indicated stage / stimulus conditions are plotted on the bottom axis. Dashed lines connect .25 and .75 quartile values, and solid lines connect .50 quartile (median) values. Data from the No Drug experiments are displayed, in light purple, for reference.

For all inter-stimulus intervals tested, changes in the phenomenology of response onset due to the block of synaptic inhibition are evident in **Figure 22**. Here, cross-modal responses, specifically, appear to be altered in both the median and interquartile range of onset times after all ISI's. Under these pharmacological conditions, when responses to cross-modal stimuli, specifically, are compared across drug treatment groups in **Figure 23a** — at the inter-stimulus interval responsible for the maximal spike number in each cell — an effect of inhibitory blockade on median first spike latency is found. More precisely, the time of median onset becomes significantly greater when synaptic inhibition is blocked with picrotoxin (Mann-Whitney rank-sum test, $P < 0.01$). **Table 6** confirms that this effect is

generalizable to all cross-modal sequences for each treatment condition, as no significant differences in response onset latency are found between the two unique input sequences.

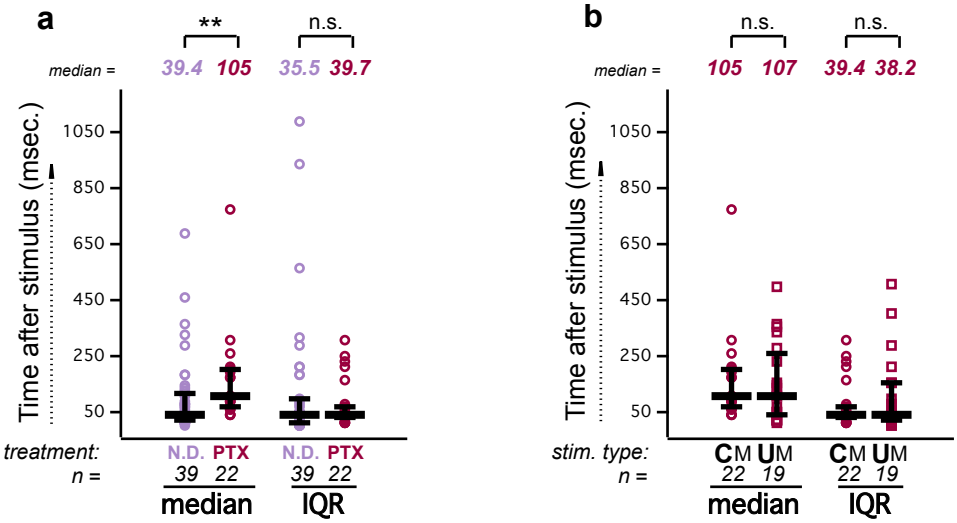

Figure 23: Synaptic inhibition influences the latency to first spike after cross-modal stimuli, but blocking synaptic inhibition reveals no difference between spike onset times after uni-modal and cross-modal pairs, at maximum MSI.
a: Values for the median time and interquartile time range of first spikes following cross-modal stimulation under picrotoxin and no drug conditions are plotted by post-stimulus time (*left axis*), and for each metric the data from these two treatment groups are compared. ** : $P < 0.01$; n.s.: not significant (Mann-Whitney rank-sum test). **b**: Values for the median time and interquartile time range of first spikes following uni- and cross-modal stimulus pairs are plotted by post-stimulus time (*left axis*) and directly compared. UM: uni-modal; CM: cross-modal. n.s.: not significant (Mann-Whitney rank-sum test).

However, when first spike latencies are examined at these same inter-stimulus intervals, no differences are evident between response onset after cross-modal and uni-modal pairs (**Fig. 23b**; Mann-Whitney rank-sum tests). Qualitatively these results resemble what is observed under normal physiological conditions, in the same developmental group (see **Figure 20**). These findings therefore cannot reject one of the potential explanations for the discrepancy between developmental changes in two measures of cross-modal sensitivity: response magnitude (i.e., total spike number) and the latency to response onset. Because $GABA_A$-receptor-mediated synaptic inhibition has an influence on the maximal response count to cross-modal stimuli, specifically, but shows no such stimulus selectivity in its influence on the onset latency of responses after the same inter-stimulus

interval, for each cell, these data do exclude the possibility that this ligand-gated chloride conductance plays different functional roles in response magnitude and response timing after paired multisensory stimuli.

		Stages 48–49; picrotoxin			**Stages 48–49; no drug**		
		Median 1st spike latency (s)	*P-value*	*Summary*	***Median 1st spike latency (s)***	*P-value*	*Summary*
Cross-Modal	***VH***	0.109 (*n* = 11)	*P* = 0.552	n.s.	0.052 (*n* = 19)	*P* = 0.474	n.s.
	HV	0.092 (*n* = 11)			0.034 (*n* = 20)		
Uni-Modal	***HH***	0.119 (*n* = 10)	*P* = 0.882	n.s.	0.118 (*n* = 13)	*P* = 0.138	n.s.
	VV	0.044 (*n* = 9)			0.054 (*n* = 13)		
		IQR 1st spike latency (s)	*P-value*	*Summary*	***IQR 1st spike latency (s)***	*P-value*	*Summary*
Cross-Modal	***VH***	0.042 (*n* = 11)	*P* = 0.432	n.s.	0.044 (*n* = 19)	*P* = 0.206	n.s.
	HV	0.032 (*n* = 11)			0.023 (*n* = 20)		
Uni-Modal	***HH***	0.047 (*n* = 10)	*P* = 0.486	n.s.	0.078 (*n* = 13)	*P* = 0.039	*
	VV	0.022 (*n* = 9)			0.048 (*n* = 13)		

Table 6: With synaptic inhibition blocked, no significant differences are found between sequences of cross-modal stimuli or between uni-modal stimulus pairs to different pathways, in either the temporal position or spread of first spikes from the maximal MSI in each cell.
Top: The median temporal position of first spikes is compared between the two cross-modal sequences and the two types of uni-modal pair. *Bottom*: The temporal spread of first spikes — represented by their interquartile range (IQR) — is compared between the two cross-modal sequences and the two types of uni-modal pair. Results from the No Drug condition are presented for comparison. *: $P < 0.05$ (Mann-Whitney rank-sum test); n.s.: not significant (Mann-Whitney rank-sum test).

During pharmacological blockade of inhibition, is somewhat surprising that at the same interval between cross-modal stimuli, for each cell, these analyses detect both a significant increase in the number of action potentials and a significantly longer latency for their onset (both versus normal physiological conditions). For example, even without an assumption of changes to the probability distribution of action potential generation, one might have expected that if a treatment were to increase the raw number of action potentials in the post-stimulus time window, then the latency to the first of these spikes would tend to become smaller. The fact that a significant shift in the opposite direction is observed instead (see **Figure 23a**) could reflect several functions of the mechanism blocked in this treatment condition — $GABA_A$-receptor-mediated inhibition. On a cellular level, for example, by contributing to membrane voltage fluctuations that facilitate action potential generation generally (Mainen and Sejnowski, 1995; Rudolph et

al., 2007) and stimulus-evoked output, specifically (Cardin et al., 2008).The analyses of the cellular data that follow will address in detail the contribution of synaptic inhibition to multisensory processes in the *Xenopus* tectum, in each developmental group and over the course of maturation.

(Results continue next page)

NEURONAL INPUTS — SYNAPTIC CONDUCTANCES

Previous studies have shown that the balance between excitatory and inhibitory synaptic conductances guides cross-modal convergence in the vertebrate OT/SC (Zheng and Knudsen, 1999) and influences the temporal characteristics of action potential generation in both the tectum (Shen et al., 2011) and primary sensory cortices (Higley and Contreras, 2006; Wehr and Zador, 2003). Data in this work, furthermore, suggest a role for synaptic inhibition in the developmentally-regulated changes in neuronal responsiveness to cross-modal stimuli, specifically.

To undertake this investigation, I performed whole-cell intracellular recordings, in the same two developmental groups as above, to isolate excitatory and inhibitory events evoked by cross-modal as well as uni-modal stimulus pairs. Excitatory condutances were isolated by clamping membrane voltage at –45mV, the chloride reversal potential (thereby eliminating electrochemical drive for synaptic inhibition), and inhibitory conductances were isolated by clamping membrane voltage at +5mV, the reversal potential for sodium and potassium (which eliminates electrochemical drive for synaptic excitation).

Figure 24 demonstrates the nature of, and general relationships between, these synaptic events. Examples of these conductances are shown in **Figure 24a**. **Figure 24b** provides an initial assessment of the effect of stimulus pairs: the raw difference between conductance recorded after paired stimulation (i.e., via OC→HB *and* HB→OC

sequences) and conductance recorded after the appropriate control stimulus — a single input to the modality targeted last in a given paired protocol (e.g., HB or OC,

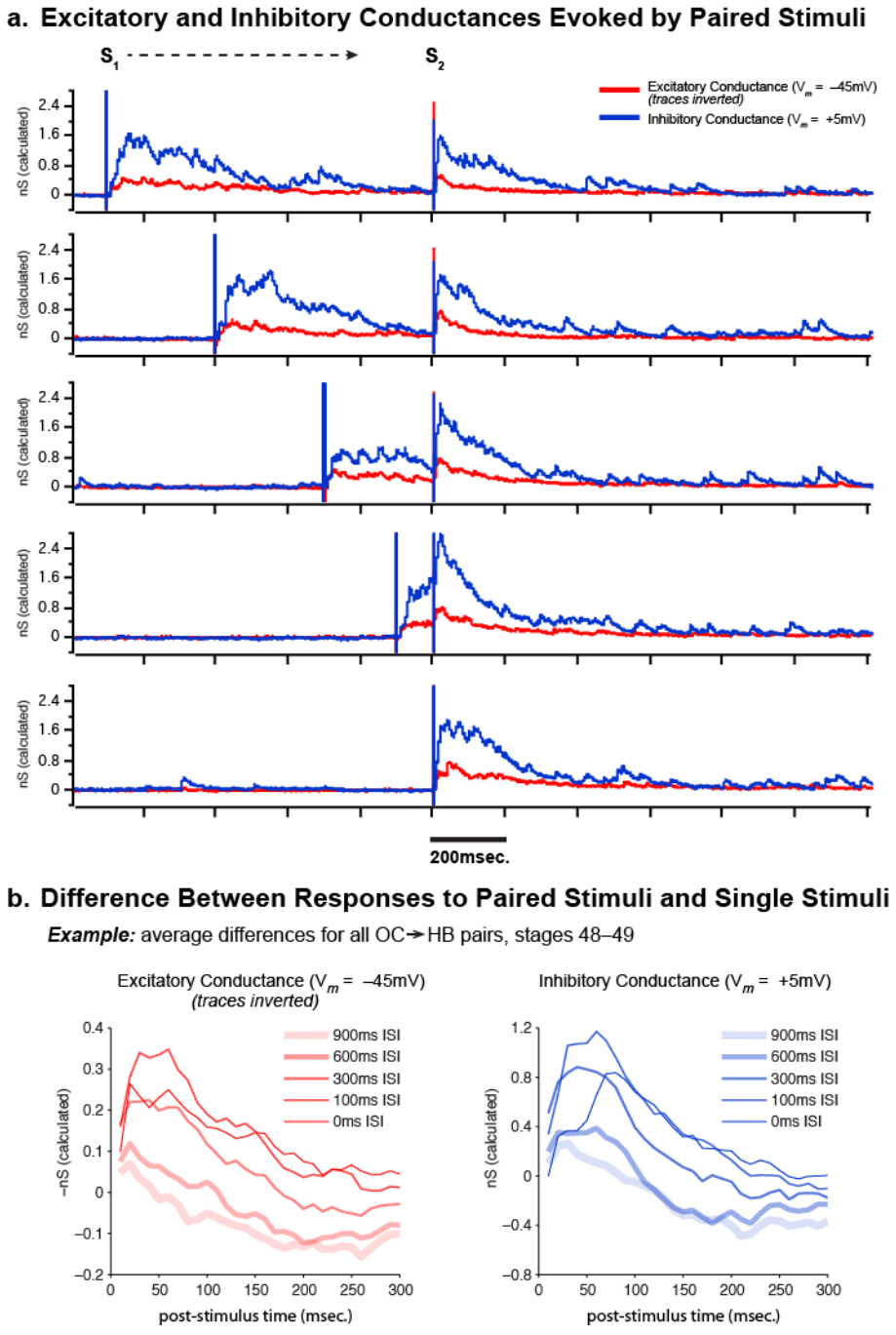

Figure 24: Synaptic conductances recorded during paired stimulation.
a. Example traces of excitatory (red) and inhibitory (blue) synaptic conductances, at different inter-stimulus intervals. S_1: first stimulus delivered in the paired stimulus protocol. S_2: second stimulus delivered in the paired stimulus protocol. **b.** The raw difference between the integrated conductance, in each 10 millisecond bin, recorded after a paired stimulus protocol (S_1S_2) and that recorded after a single stimulus protocol (S_2), delivered to whichever modality is targeted second in the pairing under investigation. This value represents the raw effect of the first stimulus on responses evoked by the second stimulus, presented alone. The temporal profile of this relationship, across cells, is shown for both excitatory (*left*) and inhibitory (*right*) conductances.

respectively). For both excitatory (*left*) and inhibitory (*right*) conductances, the curves in **Figure 24b** demonstrate that for this measure, in the temporal domain following a stimulus pair, the greatest differentiation between intracellular data from the five inter-stimulus intervals (shown in different line thickness/darkness) at, or even before, the 50 milliseconds time point. Thus, although the influence of the first input in a pair has been shown to persist for at least 1 second post-stimulus, as evident in non-zero average MSI's even for the longest intervals between inputs that were tested (**Fig. 7**), the following analyses will assess differences between experimental groups in the time range after the second stimulus where that influence is most likely to be observed. That is, the values for excitatory and inhibitory conductance below were derived from an integration of the first 50 milliseconds of the response.

Temporal Tuning of Excitatory and Inhibitory Enhancement

In **Figures 25** and **26**, population means of MSI values calculated at each inter-stimulus interval are compared directly between developmental groups, separately for excitatory and inhibitory synaptic conductances, and separately for responses to uni-modal and cross-modal stimulus pairs. The groupings between experimental conditions here, for these comparisons of synaptic inputs, are the same as in the above comparisons of neuronal output: cross-modal data represent a combination of responses to the two distinct input sequences (OC→HB and HB→OC) and uni-modal data represent a combination of responses to paired stimulation of both sensory pathways (HB→HB and

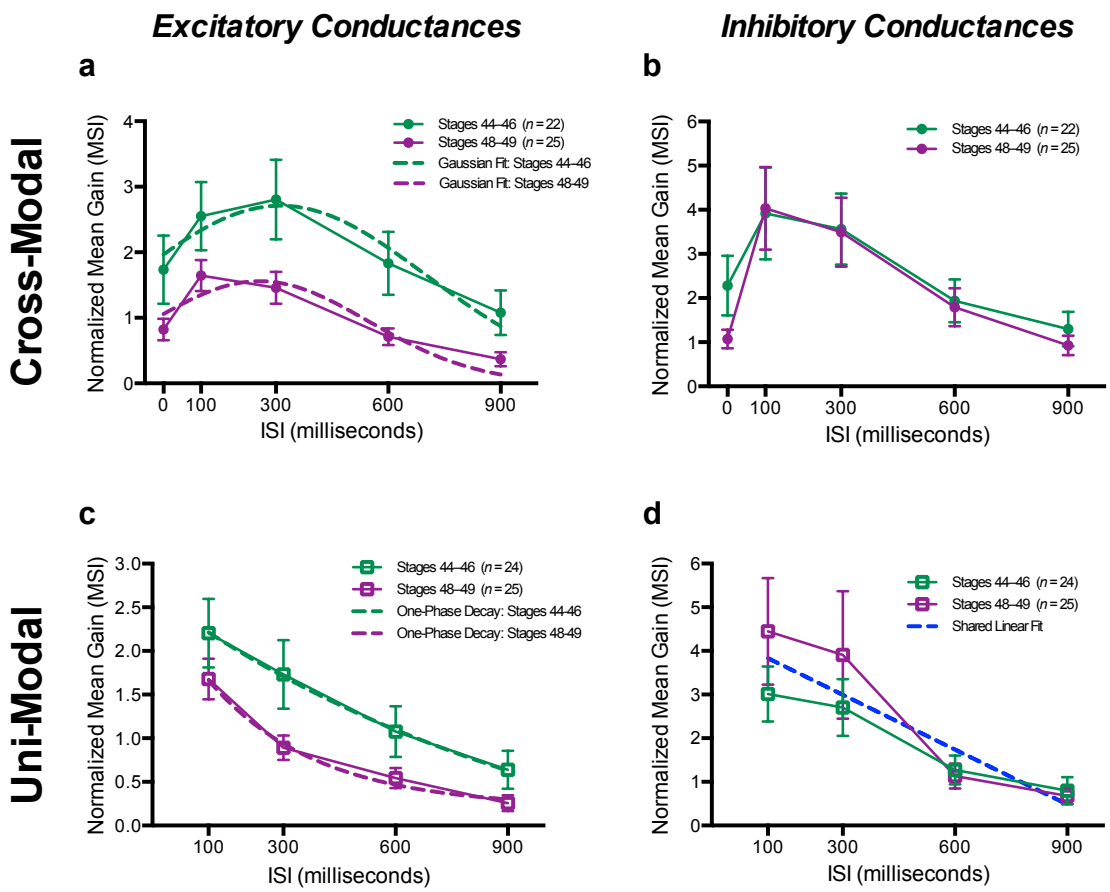

Figure 25: ISI tuning of enhancement in excitatory, but not inhibitory, conductances changes over development, for both stimulus types.
In each cell, MSI ratios are calculated from synaptic conductances integrated over the first 50 milliseconds following stimulus presentation, and averaged over presentations of given ISI. That is, for integrated conductance after each ISI, the raw difference between this pair-driven conductance and conductance recorded after the baseline stimulus (a single input to the pathway stimulated second in the respective pair) was taken, and then normalized to the conductance for that baseline stimulus input. Plotted here are the population means of these trial-averaged MSI ratios, at the ISI's tested in each condition. Error bars show +/– S.E.M. Dashed lines show curves that are best fit to the data across cells, from both developmental groups. Separate Gaussian curves were found to best fit the two data sets in **a** ($F(3, 229) = 6.755$, $P = 0.0002$) and **c** ($F(3, 182) = 3.783$, $P = 0.0115$), whereas a single linear fit was found to best describe both groups' data in **d** ($F(2, 184) = 1.271$, $P = 0.2829$). In **b**, the very close overlap between population means as well as the respective standard errors provides no basis for a hypothesis that different curves could best describe the data, and therefore no curve fitting was deemed necessary.

OC→OC). Furthermore, this quantitative assessment of synaptic inputs, across all ISI's, utilizes an analytical method similar to what was employed in the study of temporal selectivity in neuronal output (see **Figure 10**) — each data set was fit to a curve, and these curves were compared statistically. And as was the case previously, the candidate forms for these curves were determined by visual approximate from trends in the data, not by theoretical assumptions about the nature of processes from which they arise.

In the plots comparing excitatory conductances between developmental groups, the separate curve fits emphasize the finding that the two groups differ in their sensitivity to both uni-modal ISI's (**Fig. 25c**; $F(3, 182) = 3.783$, $P = 0.0115$) and cross-modal ISI's (**Fig. 25a**; $F(3, 229) = 6.755$, $P = 0.0002$). For example, after presentations of either stimulus sequence the evoked excitatory conductances produce consistently higher MSI values at stages 44–46 than at stages 48–49. Plots comparing inhibitory synaptic conductances between the two developmental groups show that any differences, after either cross-modal (**Fig. 25b**) or uni-modal (**Fig. 25d**) pairs, were not found to be statistically significant (uni-modal comparison: $F(2, 184) = 1.271$, $P = 0.2829$). Therefore, unlike in data on the number of action potentials generated in response to these same stimulus pairs, where for maximal enhancement (**Fig. 9a**, **c**) and temporal selectivity (**Fig. 10**) there exist specific developmental changes after cross-modal stimuli, these data on enhancement of both excitatory (**Fig. 25a**, **c**) and inhibitory (**Fig. 25b**, **d**) synaptic inputs show that developmentally-regulated changes in this phenomenon are not specific for one particular stimulus type.

The foregoing experiments in the stages 48–49 developmental group have shown that the developmentally-regulated responsiveness to cross-modal stimuli, specifically, depends acutely on the presence of $GABA_A$-receptor-mediated inhibition (see **Figs. 15a**, **c**; **16**). Therefore, to quantify the relationship between excitatory and inhibitory inputs at these developmental stages, I directly compared the MSI distributions for excitatory and inhibitory conductances over the range of intervals tested, in a separate plot for each type of pair. As shown in **Figure 26**, after both types of stimulus pairs the MSI values

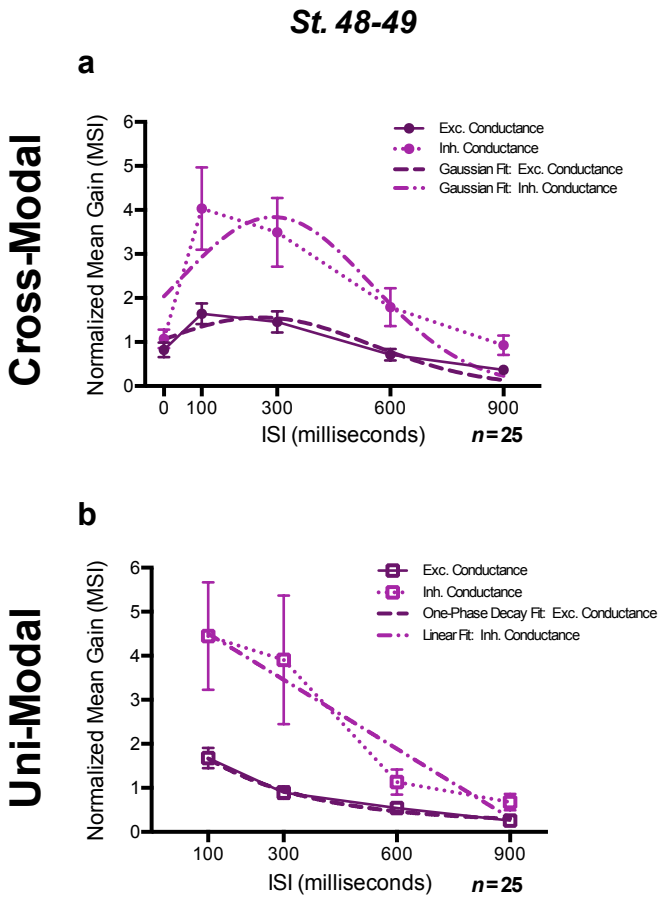

Figure 26: In the stage 48-49 developmental group, excitatory and inhibitory synaptic conductances are tuned differently to cross-modal as well as uni-modal ISI's.
Plotted over ISI are population means of trial-averaged MSI ratios calculated in each cell, from the synaptic conductances integrated over the first 50 milliseconds after stimulus presentation. Error bars show +/– S.E.M. Dashed and dash-dotted lines show curves that are best fit to the data from excitatory and inhibitory synaptic conductances. For both types of paired stimulation, different fits were found to best describe MSI ratios calculated from excitatory and inhibitory synaptic conductances

determined from excitatory and inhibitory synaptic conductances differ significantly over the range of ISI's tested (*cross-modal:* $F(3, 244) = 8.156$, $P < 0.0001$; *uni-modal, Exc.*: H_0 = straight line (vs. one-phase decay), $F(1, 97) = 4.880$, $P = 0.0295$; *uni-modal, Inh.*: H_0 = straight line (vs. one-phase decay), $F(1, 97) = 0.1554$, $P = 0.6943$). The information in these comparisons therefore would not predict the pattern of enhancements in spike number, where the block of inhibitory conductances, with picrotoxin, contributes differently to cross-modal and uni-modal effects. This set of results, then, represents another departure from the phenomenology observed in neuronal output.

Maximal Excitatory Enhancement vs. Inhibitory Enhancement — By Cell

To more directly investigate how the relationship between the MSI values describing

enhancement of excitatory and inhibitory conductances differs in response to various stimuli, for each cell recorded under a given stimulus paradigm I determined the maximal MSI value for excitatory conductances, across all intervals tested, and calculated the MSI value for inhibitory conductances at the same inter-stimulus interval which evoked the maximal excitatory response, in the same cell. I then plotted the respective index values on orthogonal axes, statistically assessed the distribution of all such data points, and used a further statistical test to compare the distributions produced by two stimulus paradigms. **Figure 27** shows the resulting plots for the stages 44–46 and stages 48–49 developmental groups. As described in **Table 7–1**, for both developmental groups, the data points for

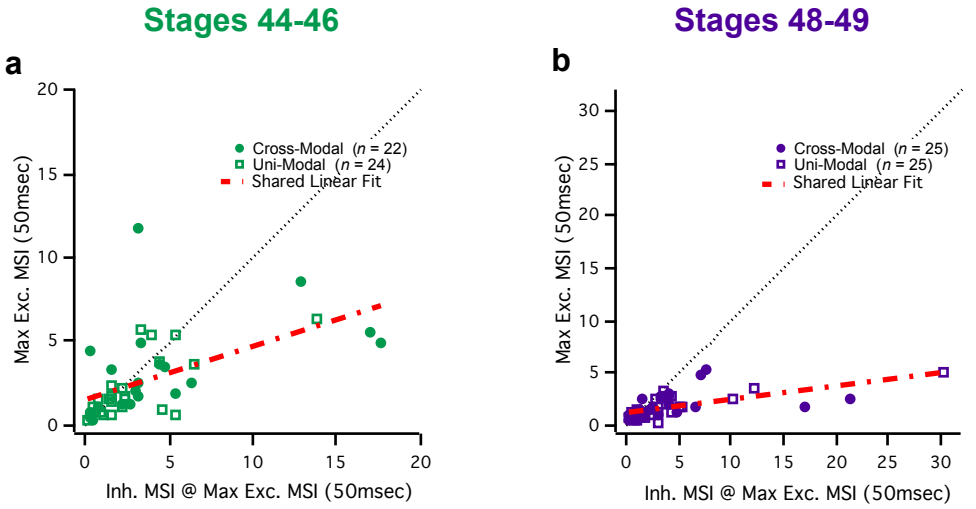

Figure 27: The type of paired stimulation has no effect on the relationship between maximum MSI ratios from excitatory and inhibitory synaptic conductances, in either developmental group.
For each cell, the maximum trial-averaged MSI ratio of excitatory conductances (over all ISI's) (*y*-axis) is plotted against the trial-averaged MSI ratio of inhibitory conductances at that same ISI (*x*-axis). Data from uni-modal and cross-modal stimulus pairs are plotted on the same sets of axes, and in both developmental groups the best description these two data sets was found to be a shared linear fit. For statistical results of curve fitting, see **Table 7–1**.

each stimulus type can be described by a linear fit with slope significantly different than 1 (i.e., the line of equality between measures), and the entirety of cell-by-cell maximal data in each developmental group (from both cross-modal and uni-modal stimulation) can be described best by a single linear fit, as shown by the red dash-dotted lines in each plot.

Comparisons		H_0: Slope = 1.0		Single fit for all data	
		H_1: Slope ≠ 1.0		Separate fits, one per data set	
		Results	*Summary*	*Results*	*Summary*
Stages 44–46	***CM***	F(1,20) = 44.93; $P < 0.0001$ ($n = 22$)	Slope ≠ 1.0	F(2,40) = 0.6314; $P = 0.5371$	Single fit
	UM	F(1,20) = 31.20; $P < 0.0001$ ($n = 22$)	Slope ≠ 1.0		
Stages 48–49	***CM***	F(1,23) = 376.5; $P < 0.0001$ ($n = 25$)	Slope ≠ 1.0	F(2,46) = 0.8141; $P = 0.4493$	Single fit
	UM	F(1,23) = 1313; $P < 0.0001$ ($n = 25$)	Slope ≠ 1.0		

Table 7–1: Statistical evaluation of the maximal excitatory MSI -vs- inhibitory MSI relationships after cross-modal and uni-modal stimuli, in both developmental groups.
Left: Statistical test to determine whether the maximal excitatory MSI -vs- inhibitory MSI relationship differs from unity (i.e., Slope = 1.0) for cross-modal and uni-modal pairs, in both developmental groups. *Right*: For both developmental groups, the totality of the data (cross-modal and uni-modal groups combined) are best described by a single linear fit, versus two separate linear fits.

These results suggest that when determined on a cell-by-cell basis, in neither developmental group is the relationship between maximal enhancement (MSI) of excitatory vs. inhibitory conductances dependent on the type of stimulus pairing, supporting the results of comparisons made between data from all inter-stimulus intervals, as in **Figure 25**. These also recapitulate the findings shown in **Figure 26**, that although the enhancement of inhibitory conductances is significantly greater than that of excitatory conductances in the later developmental group, this relationship does not differ between responses to cross-modal and uni-modal stimuli.

***A*: Stages 44–46**

Comparisons		H_0: Slope = 1.0		Single fit for all data	
		H_1: Slope ≠ 1.0		Separate fits, one per data set	
		Results	*Summary*	*Results*	*Summary*
Cross-Modal	***VH***	F(1,9) = 24.86; $P = 0.0008$ ($n = 11$)	Slope ≠ 1.0	F(2,18) = 0.8851; $P = 0.4299$	Single fit
	HV	F(1,9) = 11.34; $P = 0.0083$ ($n = 11$)	Slope ≠ 1.0		
Uni-Modal	***HH***	F(1,9) = 1.475; $P = 0.2554$ ($n = 11$)	Slope = 1.0	F(2,18) = 2.244; $P = 0.1348$	Single fit
	VV	F(1,9) = 34.00; $P = 0.0002$ ($n = 11$)	Slope ≠ 1.0		

***B*: Stages 48–49**

Comparisons		H_0: Slope = 1.0		Single fit for all data	
		H_1: Slope ≠ 1.0		Separate fits, one per data set	
		Results	*Summary*	*Results*	*Summary*
Cross-Modal	***VH***	F(1,11) = 214.3; $P < 0.0001$ ($n = 13$)	Slope ≠ 1.0	F(2,21) = 1.106; $P = 0.3495$	Single fit
	HV	F(1,10) = 31.38; $P = 0.0002$ ($n = 12$)	Slope ≠ 1.0		
Uni-Modal	***HH***	F(1,10) = 930.1; $P < 0.0001$ ($n = 12$)	Slope ≠ 1.0	F(2,21) = 0.6865; $P = 0.5143$	Single fit
	VV	F(1,11) = 32.04; $P = 0.0001$ ($n = 13$)	Slope ≠ 1.0		

Table 7–2: In a each developmental group, the maximal excitatory MSI -vs- inhibitory MSI relationship is evaluated for each sequence of cross-modal stimulation and each pathway, in cases of uni-modal stimulation.
Left: Statistical test to determine whether the maximal excitatory MSI -vs- inhibitory MSI relationship differs from unity (i.e., Slope = 1.0) for cross-modal and uni-modal pairs. *Right*: Evaluation of whether the totality of the data (cross-modal and uni-modal groups combined) can best be described by a single linear fit or two separate linear fits. **A**. Stages 44–46. **B**. Stages 48–49.

Table 7–2 confirms that in both the stages 44–46 (*top*) and stages 48–49 (*bottom*) developmental groups, data sets from the two sequences of cross-modal stimulation (OC→HB and HB→OC) and from the two pathways targeted by uni-modal stimulation (HB→HB and OC→OC) are almost all fit best by linear models with slopes significantly different than 1 (see *left* column). This table also shows that data from the respective sub-types of cross-modal and uni-modal stimuli conform to shared linear fits (see *right* column), within each of the experimental groups examined, and can therefore be considered members of the same functional class in the current analyses.

Contrast Between Enhancement of Synaptic Conductances, and of Spike Count

Critically, the preceding data on the excitatory and inhibitory synaptic inputs to *X. laevis* tectal neurons show no sign of the selectivity for cross-modal stimulus combinations which characterizes the output from the very same populations of cells. For instance, the lack of stimulus-specificity in the development of enhancement indexes (MSI values) for both synaptic conductances (**Fig. 25**) stands in contrast to the decrease in MSI values for spike output after cross-modal pairs, specifically, between the stages 44–46 and stages 48–49 developmental groups (**Figs. 7**; **9a**, **c**; **10**). Furthermore, when direct excitation vs. inhibition relationships are examined in MSI values for synaptic conductance, as in the later developmental group (**Figs. 26**; **27b**), the lack of evidence for stimulus dependence in these relationships diverges from the increase observed in MSI values for spike output after cross-modal pairs, specifically, when $GABA_A$-receptor-mediated inhibitory conductances are blocked at these stages (**Figs. 13**; **15a**, **c**; **16**). These discrepancies between synaptic conductances and neuronal output suggest that the mechanisms

underlying the selective, developmentally-regulated changes in cross-modal sensitivity lie in the subcellular targeting, or postsynaptic integration, of the synaptic inputs a neuron receives from its presynaptic partners.

Inverse Effectiveness in Synaptic Conductances

The phenomenon of inverse effectiveness has been widely deployed to identify selective

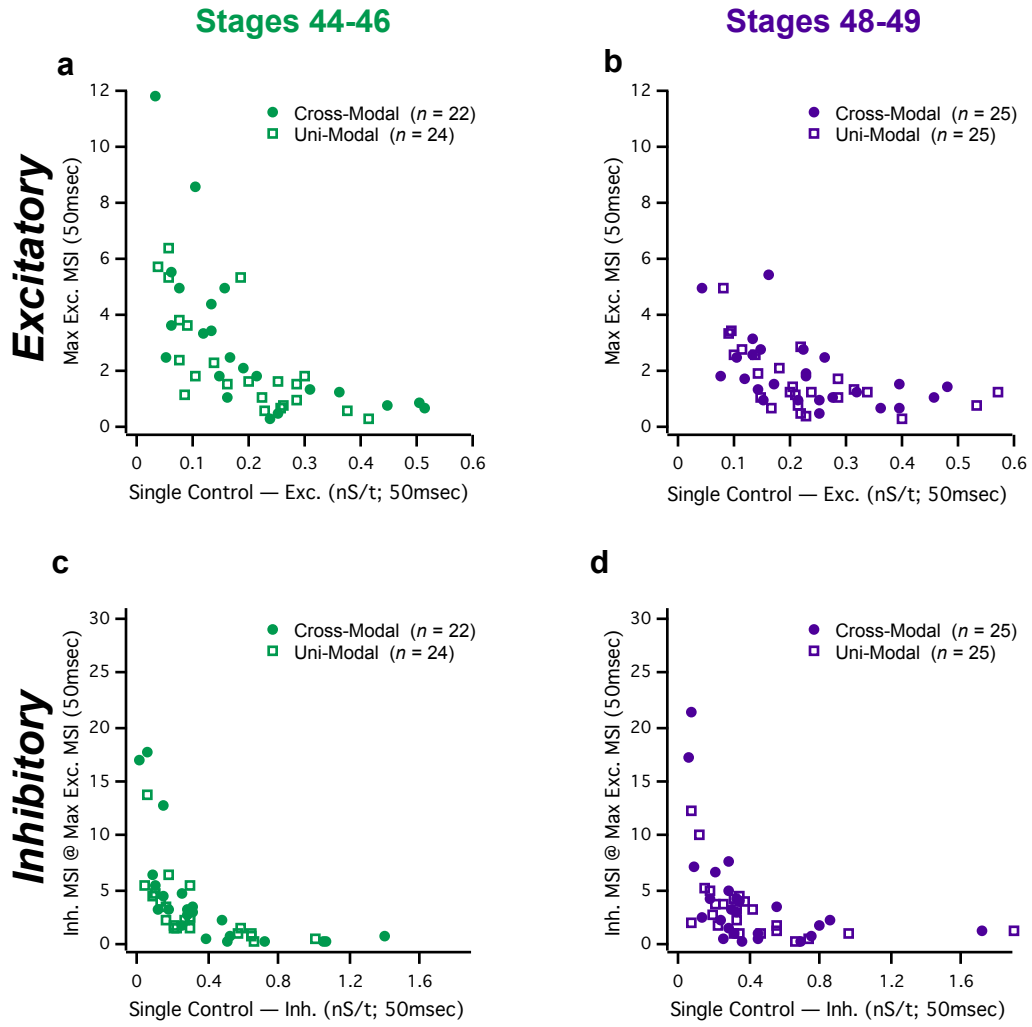

Figure 28: Maximum MSI ratios from excitatory and inhibitory synaptic conductances demonstrate inverse effectiveness, in all conditions examined.
For excitatory synaptic conductances (**a**, **b**), the maximum, trial-averaged MSI ratio (from all ISI's) in each cell is plotted against the baseline conductance, defined as the average synaptic conductance over the first 50 milliseconds after a single pulse is delivered to the modality presented second in the stimulus pair. For inhibitory synaptic conductances (**c**, **d**) the data on the *y*-axis are similar, but here the trial-averaged MSI ratio is taken from the same ISI which evokes the maximal excitatory ratio, in the same cell. Uni-modal and cross-modal data are plotted on the same sets of axes.

cross-modal processing as evidenced in both neuronal output and behavior, but its cellular origins remain unaddressed. I found that, remarkably, inverse effectiveness is present even in the underlying excitatory and inhibitory synaptic conductances, as shown in **Figure 28**. For excitatory conductances (**Fig. 28a**, **b**), for each cell the maximum MSI value calculated is plotted against the raw, trial-averaged conductance observed after a control stimulus, that being a single pulse delivered to the modality presented second in the corresponding stimulus pair. The relationship between MSI and control in inhibitory conductances is visualized similarly (**Fig. 28c**, **d**), but in this case MSI values are taken at whichever ISI evoked the maximal excitatory conductance, in the same cell. All four plots demonstrate inverse effectiveness relationships, indicating that this phenomenon holds for both conductances and in both developmental groups. Although none of the plots show an apparent difference in the distributions of cross-modal and uni-modal data points, this result is consistent with the overlap in inverse effectiveness distributions for neuronal output, for the same two stimulus paradigms (**Fig. 11**). Additionally, the presence of inverse effectiveness in inhibitory synaptic conductances, received exclusively from neurons embedded within the tectal network, indicates that at least in the context of this experimental preparation, fundamental aspects of cross-modal *and* uni-modal multisensory processing derive from polysynaptic interactions within this midbrain structure.

Role of Recurrent Intratectal Connectivity

Literature on OT/SC physiology suggests that the time course of stimulus-driven neuronal activity might indeed be related to intra-tectal connectivity. Experiments in

mammals, for instance, have demonstrated that multisensory stimuli can trigger integrative responses even when their onset times are staggered by up to 200-300ms (Meredith et al., 1987). These data strongly suggest the presence of a gate or a state of persistent activity that is maintained between the first stimulus event and the second, and which is sensitive to the onset of the second stimulus. Recent work in the laboratory has shown that after stimulation of the visual pathway of *Xenopus* tadpoles, recurrent excitatory connections from within the local circuit generate sustained activity in the tectum, persisting during the above period, and that this recurrent excitation is developmentally regulated (Pratt et al., 2008). **Figure 29** describes the stimulus protocol for isolating changes in recurrent excitation. The results described below evaluate whether developmental changes in recurrent excitatory connectivity, co-activated by cross-modal tectal inputs, could potentially explain the maturation of cross-modal sensitivity.

The following experiments assess differential "rundown" of excitatory intra-tectal connections — that is, under pharmacological blockade of $GABA_A$-receptor-mediated inhibition, during repeated stimulation of a given sensory pathway the magnitude of excitatory synaptic charge (current integrated over time) evoked by each successive input steadily decreases (see: Pratt et al., 2008). For synaptic charge integrated over a temporal window that excludes monosynaptic currents, this progressive decrease may reflect synaptic fatigue after repeated activation of the same recurrent excitatory connections. The data below, therefore, address the questions of whether (and the degree to which) cross-modal stimuli activate the same recurrent excitatory circuits, and whether

developmental changes in this cross-activation could help explain the selective, developmentally-regulated changes in sensitivity to cross-modal stimulus pairs.

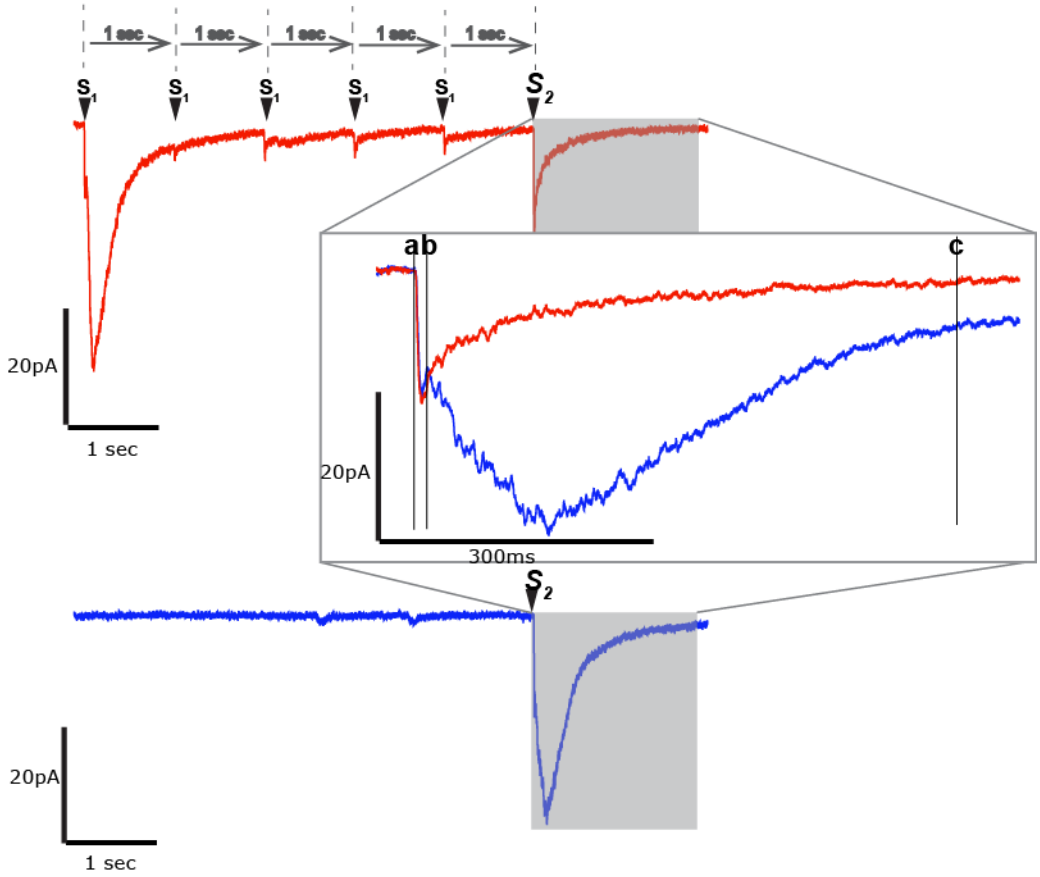

Figure 29: Cross-modal rundown of shared recurrent excitation.
Repeated 1Hz stimulation of one sensory pathway (S_1) selectively reduces the recurrent activity evoked by a second sensory pathway (S_2) (*red trace*), relative to the response evoked by a single, control stimulus (*blue trace*). This effect is highlighted in the inset, where the response to S_2 is largely unchanged in the first 20msec (bounded by vertical lines "a" and "b"), containing monosynaptic activity, but is visibly reduced between 20 and 600msec after the stimulus (bounded by vertical lines "b" and "c"), containing recurrent, polysynaptic activity.

To determine, first, whether data from the two directions/presentation sequences of cross-modal stimulation reveal any differences in the ability of one sensory pathway to influence recurrent circuits activated by the other, the two cross-modal sequences (V→H; H→V) were compared with respect to the ratios for "percent-remaining" synaptic charge in the monosynaptic window ('Early'; 0–20msec.) and in the polysynaptic/recurrent window ('Late'; 20–600msec.). As shown in **Table 8**, no differences were detected in their ability to influence polysynaptic, or recurrent, excitatory connections. For

		Stages 44–46				Stages 48–49			
		Median	*IQR*	*P-value*	*Summary*	*Median*	*IQR*	*P-value*	*Summary*
Early Ratio	***VH***	0.83 (*n* = 7)	0.4	*P* = 0.688	n.s.	0.335 (*n* = 12)	0.4075	*P* = 0.027	*
	HV	0.74 (*n* = 7)	0.18			0.91 (*n* = 12)	0.7925		
Late Ratio	***VH***	0.37 (*n* = 7)	0.29	*P* = 0.938	n.s.	0.235 (*n* = 12)	0.335	*P* = 0.765	n.s.
	HV	0.41 (*n* = 7)	0.36			0.155 (*n* = 12)	0.2775		

Table 8: Comparison between the two cross-modal rundown paradigms — V→H and H→V — at both developmental stages.
No difference in rundown of recurrent, polysynaptic activity in either developmental group (Late integration window; 0–20msec.). Greater rundown of the monosynaptic response for the V→H sequence, in the stages 48–49 developmental group (Early integration window; 20–600msec.). * : $P < 0.05$; n.s. : not significant (Wilcoxon matched-pairs signed rank test).

subsequent analyses, therefore, data derived from both cross-modal sequences, or directions of stimulation, were combined in each developmental group. **Figure 30** directly compares the results of cross-modal rundown across developmental groups. This

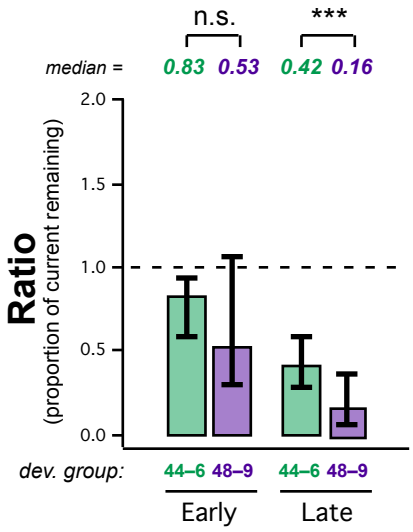

Figure 30: Rundown of polysynaptic recurrent connectivity is significantly greater at stage 48–49.
The proportion of current remaining in the Early (0–20msec.) and Late (20–600msec.) integration windows after cross-modal rundown are compared across developmental group. *** : $P < 0.001$; n.s.: not significant (Mann-Whitney rank-sum test). *stages 44–46*: $n = 19$, *stages 48–49*: $n = 27$.

protocol reveals no significant developmental changes for monosynaptic currents, but instead shows that cross-modal rundown is significantly greater in the stages 48–49 developmental group (Mann-Whitney rank-sum test: $P < 0.001$). These data are therefore consistent with a correlation between recurrent excitatory connectivity and the development of selective responsiveness to cross-modal stimuli. They further suggest that the extent of the recurrent tectal circuitry which can be activated by both sensory modalities increases over development.

DISCUSSION

This work aims to provide new insight into the synaptic and circuit-level mechanisms which underlie multisensory integration in the vertebrate optic tectum / superior colliculus. Using a reduced, *ex-vivo* preparation — the isolated brain of *Xenopus laevis* tadpoles — I provide evidence for the unique integration of cross-modal, versus uni-modal, pairs of inputs by single tectal neurons. As a body of work, this data set addresses synaptic inputs, in measures of conductance, as well as neuronal output, in measures of action potential number and onset latency.

In the preceding text I described how each of these domains of neuronal functionality depends on experimental conditions, and how these dependencies vary between developmental groups. I also highlighted, briefly, instances where the patterns in the observed changes converge for the two classes of neuronal data, and instances in which they diverge. In the following discussion I will: 1) Propose a conceptual model circuit that can account for these relationships between neuronal input and output, under different experimental conditions and in different developmental groups, 2) Explore the ethological utility of the phenomena and mechanisms evident in this model system, relative to what has been shown in mammals, 3) Note the mechanisms that remain unaddressed, or are uncontrolled for, by the experimental paradigms in this work, and 4)

Suggest new hypotheses regarding the mechanisms underlying multisensory integration, based on the knowledge created here.

Several variables influence the enhancement of action potential number by paired stimuli. For example, the maturation of tectal function that occurs between the two developmental groups studied here — stages 44–46 and stages 48–49 — is associated with both significant decreases in maximal response enhancement and a significant change in selectivity for inter-stimulus interval, resulting in narrower tuning, for responses to cross-modal stimulus pairs only. But while a significant, developmentally-regulated decrease in enhancement is found only in cross-modal data, within each developmental group the enhancement index values for responses to cross-modal stimulus pairs consistently appear lower than those to uni-modal stimulus pairs (see *y*-axis range in **Figure 7a** vs. **c**; **b** vs. **d**; **Figure 9a** vs. **c**). The presence of this relationship between uni-modal and cross-modal responses, throughout development, is underscored in **Figure 12**. Here, comparison between cumulative distribution functions of *Z*-scores (**Fig. 12c**, **d**) shows that in cells from both developmental groups responses to uni-modal stimulus pairs are more likely to demonstrate supra-linear integration, whereas responses to cross-modal stimuli are more likely to demonstrate sub-linear integration. Thus for all data on spike count enhancement, in both developmental groups, cross-modal stimulus pairs evoke relatively weaker enhancement than uni-modal pairs. The fact that responsiveness to cross-modal pairs weakens further between the stages 44–46 and stages 48–49 developmental groups suggests that whatever mechanism is responsible for this sub-linear integration becomes stronger, or more effective, as the tadpole develops.

Among candidate mechanisms, $GABA_A$-receptor-mediated synaptic inhibition is known to contribute to receptive field structure in the *X. laevis* tectum (Shen et al., 2011) and over the same developmental stages studied here, change in both its biophysical function (Akerman and Cline, 2006) and its spatiotopic properties (Tao and Poo, 2005). I therefore used the drug picrotoxin to acutely block this inhibitory conductance, at the developmental time point where relative suppression of cross-modal responsiveness is greatest: stages 48–49. As indicated by critical measures of spike count enhancement, this pharmacological treatment eliminates differences between the effectiveness of uni-modal and cross-modal stimulus pairs, by dramatically increasing responsiveness to cross-modal inputs, for the most-effective inter-stimulus interval in each cell (**Figs. 14**, **15**, and **18**) and for a narrow range of similar intervals (see *x*-axes in **Figures 16a**, **b**). These data clearly imply that $GABA_A$-receptor-mediated synaptic inhibition is selectively engaged by, and modulates cellular responses to, cross-modal stimulus pairs.

It would be reasonable to expect, therefore, that after both uni-modal and cross-modal stimulation, direct measurement of excitatory and inhibitory synaptic conductances, in a given cell, would reveal a unique relationship between excitation and inhibition after pairs of cross-modal inputs. However, as exemplified in the distributions of the relationship, determined on a cell-by-cell basis, between the greatest enhancement index value for excitatory conductance and the corresponding index value for inhibitory conductance (i.e., calculated at the same inter-stimulus interval), no distinction can be made between responses to cross-modal and uni-modal inputs, in either developmental

group (**Fig. 27**). Furthermore, for both uni-modal and cross-modal stimulus pairs, enhancement of inhibitory conductances is shown to be even greater than the enhancement observed for excitatory conductances, across all inter-stimulus intervals tested (**Fig. 26**). And it is not, in fact, the relative enhancement of inhibitory conductance that demonstrates a developmental change in this system — direct comparison between stages 44–46 data and stages 48–49 data shown that it is the pair-driven enhancement of excitatory conductances, instead, which demonstrate a decrease over development, and in a qualitatively similar fashion for both uni-modal and cross-modal responses (**Fig. 25**). Thus, enhancement of inhibitory conductances neither varies over tectal maturation nor differentiates between types of stimulus pairs, whereas the pair-driven enhancement of excitatory conductances shows a developmentally-regulated (but non-selective) decrease in strength.

Nevertheless, it is possible to account for these apparent inconsistencies between neuronal inputs and neuronal output by referencing previous findings in the *Xenopus* tadpole model system, aspects of synaptic architecture suggested by modeling studies of multisensory integration, and select assumptions about tectal afferents and intra-tectal connectivity.

For example, the developmental decrease in pair-driven enhancement of excitatory conductances (for both uni-modal *and* cross-modal combinations) appears to contradict developmental studies in mammals, where the progressive refinement of SC receptive fields is associated with the capacity for response enhancement, after paired stimulation

(Wallace and Stein, 1997). Indeed, an analogous developmental refinement of visually-driven receptive fields, specifically, is found for both excitatory and inhibitory conductances — recorded in the same neuron — in the *X. laevis* optic tectum over the same developmental stages examined here (Tao and Poo, 2005).

What likely explains the phenomenological differences in this preparation, then, is the use of bipolar stimulating electrodes to evoke action potentials throughout an afferent pathway (for visual projections, the optic nerve). This stimulation method targets afferents indiscriminately, and by its nature has no selectivity for spatiotopic organization. Each stimulus is therefore considered "whole-field," delivering impulses which carry information about randomly-distributed locations in space. And because the activation patterns evoked in two separate sensory pathways are completely independent, this observation could be particularly relevant for cross-modal stimulus pairs. That is, the likelihood that two successive, probabilistic activations will trigger axons corresponding to the same receptive field location will tend to decrease in concert with the contraction in receptive field size, over the same developmental stages. For a given postsynaptic neuron, therefore, the total excitatory synaptic drive available within its receptive field will tend to decrease, as well.

During stimulation with uni-modal pairs, however, the possibility of some axons being stimulated twice, by each of the component stimuli within the pair, must be considered. This scenario would suggest that the development of presynaptic mechanisms — especially relevant to the repeated activation of a single axon — could play a unique role

in the developmentally-regulated enhancement of conductances after uni-modal pairs, specifically. For example, the developmental increase in vesicle release probability for retino-tectal axons, and the concomitant decrease in paired-pulse facilitation (Aizenman and Cline, 2007), could lead to reduced pair-driven enhancement because any axons activated twice would produce less enhancement after the second stimulus. If many of the same axons are stimulated twice in a given uni-modal pair, the enhancement of total feed-forward excitation by uni-modal stimulus combinations could be significantly affected.

Nevertheless, there is a dissociation between the pathway specificity of these presynaptic mechanisms, which differentiate between retino-tectal and hindbrain-tectal axons, and the widely observed phenomenology of pair-driven integration, which does not differ between the two modality-specific, uni-modal pairs. Regarding presynaptic functionality, previous studies have shown that whereas retino-tectal paired-pulse facilitation (Aizenman and Cline, 2007) and quantal size (Deeg et al., 2009) both decrease over development, no such developmental changes are observed in the hindbrain-tectal projection (Deeg et al., 2009). Yet this differential development of presynaptic function across the two sensory projections is not associated with a similar specificity in the development of multi-modal integration, reflected in the relative enhancement indices for maximal excitatory conductance vs. inhibitory conductance, determined in each cell. As indicated by the statistical comparisons in **Table 7–2**, this relationship does not differ significantly between OC→OC and HB→HB uni-modal pairs, in either developmental group. If pathway-specific development of presynaptic functionality does not lead to any developmental differences in the enhancement of excitatory conductance, when

referenced to the inhibitory conductance recorded in the same cell (which is itself unchanged over development; see **Figure 25**), then the data here would suggest that presynaptic mechanisms play only a minor role, at best, in the phenomenology of pair-driven integration. This scenario would presumably apply equally well to comparisons between responses to uni-modal inputs to the two target pathways, as discussed above, and to comparisons between responses to uni-modal and cross-modal stimulus pairs, generally.

It seems likely, therefore, that the developmental changes in receptive field architecture which I hypothesize to limit the enhancement of excitatory conductances by cross-modal stimulus pairs could also be responsible for the developmental decrease in excitatory enhancement after uni-modal pairs, as well. Thus, although the repetitive activation of some number of axons remains a possibility during the pairs of uni-modal inputs used in these experiments, as well, the data suggest that the spatiotopic distributions of within-modality receptive fields activated by successive stimuli are approximately random, to the point that their overlap is similar to the overlap between randomly-activated cross-modal fields. A decrease in receptive field overlap at the later developmental stages could thereby lead to observable decreases in pair-driven enhancement of feed-forward excitation, after both uni-modal *and* cross-modal stimulus combinations.

But because this developmental decrease in enhancement of excitatory conductances occurs for both categories of paired stimulation (cross-modal *and* uni-modal), it does not help explain the relative suppression of neuronal responses to cross-modal pairs,

specifically, across all developmental stages in this study (see **Figure 12**; see also *y*-axis range in **Figures 7a** vs. **c**; **b** vs. **d**; **Fig. 9a** vs. **c**). And although the acute pharmacological blockade of synaptic inhibition abolishes this differential sensitivity — by selectively increasing cross-modal responsiveness and leaving output to uni-modal pairs unchanged (**Figs. 14**, **15**, and **18**) — no such differential sensitivity is detected in the enhancement indices for inhibitory conductances, in either developmental group (**Fig. 25b**, **d**). What these measures of synaptic conductance cannot address, however, is the manner in which these synaptic inputs might interact, postsynaptically. Indeed, the voltage-clamp method used to record conductances prevents (by definition) voltage-dependent interactions between these inputs, and does not reveal any information about their relative positions within and across the electrotonic compartments of the postsynaptic tectal neuron, which sets fundamental parameters for both their interaction and their contribution to neuronal output (Koch, 1999).

Nevertheless, theoretical and modeling studies on the biological basis of multisensory integration have suggested that differential subcellular localization of modality-specific feed-forward excitation and inhibition could explain how the synaptic conductances I observe here generate the patterns evident in neuronal output. Specifically, in series of models first introduced by Cuppini and colleagues (2010), feed-forward excitation derived from first-order sensory systems segregates by modality onto distinct, electrotonically-isolated dendritic compartments of the postsynaptic tectal neuron, which only converge at or near the point of action potential generation. Furthermore, a critical component of these models is cross-inhibition of these feed-forward excitatory inputs —

feed-forward inhibition driven, exclusively, by one first-order pathway targets only the dendrites that receive excitation from the opposite first-order pathway, and in that manner shunt the excitation derived from cross-modal sources (see: Koch, 1999).

The basic connections and structures noted here would thus describe how the synaptic conductances reported in my data could underlie the stimulus selectivity I observe in cellular output. For instance, during stimulation with a cross-modal stimulus sequence, the first input will excite both its recipient dendrite on the postsynaptic neuron and also an inhibitory neuron that, in turn, targets the dendrite which receives first-order projections from the opposite sensory modality. If the cross-modal excitatory input then arrives at its recipient dendrite at a time when this feed-forward inhibitory influence is present, its effect on local postsynaptic voltage in that dendritic compartment will be reduced, as will be the output of that compartment for downstream summation with the first of the two inputs. The temporal alignment of these excitatory and inhibitory influences would likely depend on the inter-stimulus interval, as well. For uni-modal stimulus sequences, in contrast, the convergence of first-order inputs onto the same electrotonic compartment would allow for compounding, or facilitation, of membrane voltage in the absence of feed-forward inhibition, which is directed to the other dendrite.

This architecture can also explain the changes in neuronal output observed when inhibitory synapses are blocked pharmacologically: whereas the integration of uni-modal input sequences does not depend on synaptic inhibition under normal physiological conditions, and therefore would not change in its absence, cross-modal enhancement is

highly constrained by inhibitory inputs in this model, and would be expected to increase if those inputs were blocked. Indeed, the finding that, when synaptic inhibition is blocked, maximal enhancement of responses to cross-modal pairs reaches a level nearly equal to what is observed for uni-modal pairs (**Figs. 13**, **15a**, **c**, **18**) suggests that this model is fundamentally capable of postsynaptic facilitation between excitatory inputs to separate dendritic compartments, as well as those to the same dendritic compartment, but that cross-inhibition acts specifically to suppress this function.

Some aspects of the feed-forward inhibition proposed by Cuppini et al. (2010) are not consistent with observations in this preparation, and must be amended for consideration here. Specifically, these authors put forth two dedicated, non-overlapping populations of inhibitory neurons that each receives its first-order inputs from only one sensory modality. In intracellular recordings made in the *X. laevis* tectum, however, nearly all cells receive a short-latency, monosynaptic input after stimulation of either pathway. And because inhibitory neurons are distributed within the cell body layer at the location of these recordings (Miraucourt et al., 2012), and cannot be identified visually, it must be assumed that all data apply equally to GABA-ergic interneurons and glutamatergic cells. Therefore, I would propose that cross-modal specificity in feed-forward inhibition be maintained by a rule where the postsynaptic target of each inhibitory neuron corresponds to the modality from which they receive the weakest first-order excitation. To maintain a spatiotopic organization of inhibition, GABA-ergic interneurons would receive inputs from the same first-order axons as their nearest glutamatergic neighbors, and in turn make local connections only, with cells that receive the same ascending processes. These

local connections, then, could participate in the developmental processes that align inhibitory receptive fields with excitatory receptive fields, as they both refine and contract over the same stages examined here (Tao and Poo, 2005).

Multi-modal recurrent circuits, engaged specifically by pairs of unlike inputs and shown to grow more robust over these stages of development (**Fig. 30**), could also contribute to the synaptic conductances recorded in these experiments. Indeed, even though enhancement indices for excitatory and inhibitory conductances are calculated only over the first 50msec after the second stimulus in a cross-modal or uni-modal pair, conductances integrated in this window would still reflect the influence of recurrent activity, initiated by the first stimulus in the pair and persisting in the tectal circuit through the inter-stimulus interval. And although the blockade of synaptic inhibition is required to fully expose excitatory recurrent connectivity, recurrent excitation may ultimately drive inhibitory neurons, as well. This leaves open the possibility that under normal physiological conditions, these excitatory connections could be balanced in some manner by reciprocal, feed-back inhibition.

Indeed, despite the evidence for greater excitatory interconnectivity between the targets of cross-modal stimulation (**Fig. 30**), there is no indication that this leads to the differential enhancement of excitatory conductance by cross-modal pairs, versus uni-modal pairs (**Fig. 26**). In contrast, pair-driven enhancement of excitation actually decreases over development, and equally for cross-modal and uni-modal pairs (**Fig. 25a**, **c**). Some aspects of the data, however, could suggest that an important function of

recurrent activity is to activate, and thereby link, otherwise disparate groups of inhibitory interneurons. If the proposed link between receptive field contraction and reduction in pair-driven enhancement over development also applies to feed-forward inhibition, as it does to feed-forward excitation, then this developmental effect should be seen in **Figure 25b**, **d**. The fact that inhibitory enhancement is shown to remain constant over development indicates that either: 1) receptive field refinement does not, in fact, equivalently affect excitatory and inhibitory enhancement, or 2) later in development an additional inhibitory influence, not dependent on local spatiotopic factors, is recruited by paired stimulation. In the second scenario, this additional inhibitory influence could driven by recurrent excitatory connections that act upon local inhibitory interneurons.

The fact these developmental changes concern recurrent activity initiated by cross-modal stimulus pairs, particularly, does not preclude its involvement in synaptic activity initiated by uni-modal pairs. Indeed, because the relationships between conductances measured after uni-modal and cross-modal pairs do not differ in any qualitative fashion, there is no evidence to suggest that responses to these two classes of stimuli are mediated by non-overlapping networks in the tectum. Thus, the finding that enhancement of inhibitory conductances after uni-modal stimuli, as well, remains unchanged over development (**Fig. 25d**) could reflect the influence of non-specific feed-back inhibition, which although driven best by cross-modal combinations, may yet be consistent with the second the two scenarios proposed for the findings in **Figure 25**, as described above.

The selective, developmentally-regulated suppression of cross-modal responsiveness in

these experiments, associated with a unique contribution from $GABA_A$-receptor-mediated synaptic inhibition, represents a departure from results reported for *in-vivo* experiments in mammals. Specifically, I see that the average magnitude of cross-modal response enhancement decreases over development, rather than an increases (Wallace and Stein, 1997), and that relative to enhancement from uni-modal stimulus pairs, pair-driven enhancement after cross-modal stimulation is weaker, not stronger (Alvarado et al., 2007b).

Another possible explanation lies in the nature of the *ex-vivo* preparation itself: it is cut off from the sensory organs and systems which endogenously provide feed-forward excitation to the brain, as the animal traverses its environment. With these sources of excitatory drive removed, the brain might be left in a relatively quiescent state. And in comparison to the degree of background synaptic excitation observed in *in-vivo* preparations in the laboratory (Dong and Aizenman, 2012; Dong et al., 2009; Khakhalin et al., 2014), a degree of hypo-activity can be seen in the background excitation received by tectal neurons within an isolated brain (for example, see: Bell et al., 2011). This might leave an imbalance of synaptic inhibition, given that its magnitude and dynamic properties have been developed in the context of an intact animal. However, quiescence in the baseline activity of tectal neurons themselves is inversely correlated with the magnitude of enhancement seen in their cross-modal pair-induced responses (Perrault et al., 2003). It is important to note that in both the intact animal and isolated brain, at least some background excitation represents the output of excitatory neurons within the tectal population itself. The relatively lower background excitation in the isolated brain could

therefore reflect a decrease in the spontaneous activity of neurons residing within the tectum. As such, it leaves open the possibility that these neurons should be able to generate greater cross-modal enhancement in the conditions of this preparation, not less — this capability would lend even greater weight to the selective suppression of cross-modal responses that is seen in the data.

In support of the functional relevance of the findings in this study, antagonism between cross-modal stimuli has recently been found at the behavioral level in *X. laevis* tadpoles, at the same developmental stages in this study, in their orienting responses (Simmons et al., 2015). As shown in this report, the presence of discreet visual cues decreases the accuracy of, and increases the latency to, their rheotaxis (body orientation into a directional current) relative to what is seen under conditions of single-modality stimulation, that is, a purely mechanosensory environment without visual stimuli. These findings complement my data on tectal responsiveness under cross-modal stimulation and support the notion that in the premetamorphic tadpole, cross-modal stimuli suppress function, rather than enhance it.

If the results described here are indeed valid, though, they raise two important questions about tectal function: first, why this species develops with cross-modal inputs to tectal neurons, if those inputs only disrupt behavior, and second, how effective behavioral responses can be generated at all, under such conditions. Indeed, a study of cross-modal, experience-dependent plasticity at the stages examined here reinforces the robust nature

of these cross-modal inputs by describing how tectal neurons express homeostatic changes that maintain cross-modal synaptic drive, rather than select for inputs from the stronger of the two sensory pathways (Deeg and Aizenman, 2011), as would be expected from a purely Hebbian response.

One possible explanation could be that it is energetically more favorable, in the tadpole, to have the one circuit mediate responses to two sensory modalities — with the supposition that behaviorally-relevant information would not be present simultaneously, at the same spatiotopic position, in the two modalities. The behavioral characteristics of *X. laevis* tadpoles would seem to support this conclusion. Their repertoire of routine visually-guided behaviors is limited, as they scavenge food as it is encountered (not engaging in tracking behavior that might rely on vision) and are nocturnal in the wild. Although tadpoles do use vision to avoid and evade dark objects (Dong et al., 2009; Khakhalin et al., 2014), these responses may be associated with such close-range, immediate avoidance that the relevant visual information is very strong, and there would be no additional information to be gained by incorporating cross-modal, mechanosensory signals.

Decisive experiments are therefore necessary to determine how, in face the ongoing cross-modal stimulation that characterizes most naturally-occurring environments, a tadpole can maintain appropriate responses to both appetitive and aversive stimuli. Surely, if the patterns of activity in an animal's cross-modal pathways were to continuously suppress the output of each tectal neuron that receives such inputs, all adaptive behaviors

— to each sensory modality — would be compromised.

One possible outcome is that real-time behavioral responses to uni-modal information both modalities are mediated by the 'switching' of tectal neurons, and their local tectal circuits, to transmit information about the modality which carries the strongest, or most salient, stimulus at a particular spatiotopic location, on a moment-to-moment basis. Ambiguous or unchanging cross-modal environments might not allow for or maintain such transient uni-modal selectivity, and therefore create suppressive effects, similar to what is reported above. This mechanistic principle would therefore appear to be at least partially reflected in the predicted "winner-take-all" responses of collicular neurons upon stimulation with paired heterologous inputs, in the absence of cortical influence, as seen in the formalized computational models of Cuppini and colleagues (2012; 2010). These are the same models from which the candidate conceptual mechanism for cross-modal suppression in *X. laevis* tadpoles was derived, above. The alternative outcome, therefore, represents a scenario in which the output of tectal neurons in changeable cross-modal conditions does, in fact, remain suppressed relative what would be observed in an experimentally-controlled, uni-modal environment. However, while in this case the absolute magnitude of response enhancement might not be instructive, it remains possible that unique information carried in other aspects of each neuron's responses could allow a downstream cell population, further along the output pathway in the tectum or elsewhere, to decode this information and thus direct an adaptive behavior.

These two possibilities can be readily distinguished in the tadpole tectum, either *in-vivo*

or *ex-vivo*, by using techniques currently deployed in the laboratory. For example, members of the group have used a CCD camera to detect changes in signal from a membrane-permeable, calcium-sensitive fluorescence indicator at a rate of 125 frames per second, and then an empirically-determined and systematized method to reconstruct action potentials with the relatively low timing error of 0 – 16 milliseconds (Khakhalin et al., 2014; Xu et al., 2011). When deployed to record concurrent spike output from the 30–90 cells in a given imaging area, this technique is well-suited to collect data on how tectal neurons evolve their responses relative to each other, and how these stimulus-driven relationships change on a moment-to-moment basis. Thus, experiments conducted with this method would be able to detect both of the distinct, but not mutually-exclusive, possibilities suggested above: that the magnitude of spike count enhancement is uniformly suppressed by cross-modal stimulus pairs, with potentially more information in other aspects of their output (such as temporal patterns, for example), and that relative sensitivity within this population might change such that some neurons become more responsive to one or the other modality during the course of ongoing, variable cross-modal stimulation.

CONCLUSIONS

Taken as whole, then, this body of work reveals relationships between synaptic conductances and neuronal output in the context of a powerful sensory phenomenon, evident across species in both behavior and neural properties, for which the synaptic and circuit-level mechanisms were entirely unknown. And, in utilizing a reduced preparation and simple stimuli, this study achieves a broader reach and deeper impact than any report from a more specialized system.

My hope is that these fundamental strengths allow these data to serve as a foundational reference for vertebrate researchers working in diverse species, and with a wide array of experimental paradigms, in the ongoing effort to expand our insight into this core principle for the biological basis of perception — multisensory integration.

BIBLIOGRAPHY

Aizenman, C.D., and Cline, H.T. (2007). Enhanced visual activity in vivo forms nascent synapses in the developing retinotectal projection. J Neurophysiol *97*, 2949-2957.

Akerman, C.J., and Cline, H.T. (2006). Depolarizing GABAergic conductances regulate the balance of excitation to inhibition in the developing retinotectal circuit in vivo. J Neurosci *26*, 5117-5130.

Alvarado, J.C., Stanford, T.R., Rowland, B.A., Vaughan, J.W., and Stein, B.E. (2009). Multisensory integration in the superior colliculus requires synergy among corticocollicular inputs. J Neurosci *29*, 6580-6592.

Alvarado, J.C., Stanford, T.R., Vaughan, J.W., and Stein, B.E. (2007a). Cortex mediates multisensory but not unisensory integration in superior colliculus. J Neurosci *27*, 12775-12786.

Alvarado, J.C., Vaughan, J.W., Stanford, T.R., and Stein, B.E. (2007b). Multisensory versus unisensory integration: contrasting modes in the superior colliculus. J Neurophysiol *97*, 3193-3205.

Anastasio, T.J., and Patton, P.E. (2003). A two-stage unsupervised learning algorithm reproduces multisensory enhancement in a neural network model of the corticotectal system. J Neurosci *23*, 6713-6727.

Anastasio, T.J., Patton, P.E., and Belkacem-Boussaid, K. (2000). Using Bayes' rule to model multisensory enhancement in the superior colliculus. Neural Comput *12*, 1165-1187.

Behrend, O., Branoner, F., Zhivkov, Z., and Ziehm, U. (2006). Neural responses to water surface waves in the midbrain of the aquatic predator Xenopus laevis laevis. Eur J Neurosci *23*, 729-744.

Bell, M.R., Belarde, J.A., Johnson, H.F., and Aizenman, C.D. (2011). A neuroprotective role for polyamines in a Xenopus tadpole model of epilepsy. Nat Neurosci *14*, 505-512.

Binns, K.E., and Salt, T.E. (1996). Importance of NMDA receptors for multimodal integration in the deep layers of the cat superior colliculus. J Neurophysiol *75*, 920-930.

Bolognini, N., Leo, F., Passamonti, C., Stein, B.E., and Ladavas, E. (2007). Multisensory-mediated auditory localization. Perception *36*, 1477-1485.

Cardin, J.A., Palmer, L.A., and Contreras, D. (2008). Cellular mechanisms underlying stimulus-dependent gain modulation in primary visual cortex neurons in vivo. Neuron *59*, 150-160.

Cuppini, C., Magosso, E., Rowland, B., Stein, B., and Ursino, M. (2012). Hebbian mechanisms help explain development of multisensory integration in the superior colliculus: a neural network model. Biol Cybern *106*, 691-713.

Cuppini, C., Ursino, M., Magosso, E., Rowland, B.A., and Stein, B.E. (2010). An emergent model of multisensory integration in superior colliculus neurons. Front Integr Neurosci *4*, 6.

Deeg, K.E., and Aizenman, C.D. (2011). Sensory modality-specific homeostatic plasticity in the developing optic tectum. Nat Neurosci *14*, 548-550.

Deeg, K.E., Sears, I.B., and Aizenman, C.D. (2009). Development of multisensory convergence in the Xenopus optic tectum. J Neurophysiol *102*, 3392-3404.

Diederich, A., and Colonius, H. (2004). Bimodal and trimodal multisensory enhancement: effects of stimulus onset and intensity on reaction time. Percept Psychophys *66*, 1388-1404.

Dong, W., and Aizenman, C.D. (2012). A competition-based mechanism mediates developmental refinement of tectal neuron receptive fields. J Neurosci *32*, 16872-16879.

Dong, W., Lee, R.H., Xu, H., Yang, S., Pratt, K.G., Cao, V., Song, Y.K., Nurmikko, A., and Aizenman, C.D. (2009). Visual avoidance in Xenopus tadpoles is correlated with the maturation of visual responses in the optic tectum. J Neurophysiol *101*, 803-815.

Doubell, T.P., Skaliora, I., Baron, J., and King, A.J. (2003). Functional connectivity between the superficial and deeper layers of the superior colliculus: an anatomical substrate for sensorimotor integration. J Neurosci *23*, 6596-6607.

Drager, U.C., and Hubel, D.H. (1975a). Physiology of visual cells in mouse superior colliculus and correlation with somatosensory and auditory input. Nature *253*, 203-204.

Drager, U.C., and Hubel, D.H. (1975b). Responses to visual stimulation and relationship between visual, auditory, and somatosensory inputs in mouse superior colliculus. J Neurophysiol *38*, 690-713.

Drager, U.C., and Hubel, D.H. (1976). Topography of visual and somatosensory projections to mouse superior colliculus. J Neurophysiol *39*, 91-101.

Edwards, C.J., and Kelley, D.B. (2001). Auditory and lateral line inputs to the midbrain of an aquatic anuran: neuroanatomic studies in Xenopus laevis. J Comp Neurol *438*, 148-162.

Fetsch, C.R., DeAngelis, G.C., and Angelaki, D.E. (2013). Bridging the gap between theories of sensory cue integration and the physiology of multisensory neurons. Nat Rev Neurosci *14*, 429-442.

Gaze, R.M., Chung, S.H., and Keating, M.J. (1972). Development of the retinotectal projection in Xenopus. Nat New Biol *236*, 133-135.

Gaze, R.M., Keating, M.J., and Chung, S.H. (1974). The evolution of the retinotectal map during development in Xenopus. Proc R Soc Lond B Biol Sci *185*, 301-330.

Ghose, D., Barnett, Z.P., and Wallace, M.T. (2012). Impact of response duration on multisensory integration. J Neurophysiol *108*, 2534-2544.

Ghose, D., Maier, A., Nidiffer, A., and Wallace, M.T. (2014). Multisensory response modulation in the superficial layers of the superior colliculus. J Neurosci *34*, 4332-4344.

Ghose, D., and Wallace, M.T. (2014). Heterogeneity in the spatial receptive field architecture of multisensory neurons of the superior colliculus and its effects on multisensory integration. Neuroscience *256*, 147-162.

Graybiel, A.M. (1975). Anatomical organization of retinotectal afferents in the cat: an autoradiographic study. Brain Res *96*, 1-23.

Graziano, M.S., and Gross, C.G. (1998). Spatial maps for the control of movement. Curr Opin Neurobiol *8*, 195-201.

Hardy, O., Leresche, N., and Jassik-Gerschenfeld, D. (1985). Morphology and laminar distribution of electrophysiologically identified cells in the pigeon's optic tectum: an intracellular study. J Comp Neurol *233*, 390-404.

Harting, J.K., and Van Lieshout, D.P. (1991). Spatial relationships of axons arising from the substantia nigra, spinal trigeminal nucleus, and pedunculopontine tegmental nucleus within the intermediate gray of the cat superior colliculus. J Comp Neurol *305*, 543-558.

Hecht, D., Reiner, M., and Karni, A. (2008a). Enhancement of response times to bi- and tri-modal sensory stimuli during active movements. Experimental brain research *185*, 655-665.

Hecht, D., Reiner, M., and Karni, A. (2008b). Multisensory enhancement: gains in choice and in simple response times. Experimental brain research *189*, 133-143.

Higley, M.J., and Contreras, D. (2006). Balanced excitation and inhibition determine spike timing during frequency adaptation. J Neurosci *26*, 448-457.

Hiramoto, M., and Cline, H.T. (2009). Convergence of multisensory inputs in Xenopus tadpole tectum. Dev Neurobiol *69*, 959-971.

Holt, C.E. (1989). A single-cell analysis of early retinal ganglion cell differentiation in Xenopus: from soma to axon tip. J Neurosci *9*, 3123-3145.

Jay, M.F., and Sparks, D.L. (1987). Sensorimotor integration in the primate superior colliculus. II. Coordinates of auditory signals. J Neurophysiol *57*, 35-55.

Jiang, W., Jiang, H., Rowland, B.A., and Stein, B.E. (2007). Multisensory orientation behavior is disrupted by neonatal cortical ablation. J Neurophysiol *97*, 557-562.

Jiang, W., Jiang, H., and Stein, B.E. (2002). Two corticotectal areas facilitate multisensory orientation behavior. J Cogn Neurosci *14*, 1240-1255.

Jiang, W., and Stein, B.E. (2003). Cortex controls multisensory depression in superior colliculus. J Neurophysiol *90*, 2123-2135.

Jiang, W., Wallace, M.T., Jiang, H., Vaughan, J.W., and Stein, B.E. (2001). Two cortical areas mediate multisensory integration in superior colliculus neurons. J Neurophysiol *85*, 506-522.

Khakhalin, A.S., Koren, D., Gu, J., Xu, H., and Aizenman, C.D. (2014). Excitation and inhibition in recurrent networks mediate collision avoidance in Xenopus tadpoles. Eur J Neurosci *40*, 2948-2962.

Knudsen, E.I. (1982). Auditory and visual maps of space in the optic tectum of the owl. J Neurosci *2*, 1177-1194.

Knudsen, E.I. (1983). Early auditory experience aligns the auditory map of space in the optic tectum of the barn owl. Science *222*, 939-942.

Knudsen, E.I. (2002). Instructed learning in the auditory localization pathway of the barn owl. Nature *417*, 322-328.

Knudsen, E.I., and Brainard, M.S. (1991). Visual instruction of the neural map of auditory space in the developing optic tectum. Science *253*, 85-87.

Knudsen, E.I., du Lac, S., and Esterly, S.D. (1987). Computational maps in the brain. Annu Rev Neurosci *10*, 41-65.

Knudsen, E.I., and Knudsen, P.F. (1983). Space-mapped auditory projections from the inferior colliculus to the optic tectum in the barn owl (Tyto alba). J Comp Neurol *218*, 187-196.

Koch, C. (1999). Biophysics of computation : information processing in single neurons (New York, Oxford University Press).

Lázár, G. (1973). The development of the optic tectum in Xenopus laevis: a Golgi study. J Anat *116*, 347-355.

Lee, C., Rohrer, W.H., and Sparks, D.L. (1988). Population coding of saccadic eye movements by neurons in the superior colliculus. Nature *332*, 357-360.

Lee, P.H., Helms, M.C., Augustine, G.J., and Hall, W.C. (1997). Role of intrinsic synaptic circuitry in collicular sensorimotor integration. Proc Natl Acad Sci U S A *94*, 13299-13304.

Lippert, M., Logothetis, N.K., and Kayser, C. (2007). Improvement of visual contrast detection by a simultaneous sound. Brain Res *1173*, 102-109.

Lowe, D.A. (1986). Organisation of lateral line and auditory areas in the midbrain of Xenopus laevis. J Comp Neurol *245*, 498-513.

Luksch, H. (2003). Cytoarchitecture of the avian optic tectum: neuronal substrate for cellular computation. Rev Neurosci *14*, 85-106.

Mainen, Z.F., and Sejnowski, T.J. (1995). Reliability of spike timing in neocortical neurons. Science *268*, 1503-1506.

May, P.J. (2006). The mammalian superior colliculus: laminar structure and connections. Prog Brain Res *151*, 321-378.

Meredith, M.A., and King, A.J. (2004). Spatial distribution of functional superficial-deep connections in the adult ferret superior colliculus. Neuroscience *128*, 861-870.

Meredith, M.A., Nemitz, J.W., and Stein, B.E. (1987). Determinants of multisensory integration in superior colliculus neurons. I. Temporal factors. J Neurosci *7*, 3215-3229.

Meredith, M.A., and Stein, B.E. (1983). Interactions among converging sensory inputs in the superior colliculus. Science *221*, 389-391.

Meredith, M.A., and Stein, B.E. (1985). Descending efferents from the superior colliculus relay integrated multisensory information. Science *227*, 657-659.

Meredith, M.A., and Stein, B.E. (1986a). Spatial factors determine the activity of multisensory neurons in cat superior colliculus. Brain Res *365*, 350-354.

Meredith, M.A., and Stein, B.E. (1986b). Visual, auditory, and somatosensory convergence on cells in superior colliculus results in multisensory integration. J Neurophysiol *56*, 640-662.

Meredith, M.A., and Stein, B.E. (1996). Spatial determinants of multisensory integration in cat superior colliculus neurons. J Neurophysiol *75*, 1843-1857.

Miraucourt, L.S., Silva, J.S., Burgos, K., Li, J., Abe, H., Ruthazer, E.S., and Cline, H.T. (2012). GABA expression and regulation by sensory experience in the developing visual system. PLoS One *7*, e29086.

Munoz, A., Munoz, M., Gonzalez, A., and Ten Donkelaar, H.J. (1995). Anuran dorsal column nucleus: organization, immunohistochemical characterization, and fiber connections in Rana perezi and Xenopus laevis. J Comp Neurol *363*, 197-220.

Nieuwkoop, P.D., and Faber, J. (1956). Normal Table of Xenopus laevis (Daudin) (New York, Garland).

Patton, P.E., and Anastasio, T.J. (2003). Modeling cross-modal enhancement and modality-specific suppression in multisensory neurons. Neural Comput *15*, 783-810.

Perrault, T.J., Jr., Vaughan, J.W., Stein, B.E., and Wallace, M.T. (2003). Neuron-specific response characteristics predict the magnitude of multisensory integration. J Neurophysiol *90*, 4022-4026.

Pratt, K.G., and Aizenman, C.D. (2007). Homeostatic regulation of intrinsic excitability and synaptic transmission in a developing visual circuit. J Neurosci *27*, 8268-8277.

Pratt, K.G., and Aizenman, C.D. (2009). Multisensory integration in mesencephalic trigeminal neurons in Xenopus tadpoles. J Neurophysiol *102*, 399-412.

Pratt, K.G., Dong, W., and Aizenman, C.D. (2008). Development and spike timing-dependent plasticity of recurrent excitation in the Xenopus optic tectum. Nat Neurosci *11*, 467-475.

Richards, B.A., Voss, O.P., and Akerman, C.J. (2010). GABAergic circuits control stimulus-instructed receptive field development in the optic tectum. Nat Neurosci *13*, 1098-1106.

Roberts, A., Feetham, B., Pajak, M., and Teare, T. (2009). Responses of hatchling Xenopus tadpoles to water currents: first function of lateral line receptors without cupulae. J Exp Biol *212*, 914-921.

Robinson, D.A. (1972). Eye movements evoked by collicular stimulation in the alert monkey. Vision Res *12*, 1795-1808.

Rowland, B.A., Quessy, S., Stanford, T.R., and Stein, B.E. (2007a). Multisensory integration shortens physiological response latencies. J Neurosci *27*, 5879-5884.

Rowland, B.A., Stanford, T.R., and Stein, B.E. (2007b). A model of the neural mechanisms underlying multisensory integration in the superior colliculus. Perception *36*, 1431-1443.

Rowland, B.A., and Stein, B.E. (2007). Multisensory integration produces an initial response enhancement. Front Integr Neurosci *1*, 4.

Rowland, B.A., and Stein, B.E. (2014). A model of the temporal dynamics of multisensory enhancement. Neurosci Biobehav Rev *41*, 78-84.

Rudolph, M., Pospischil, M., Timofeev, I., and Destexhe, A. (2007). Inhibition determines membrane potential dynamics and controls action potential generation in awake and sleeping cat cortex. J Neurosci *27*, 5280-5290.

Shen, W., Da Silva, J.S., He, H., and Cline, H.T. (2009). Type A GABA-receptor-dependent synaptic transmission sculpts dendritic arbor structure in Xenopus tadpoles in vivo. J Neurosci *29*, 5032-5043.

Shen, W., McKeown, C.R., Demas, J.A., and Cline, H.T. (2011). Inhibition to excitation ratio regulates visual system responses and behavior in vivo. J Neurophysiol *106*, 2285-2302.

Simmons, A.M., Warnecke, M., Vu, T.T., and Smith, A.T. (2015). Flow sensing in developing Xenopus laevis is disrupted by visual cues and ototoxin exposure. J Comp Physiol A Neuroethol Sens Neural Behav Physiol *201*, 215-233.

Skaliora, I., Doubell, T.P., Holmes, N.P., Nodal, F.R., and King, A.J. (2004). Functional topography of converging visual and auditory inputs to neurons in the rat superior colliculus. J Neurophysiol *92*, 2933-2946.

Sparks, D.L. (1986). Translation of sensory signals into commands for control of saccadic eye movements: role of primate superior colliculus. Physiol Rev *66*, 118-171.

Stanford, T.R., Quessy, S., and Stein, B.E. (2005). Evaluating the operations underlying multisensory integration in the cat superior colliculus. J Neurosci *25*, 6499-6508.

Stein, B.E. (1984). Development of the superior colliculus. Annu Rev Neurosci *7*, 95-125.

Stein, B.E., Huneycutt, W.S., and Meredith, M.A. (1988). Neurons and behavior: the same rules of multisensory integration apply. Brain Res *448*, 355-358.

Stein, B.E., Labos, E., and Kruger, L. (1973). Sequence of changes in properties of neurons of superior colliculus of the kitten during maturation. J Neurophysiol *36*, 667-679.

Stein, B.E., Meredith, M.A., Huneycutt, W.S., and McDade, L. (1989). Behavioral Indices of Multisensory Integration: Orientation to Visual Cues is Affected by Auditory Stimuli. J Cogn Neurosci *1*, 12-24.

Stein, B.E., and Stanford, T.R. (2008). Multisensory integration: current issues from the perspective of the single neuron. Nat Rev Neurosci *9*, 255-266.

Stein, B.E., Stanford, T.R., Ramachandran, R., Perrault, T.J., Jr., and Rowland, B.A. (2009). Challenges in quantifying multisensory integration: alternative criteria, models, and inverse effectiveness. Exp Brain Res *198*, 113-126.

Straznicky, K., and Gaze, R.M. (1972). The development of the tectum in Xenopus laevis: an autoradiographic study. J Embryol Exp Morphol *28*, 87-115.

Székely, G., and Lázár, G. (1976). Cellular and synaptic architecture of the optic tectum. In Frog Neurobiology, R. Llinás, and W. Precht, eds. (Berlin, Springer-Verlag), pp. 407-434.

Tao, H.W., and Poo, M.M. (2005). Activity-dependent matching of excitatory and inhibitory inputs during refinement of visual receptive fields. Neuron *45*, 829-836.

Tsurudome, K., Li, X., and Matsumoto, N. (2005). Intracellular and current source density analyses of somatosensory input to the optic tectum of the frog. Brain Res *1064*, 32-41.

Wallace, M.T., Meredith, M.A., and Stein, B.E. (1993). Converging influences from visual, auditory, and somatosensory cortices onto output neurons of the superior colliculus. J Neurophysiol *69*, 1797-1809.

Wallace, M.T., and Stein, B.E. (1997). Development of multisensory neurons and multisensory integration in cat superior colliculus. J Neurosci *17*, 2429-2444.

Wallace, M.T., and Stein, B.E. (2000). Onset of cross-modal synthesis in the neonatal superior colliculus is gated by the development of cortical influences. J Neurophysiol *83*, 3578-3582.

Wallace, M.T., and Stein, B.E. (2007). Early experience determines how the senses will interact. J Neurophysiol *97*, 921-926.

Wehr, M., and Zador, A.M. (2003). Balanced inhibition underlies tuning and sharpens spike timing in auditory cortex. Nature *426*, 442-446.

Wilczynski, W., and Northcutt, R.G. (1977). Afferents to the optic tectum of the leopard frog: an HRP study. J Comp Neurol *173*, 219-230.

Will, U., Luhede, G., and Görner, P. (1985a). The area octavo-lateralis in *Xenopus laevis* I. The primary afferent projections. Cell and Tissue Research *239*, 147-161.

Will, U., Luhede, G., and Görner, P. (1985b). The area octavo-lateralis in *Xenopus laevis* II. Second order projections and cytoarchitecture. Cell and Tissue Research *239*, 163-172.

Wu, G., Malinow, R., and Cline, H.T. (1996). Maturation of a central glutamatergic synapse. Science *274*, 972-976.

Wu, G.Y., and Cline, H.T. (2003). Time-lapse in vivo imaging of the morphological development of Xenopus optic tectal interneurons. J Comp Neurol *459*, 392-406.

Xu, H., Khakhalin, A.S., Nurmikko, A.V., and Aizenman, C.D. (2011). Visual experience-dependent maturation of correlated neuronal activity patterns in a developing visual system. J Neurosci *31*, 8025-8036.

Yu, L., Stein, B.E., and Rowland, B.A. (2009). Adult plasticity in multisensory neurons: short-term experience-dependent changes in the superior colliculus. J Neurosci *29*, 15910-15922.

Zahar, Y., Reches, A., and Gutfreund, Y. (2009). Multisensory enhancement in the optic tectum of the barn owl: spike count and spike timing. J Neurophysiol *101*, 2380-2394.

Zhang, L.I., Tao, H.W., Holt, C.E., Harris, W.A., and Poo, M. (1998). A critical window for cooperation and competition among developing retinotectal synapses. Nature *395*, 37-44.

Zheng, W., and Knudsen, E.I. (1999). Functional selection of adaptive auditory space map by GABAA-mediated inhibition. Science *284*, 962-965.

Zittlau, K.E., Claas, B., and Munz, H. (1988). Horseradish peroxidase study of tectal afferents in Xenopus laevis with special emphasis on their relationship to the lateral-line system. Brain Behav Evol *32*, 208-219.